# Functional spectrum and structural specificity of mitochondrial ferredoxins FDX1 and FDX2

3	
4	Vinzent Schulz <sup>1</sup> , Somsuvro Basu <sup>1,#</sup> , Sven-A. Freibert <sup>1</sup> , Holger Webert <sup>1</sup> , Linda Boß <sup>1</sup> ,
5	Ulrich Mühlenhoff <sup>1</sup> , Fabien Pierrel <sup>2</sup> , Lars-O. Essen <sup>3</sup> , Douglas M. Warui <sup>4</sup> , Squire Booker <sup>4,5,6</sup> ,
6	Oliver Stehling <sup>1,7,*</sup> , and Roland Lill <sup>1,7,*</sup>
7 8 9	<sup>1</sup> Institut für Zytobiologie, Philipps-Universität Marburg, Karl-von-Frisch-Str. 14, 35032 Marburg, Germany
10	<sup>2</sup> Univ. Grenoble Alpes, CNRS, UMR 5525, VetAgro Sup, Grenoble INP, TIMC, 38000
11 12 13	Grenoble, France <sup>3</sup> Department of Biochemistry, Faculty of Chemistry, Philipps-Universität Marburg, Hans-Meerwein-Str. 4, 35032 Marburg, Germany
14	<sup>4</sup> Department of Chemistry, The Pennsylvania State University, University Park, PA 16802
15 16 17	USA <sup>5</sup> Department of Biochemistry and Molecular Biology, The Pennsylvania State University University Park, PA 16802, USA
18 19	<sup>6</sup> The Howard Hughes Medical Institute, The Pennsylvania State University, University Park PA 16802, USA
20 21 22	<sup>7</sup> Zentrum für Synthetische Mikrobiologie Synmikro, Karl-von-Frisch-Str. 14, 35032 Marburg Germany
23 24 25	* Present affiliation and address: Freelance medical communications consultant; Vídeňská 281/77, 63900 Brno, Czech Republic
26 27 28	*Corresponding authors: Roland Lill E-mail: Lill@staff.uni-marburg.de, phone: +49-6421-286 6449
29 30 31	Oliver Stehling E-mail: Stehling@staff.uni-marburg.de, phone: +49-6421-286 4044
32	
33	
34	<b>Keywords:</b> Iron-sulfur proteins, lipoyl synthase, biogenesis, heme, coenzyme Q
35	mitochondria, cellular respiration, elesclomol.
36	

#### **Abstract**

Ferredoxins comprise a large family of iron-sulfur (Fe/S) proteins that shuttle electrons in diverse biological processes. Human mitochondria contain two isoforms of [2Fe-2S] ferredoxins, FDX1 (aka adrenodoxin) and FDX2, with known functions in cytochrome P450-dependent steroid transformations and Fe/S protein biogenesis. Here, we show that only FDX2, but not FDX1, is involved in Fe/S protein maturation. Vice versa, FDX1 is specific not only for steroidogenesis, but also for heme *a* and lipoyl cofactor biosyntheses. In the latter pathway, FDX1 provides electrons to kickstart the radical chain reaction catalyzed by lipoyl synthase. We also identified lipoylation as a target of the toxic anti-tumor copper ionophore elesclomol. Finally, the striking target specificity of each ferredoxin was assigned to small conserved sequence motifs. Swapping these motifs changed the target specificity of these electron donors. Together, our findings identify new biochemical tasks of mitochondrial ferredoxins and provide structural insights into their striking functional specificity.

#### 52 Introduction

Ferredoxins (FDXs) comprise a large family of redox proteins found in all kingdoms of life<sup>1,2</sup>. Their iron-sulfur (Fe/S) cofactors allow electron transfer to numerous targets in diverse biological pathways. FDXs from pathogens may serve as drug targets<sup>3,4</sup>. Mitochondria harbor the [2Fe-2S] cluster-containing FDXs that are evolutionarily derived from bacteria, and receive their electrons from NADPH via ferredoxin reductase (FDXR)<sup>1</sup>. The long-known mammalian mitochondrial FDX1 (aka adrenodoxin) functions in the metabolism of steroid hormones, bile acids, and vitamins A and D transferring electrons to all seven class I mitochondrial cytochrome P450 enzymes<sup>5</sup>. Mammals, including humans, possess the additional [2Fe-2S] FDX2 which, however, cannot take over the function of FDX1 in cortisol formation<sup>6</sup>. Instead, FDX2 and its fungal counterparts including S. cerevisiae Yah1 are central components of the core iron-sulfur cluster assembly (ISC) machinery, and hence are present in virtually all mitochondria or in mitochondria-related, ISC-containing mitosomes and hydrogenosomes<sup>4,6-11</sup>. FDX2 is required twice in mitochondrial Fe/S protein maturation. Initially, it interacts with the cysteine desulfurase complex NFS1-ISD11-ACP112-14 and reduces a persulfide (-SSH) bound to the scaffold protein ISCU2 to sulfide, thereby inducing *de novo* [2Fe-2S] cluster synthesis<sup>9,15-17</sup>. Later in mitochondrial [4Fe-4S] cluster assembly, FDX2 facilitates reductive fusion of two [2Fe-2S] to a [4Fe-4S] cluster on the ISCA proteins 18. The importance of human FDX2 and FDXR is reflected by severe genetic diseases including mitochondrial myopathy and sensory neuropathies<sup>19-22</sup>. Moreover, FDXR is a p53-dependent tumor suppressor, and its deficiency leads to tumor formation and liver disease in a mouse model<sup>23</sup>.

Beyond steroidogenesis and Fe/S protein biogenesis, mitochondrial FDXs were reported to be involved in other metabolic reactions. For instance, yeast mitochondrial Yah1, together with its reductase Arh1, provides electrons to the hydroxylase Cox15, thereby yielding heme  $a/a_3$  of cytochrome c oxidase (COX)<sup>24-26</sup>. Since FDX2 knockdown in human cells is associated with a partial COX defect, the protein was suggested to perform a similar function as Yah1<sup>6</sup>. Additionally, Yah1-Arh1 are required for coenzyme Q (ubiquinone or yeast CoQ<sub>6</sub>) biosynthesis, supposedly to reduce the Coq6 protein that catalyzes C5-hydroxylation of a CoQ<sub>6</sub> intermediate<sup>27,28</sup>. Neither human FDX1 nor FDX2 can replace Yah1 in yeast CoQ<sub>6</sub> synthesis, leaving open whether these electron donors might support CoQ<sub>10</sub> biosynthesis in humans. Conflicting results have been reported for the involvement of human FDX1 in cellular Fe/S protein biogenesis. Earlier studies, using *in vivo* complementation in yeast and RNA interference (RNAi) experiments in human cell culture, identified FDX2 as the sole Fe/S protein biogenesis-related FDX<sup>6</sup>. Accordingly, FDX2 but not FDX1 was crucial for *in vitro* reconstitution of both [2Fe-2S] and [4Fe-4S] cluster formation<sup>9,16,18,29</sup>. In principle, the specialized functions of human FDX1 and FDX2 fit their strikingly different tissue distribution identified by

immunostaining<sup>6</sup> (Suppl. Fig. 1a; see legend for details). However, systematic transcript analyses indicate significant expression of *FDX1* mRNA in a variety of tissues despite undetectable protein levels, raising the question of a broader function of FDX1 (Suppl. Fig. 1b). Accordingly, two reports proposed FDX1 to function also in Fe/S protein biogenesis, based on RNAi depletion experiments and *in vitro* [2Fe-2S] cluster synthesis on ISCU2 using FDXs chemically reduced by dithionite (DT)<sup>8,30</sup>. It remained unexplained, however, why the two FDXs would not functionally complement each other *in vivo* in Fe/S protein biogenesis.

Here, we aimed to clarify these important issues and identified so far unknown functions of the human FDXs in mitochondrial metabolism, most prominently the essential role of FDX1 to kickstart the radical chain reaction of lipoyl synthase (LIAS). Knowledge of the functional capacity of the two FDXs is crucial for understanding their impact on both mitochondrial metabolism and mitochondria-cytoplasm interaction, particularly in (tumorigenic) cells that shutdown their dependence on mitochondrial respiration<sup>31-33</sup>. We also report a striking target specificity of the two FDXs, and hence examined the structural basis of target recognition by site-directed mutagenesis, leading to the identification of small structural segments that functionally discriminate the two FDXs. Our work defining the functional spectrum of the human FDXs may have possible implications for better understanding disease phenotypes and for biotechnological applications of these unique electron donors<sup>34</sup>.

#### Results

107

108

109

110

111

112113

114

115

116

117

118119

120

121

122

123

124

125

126127

128

129

130

131

132

133

134

135

136137

138

139

#### FDX2 but not FDX1 is required for cellular Fe/S protein biogenesis

In vivo and in vitro studies have provided conflicting results on the function of human FDX1 in Fe/S protein biogenesis, while the involvement of FDX2 in this process is undisputed<sup>6,8,9,30</sup>. Reevaluation of these experiments confirmed that substantial depletion of FDX1 by RNAi did not induce any significant growth defect or reduction in the levels of various mitochondrial and cytosolic-nuclear Fe/S proteins, in contrast to depletion of FDX2, which is essential for the biogenesis of cellular Fe/S proteins including FDX1 (Fig. 1a; Suppl. Fig. 2a,b)<sup>6</sup>. To exclude that our RNAi knockdown of FDX1 was too weak to elicit a detectable phenotype, we knocked out FDX1 (or FDX2 as a control) by CRISPR-Cas9 technology. Application of three different FDX2-directed guide RNAs (gRNAs) did not yield viable FDX2-depleted cells after puromycin selection, consistent with the indispensable function of FDX2 in Fe/S protein assembly<sup>6,8</sup>. Two of three FDX1-directed gRNAs (CC1 and CC2; Suppl. Table 1) efficiently depleted FDX1, and, in contrast to the RNAi findings, profoundly decreased cell growth over time, while gRNA CC3 was ineffective (Fig. 1b; Extended data Fig. 1a,b). The results suggested a critical in vivo role of FDX1 disclosed only upon strong depletion. CC1- or CC2-mediated FDX1 knockout hardly affected the levels of the mitochondrial Fe/S-cluster-containing respiratory chain subunits NDUFS1, NDUFS8, NDUFV2, SDHB, and UQCRFS1, in contrast to the RNAi-mediated FDX2 knockdown (Fig. 1a,b; Extended data Fig. 1b; Suppl. Fig. 2b). Consistently, the enzyme activities of key mitochondrial Fe/S proteins, i.e. aconitase and succinate dehydrogenase (SDH), were not altered upon FDX1 knockout (Fig. 1c; Extended data Fig. 1c-e), unlike upon FDX2 RNAi depletion<sup>6,8</sup>. Together, these findings strongly argue against a critical *in vivo* role of FDX1 in cellular Fe/S protein biogenesis.

We next compared the capacities of FDX1 and FDX2 to *in vitro* donate electrons to the initial step of Fe/S protein biogenesis, i.e. the *de novo* [2Fe-2S] cluster synthesis on the scaffold protein ISCU2 by enzymatic function of the cysteine desulfurase complex NFS1-ISD11-ACP1 (NIA) and frataxin (FXN)<sup>9,15,30</sup>. [2Fe-2S] cluster formation was measured by circular dichroism (CD) spectroscopy, and strictly depended on FDX2 addition up to equimolar amounts to NIA (Fig. 1d; Extended data Fig. 2). In contrast, even a fivefold excess of FDX1 over NIA did not support any [2Fe-2S] cluster synthesis above control reactions performed without any FDX. In summary, our *in vivo* and *in vitro* results do not indicate a direct role of FDX1 in human Fe/S protein biogenesis, in contrast to previous suggestions<sup>8,30</sup>. Rather, the data support and extend earlier findings indicating a vital role of FDX2 as the exclusive physiological electron donor in mitochondrial Fe/S protein biogenesis<sup>6,9,18</sup>.

#### A crucial role of FDX1 in heme a-dependent cytochrome c oxidase activity

We next sought to find an explanation for the substantial growth retardation upon *FDX1* gene knockout. The culture medium of FDX1-deficient cells showed a profound acidification (Extended data Fig. 3a), indicating a metabolic switch from mitochondrial oxidative phosphorylation to glycolysis. Since respiratory complexes I-III and aconitase were unaffected in these cells (cf. Fig. 1b,c), we analyzed the activity of respiratory complex IV (cytochrome *c* oxidase, COX). We found a diminution in the levels of COX2 and COX6A subunits and a substantial decrease in COX enzyme activity (Fig. 2a,b; Extended data Fig. 3b). These effects were specific because complementation of FDX1-deficient cells by mitochondria-targeted FDX1 recovered both COX subunit levels and activity (Extended data Fig. 3c,d).

COX lacks Fe/S clusters, and consistently RNAi-mediated depletion of FDX2 only weakly affected COX2 or COX6A subunit levels, in contrast to the severe decrease upon FDX1 gene knockout (Fig. 2a; Suppl. Fig. 2b). COX contains two Cu centers and heme a/a₃ cofactors that are derived from heme b by COX10-dependent farnesylation (yielding the intermediate heme o) and COX15-catalyzed formylation  $^{24,26,35-37}$ . A role of FDX1 in heme b synthesis as an explanation for the COX defect was excluded, because heme b-containing complexes II and III were not altered in FDX1 knockout cells (Fig. 1b,c; Extended data Fig. 1b-d). In S. cerevisiae, Cox15-dependent heme a formation requires the function of ferredoxin Yah1, suggesting that the impaired COX function in FDX1 knockout cells may be caused by a heme a synthesis defect. A direct measurement of heme a levels by HPLC<sup>24</sup> or mass spectrometry failed due to detection limits. Notably, FDX1-deficient cells (CC2-based knockout) retained 33% of wild-type COX activity, likely due to the presence of FDX2 (Fig. 2b; Extended data Fig. 3b). Consistently, RNAi depletion of FDX2 was associated with some decrease in COX subunit levels and activity (Suppl. Fig. 2b)<sup>6</sup>. Since this effect is also seen upon depletion of other ISC factors including the ISCA-IBA57 proteins<sup>38</sup>, it may be an indirect consequence of FDX2 depletion on COX. Collectively, FDX1 performs a critical role for COX activity, presumably by its function in heme a synthesis, yet FDX2 may partially replace FDX1 in this process.

Our previous FDX1 and FDX2 complementation studies in Yah1-depleted Gal-YAH1 yeast cells had indicated a (weak) requirement of FDX2 but not FDX1 for yeast COX activity<sup>6</sup>, challenging our results with human cells. We reasoned that this discrepancy may be due to a failure of human FDX1 to properly interact with yeast Cox15 during heme o to heme a conversion. We therefore expressed human COX15 in the regulatable yeast strain Gal- $YAH1-cox15\Delta$  in which yeast COX15 was deleted. When Yah1 was depleted by growth in the presence of glucose (Glc) or glycerol (Gly)<sup>7</sup>, cells showed a growth defect that could be rescued only by expression of FDX2 but not by FDX1, consistent with the vital function of FDX2 in Fe/S protein biogenesis (Fig. 2c). However, under respiratory growth conditions (Gly-

containing medium) only the combined expression of FDX1 and FDX2 resulted in full growth complementation, indicating independent, complementary functions of the two human FDXs. Measurement of COX activity in extracts of Yah1-depleted Gal-YAH1-cox15∆ cells still showed low residual COX activity, due to the leaky *GAL* promoter (Fig. 2d). Upon FDX1 complementation, COX activity increased ca. 3-fold, despite the severe growth defect under this condition. In contrast, FDX2 complementation did not recover COX activity, despite normal cell growth on glucose-containing medium due to restored Fe/S protein biogenesis. These results for COX15-humanized yeast perfectly support our observations with human cells, implying that FDX1 is the predominant human ferredoxin supporting COX15-dependent heme a formation.

#### Both human ferredoxins are dispensable for ubiquinone biosynthesis

In S. cerevisiae, both Yah1 and Arh1 are essential for the biosynthesis of ubiquinone by supporting Coq6-catalyzed hydroxylation of precursor (coenzyme Q<sub>6</sub>;  $CoQ_6)$ compounds<sup>27,28</sup>. The electron donor for the biosynthesis of human ubiquinone (CoQ<sub>10</sub>) is unknown, and we therefore tested the potential function of the two human FDXs in this process. Determination of cellular CoQ<sub>10</sub> levels in *FDX1* knockout cells did not diminish CoQ<sub>10</sub> levels, not even upon prolonged tissue culture following puromycin selection (Fig. 2e). Likewise, FDX2-deficient cells contained wild-type levels of CoQ<sub>10</sub> even after 9 days of RNAi-mediated depletion (Fig. 2f, left) when cells showed a growth defect (Extended data Fig. 4a). We analyzed CoQ<sub>10</sub> levels in FDX2-depleted FDX1 knockout cells to test a potential redundant function of the FDXs. The FDX double-deficient cells showed a more profound growth retardation compared to single depletions (Extended data Fig. 4a), yet no significant changes in CoQ<sub>10</sub> levels (Fig. 2f, right), despite severe diminution of mitochondrial Fe/S protein levels (Extended data Fig. 4b). This result indicates that CoQ<sub>10</sub> synthesis in human cells is FDXindependent, and, unlike in yeast, may involve another, still unknown oxidoreductase.

#### FDX1 functions as a radical chain starter for LIAS-dependent lipoyl synthesis

To search for reasons of the growth defect and metabolic switch of *FDX1* knockout cells, we next performed anti-lipoyl immunostaining, and thereby identified a strong lipoylation defect of the E2 subunits dihydrolipoyl transacetylase (DLAT) and dihydrolipoyl succinyl transferase (DLST) of pyruvate dehydrogenase (PDH) and  $\alpha$ -ketoglutarate dehydrogenase (KGDH), respectively (Fig. 3a)<sup>39</sup>. The steady-state levels of the DLAT protein and of the radical *S*-adenosyl methionine (SAM) Fe/S enzyme lipoyl synthase (LIAS) remained unchanged. Complementation of FDX1-deficient cells by expression of mitochondria-targeted Su9-FDX1

recovered DLAT lipoylation (Extended data Fig. 5). This finding suggests a crucial function of FDX1 in lipoylation, an observation not revealed by the less severe RNAi depletion of FDX1 (cf. Suppl. Fig. 2b).

We surmised that FDX1 could act as the so far unknown electron donor starting the radical chain reaction of LIAS (explained in Extended data Fig. 6a)<sup>40,41</sup>. To test this idea, we adapted an in vitro assay for bacterial lipoyl synthase (LipA) for human LIAS<sup>40</sup>. An octapeptide containing the octanoyllysyl precursor served as a substrate analogue, and the SAMdependent formation of both the 6-thiooctanoyl intermediate and lipoyl product under strictly anaerobic conditions was measured and quantified by HPLC-MS. In the presence of the nonphysiological reductant DT, normally used to artificially start the radical chain, both the intermediate and product of the LIAS reaction were formed strictly dependent on the presence of DT, SAM, and LIAS (Fig. 3b,c). Strikingly, reduced FDX1 (by action of NADPH and FDXR) could replace DT much more efficiently as an electron source. Both the time courses and final yields for intermediate and product formation differed, comparable to reports for bacterial LipA<sup>40</sup>, assigning the second sulfur insertion step as being rate-limiting under *in vitro* conditions (Extended data Fig. 6b). We observed 29- and 61-fold, respectively, lower yields of intermediate and product with reduced FDX2 instead of FDX1 (Fig. 3b,c). This substantial difference suggested FDX1 being the physiological electron donor for LIAS, consistent with our in vivo experiments.

We further took advantage of human LIAS-expressing yeast cells lacking the endogenous *LIP5* gene to verify the FDX1 function and specificity in lipoylation. Yeast Gal-*YAH1-lip5*Δ cells were transformed with plasmids harboring human *LIAS*, *FDX1* and/or *FDX2*, followed by growth in the presence of either glucose or galactose. As expected, anti-lipoyl staining showed no lipoylation in extracts of Yah1-depleted Gal-*YAH1-lip5*Δ cells (lacking human LIAS) compared to wild-type cells (Fig. 3d). Lipoylation could be restored to wild-type levels by complementation with LIAS when cells were grown under Yah1-inducing conditions (galactose), but only weakly upon depletion (glucose) of Yah1 that is needed for LIAS Fe/S cluster maturation during ectopic expression. FDX1 but not FDX2 fully complemented the severe lipoylation defect of LIAS-containing, Yah1-depleted Gal-*YAH1-lip5*Δ cells. Apparently, the low residual levels of Yah1 in this condition (leaky Gal promoter) were adequate to mature enough FDX1 and LIAS for sufficient lipoylation. The humanized yeast model fully supports the dedicated role of human FDX1 in lipoylation.

To confirm this notion, we measured the enzyme activities of the lipoyl-dependent yeast KGDH and the Fe/S enzyme aconitase in this yeast model (Fig. 3e). As expected,  $lip5\Delta$  deletion cells lacked KGDH activity, and aconitase activity dropped by half, likely as an indirect effect of impaired mitochondrial metabolism. In Yah1-depleted Gal-YAH1- $lip5\Delta$  cells, absent KGDH and low aconitase activities were rescued to the  $lip5\Delta$  levels only by expression of LIAS,

FDX1, and FDX2. The findings indicate the specific, non-overlapping functions of FDX1 and FDX2 in LIAS-dependent lipoylation and Fe/S protein biogenesis, respectively. This view perfectly agrees with the growth behavior of the various LIAS-expressing Gal-YAH1-lip5 $\Delta$  cells in different liquid or solid media (Extended data Fig. 7).

#### Lipoylation is a primary target of the elesclomol-copper complex

FDX1 has been proposed to the target of the anti-cancer drug elesclomol (Ele) because CRISPR-Cas9 deletion of *FDX1* desensitizes these cells against treatment with Ele <sup>32</sup>. Ele was shown to be toxic for proteasome inhibitor-resistant cells depending on increased mitochondrial energy metabolism, and it was proposed that Ele imparts a toxic gain of FDX1's function in Fe/S protein biogenesis. The toxic effect was further shown to be mediated by the complex of Ele with Cu (Ele:Cu) rather than Ele alone<sup>32</sup>, which is consistent with earlier reports that Ele acts as a Cu ionophore transporting Cu to mitochondria, thereby restoring COX function in Cu deficiency<sup>42,43</sup>. A study published during review of this work suggested both FDX1 and lipoylation as targets of Ele:Cu toxicity, but no molecular explanations were described<sup>33</sup>. Our *in vivo* and *in vitro* findings refuting FDX1 function in Fe/S protein biogenesis, but showing its role in lipoylation, urged for a biochemical evaluation of the toxic role of Ele:Cu.

We first tested the effects of Ele and/or Cu on LIAS- and FDX1-dependent lipoyl synthesis *in vitro*. Addition of Ele alone did not affect 6-thiooctanoyl and lipoyl formation, even at a 14-fold excess over FDX1 (Fig. 4a,b; left). In contrast, both Cu and Ele:Cu imposed severe effects on these reactions in a dose-dependent manner (Fig. 4a,b; middle and right), fully consistent with reports indicating toxic effects of Ele only in the presence of Cu or other metals<sup>32,33,42,44,45</sup>. Notably, an excess of Ele over Cu slightly attenuated the synthesis defect. The high stability constant of K<sub>Ele:Cu(II)</sub>=10<sup>24,2</sup> L/mol<sup>46</sup> suggests that both Cu and Ele:Cu inhibit lipoylation, with Cu being slightly more potent. Similar relative impacts of Cu and Ele:Cu have been observed for superoxide dismutase enzyme activity<sup>44</sup>. Collectively, our *in vitro* results identify lipoylation rather than Fe/S protein biogenesis as a sensitive target of Ele:Cu toxicity. In particular, the second sulfur insertion step appears to be most affected (Fig. 4a,b; Extended data Fig. 6a). Since lipoyl-dependent PDH and KGDH are central components of mitochondrial metabolism, our findings satisfactorily explain why particularly cells dependent on this process are most vulnerable to Ele treatment<sup>32</sup>.

The *in vitro* lipoylation assay did not readily allow the discrimination between FDX1 and/or LIAS as potential targets of the Ele:Cu toxicity. To address this issue biochemically, we first studied the impact of Ele and/or Cu on FDX1 during NADPH-FDXR-FDX1-dependent electron transfer to cytochrome *c*. Reduction of cytochrome *c* was not affected by addition of Ele or Ele:Cu, yet was fully abolished by Cu (Fig. 4c). The striking difference of this result to

the observed inhibition of lipoylation by both Cu and Ele:Cu indicates the LIAS reaction as the preferential target of Ele:Cu and FDX1 as target of Cu only. Consistently, only Cu but not Ele or Ele:Cu destroyed the Fe/S clusters of both FDX1 and FDX2 (Fig. 4d,e; Suppl. Fig. 3), in agreement with the Cu sensitivity of yeast Yah1<sup>47</sup>. Our *in vitro* findings identifying LIAS function in lipoylation as a target of the toxic effect of Ele:Cu are further supported *in vivo*. Human cells treated with Ele or Ele:Cu showed a strong impairment of lipoylation and a destabilization of LIAS (not seen upon *FDX1* knockout), while DLAT protein and the two FDXs were hardly affected (Fig. 4f). In contrast, Cu alone elicited no detectable effects. Collectively, the biochemical and cell biological results document that the Ele:Cu complex strongly affects LIAS function in lipoylation and may be the target of the toxic effect of Ele (see Suppl. Discussion).

#### Converting FDX1 into a ferredoxin functional in Fe/S protein biogenesis

To address the structural basis of the functional specificity of the two human FDXs, we solved the crystal structure of mature FDX2 (residues 66-171; PDB ID: 2Y5C; Suppl. Table 2; Suppl. Results) for comparison with the known FDX1 structure (PDB ID: 3P1M). Significant structural differences between FDX1 and FDX2 were observed only for the loop between helix C and the Fe/S cluster binding site, because the Phe-Gly (FG) dipeptide is missing in FDX2 (Fig. 5a; Extended data Fig. 8; Suppl. Fig. 4; Suppl. Results). Comparison of the surface potentials<sup>48</sup> revealed a less negatively charged area of FDX2 (Fig. 5b; Suppl. Fig. 5; Suppl. Results; for details see Discussion), mainly due to exchanges of semi-conserved Asp91<sup>FDX1</sup> by His95<sup>FDX2</sup> and Glu133<sup>FDX1</sup> by Arg135<sup>FDX2</sup> (Extended data Fig. 8). Overall, the 3D structures of FDX1 and FDX2 display only minor differences in backbone geometry.

Consequently, we compared multi-sequence alignments of FDX1-, FDX2-, fungal- and bacterial-type FDXs (Extended data Fig. 8). Ten regions (including those structurally pinpointed above) were identified that distinguish FDX1- and FDX2-type proteins (named M1 to M10). We first tested the importance of these regions for FDX2 function by introducing the corresponding FDX1 M1-M10 sequences (Suppl. Table 3), and we examined N- and C-terminal truncations of FDX2 (termed  $\Delta$ N13 and  $\Delta$ C12). FDX2 mutant proteins were expressed in Yah1-depleted Gal-YAH1 cells, and growth was analyzed (Extended data Fig. 9). Exchanges of regions M3 to M7 decreased the Yah1-rescuing function of FDX2, with segment M7 showing the most pronounced growth defect. Moreover, the C terminus ( $\Delta$ C12) but not the N terminus ( $\Delta$ N13) of mature FDX2 was critical for growth. Hence, region M7 and the FDX2 C terminus are important structural elements for FDX2 function.

Second, we introduced FDX2 segments M1-M10 (either alone or in combination) into FDX1, and we transferred 14 or 27 C-terminal FDX2 residues into FDX1 (exC14 and exC27), in an attempt to generate FDX2 functionality in FDX1 (Fig. 5c,d). Like FDX1<sup>6</sup>, most FDX1

variants did not detectably rescue the growth defect of Yah1-depleted Gal-YAH1 yeast, even though all recombinantly purified proteins contained a [2Fe-2S] cluster, except for FDX1-M5 (deletion of the FG motif), explaining why this mutant is non-functional (Fig. 5d; Suppl. Fig. 6). However, partial growth restoration was observed by introducing the FDX2 C terminus into FDX1. Further growth improvement was obtained by additional exchange of segment M7, particularly in combination with either M3 or M6. Consistent with the findings above (Extended data Fig. 9), region M7 and the C terminus are decisive features of FDX2 functionality, while regions M3 and M6 fulfil a weak auxiliary role. To extend these findings, we measured the enzyme activities of aconitase and catalase (a non-Fe/S protein, yet indirectly affected by Fe/S protein synthesis defects<sup>6,49</sup>) in Yah1-depleted Gal-YAH1 yeast complemented with FDX1, FDX2, or the growth-restoring FDX1-M3+M7+exC27 or FDX1-M6+M7+exC27 mutant proteins (Fig. 5e,f). While wild-type FDX1 showed no improvement of both enzyme activities in Yah1-depleted cells, both FDX1 mutant proteins restored ca. 30-50% of the activities seen in FDX2-complemented cells. Apparently, small increases in Fe/S protein biogenesis activity by introducing FDX2 functionality into FDX1 can lead to partial growth restoration.

#### Converting FDX2 into a ferredoxin with FDX1 functionality

In a reversed approach, we sought to identify regions specific for FDX1 functionality. We introduced the FDX-discriminating regions M1-M10 from FDX1 into FDX2, and we deleted the conserved FDX2 C terminus (\( \Delta C12 \); Fig. 6a; Extended data Fig. 8; Suppl. Table 3). Because simple cell-based in vivo assays were not readily feasible to test restoration of FDX1-specific functions in FDX2, we studied two specifically FDX1-catalyzed reactions in vitro, namely the cytochrome P450-dependent cortisol synthesis from the 11-deoxycortisol precursor<sup>5,6</sup> (Suppl. Fig. 7) and lipoylation (cf. Fig. 3b,c). The various FDX2 mutant proteins were recombinantly expressed and purified. They showed close to wild-type UV/Vis spectral properties, except for FDX2-M7 which did not bind any Fe/S cluster, explaining why this segment was essential for FDX2 function (see above; Extended data Fig. 9; Suppl. Fig. 6). Cortisol formation by cytochrome P450 CYP11B1 was efficiently catalyzed by FDX1, but not by FDX26 or several mutant proteins (Fig. 6b,c). In contrast, mutant FDX2-R135E showed a strong (35-fold) increase in cortisol formation compared to wild-type FDX2. Further small improvements were seen by combining this site-specific exchange with the C-terminal deletion (FDX2-R135E+ $\Delta$ C12) and segment M5 (FDX2-M5+R135E+ $\Delta$ C12) to yield a 42- and 45-fold stimulation, respectively. Overall, up to 9% of the FDX1-catalyzed cortisol levels were generated, showing that mutated FDX2 is now well, yet not fully capable of steroid production. We conclude that FDX1-specific Glu133 represents a decisive functional element for steroid formation, and the C-terminal truncation provides a further minor contribution. Interestingly, the fungal-type *S. cerevisiae* Yah1 and *S. pombe* Etp1<sup>fd</sup> also supported cortisol synthesis at 20-60% efficiencies compared to FDX1-type human FDX1 and *Bos taurus* Adx<sup>50,51</sup> (Fig. 6c). These fungi contain only one FDX and do not possess mitochondrial cytochrome P450 enzymes<sup>52</sup>. However, both fungal proteins contain a negatively charged Asp at position Glu133<sup>FDX1</sup>, re-emphasizing the importance of negative charge at this position for steroid formation.

Analogously, the FDX2 mutant proteins were assayed by FDX1-specific lipoylation (cf. Fig. 3b,c). Surprisingly, FDX2-R135E did not significantly improve lipoylation compared to wild-type FDX2 (Fig. 6d,e). Instead, the C-terminally truncated FDX2-ΔC12 variants (without or with additional modifications) showed robust activity increases, enabling up to 49% 6-thiooctanoyl and 21% lipoyl formation compared to FDX1, equivalent to a 6-10-fold increase over FDX2-catalyzed levels. Thus, the C terminus of FDX2 appears to negatively interfere with LIAS interaction, an effect also evident from the ca. 3-fold higher lipoylation (compared to FDX2) by *S. cerevisiae* Yah1 hosting a shorter C terminus distinct from FDX2 (Fig. 6d,e; Extended data Fig. 8). This result agrees well with the *in vivo* complementation experiments with LIAS-humanized yeast (cf. Fig. 3d). Collectively, our mutational studies identify different regions of FDX1 (highlighted in Fig. 6a) with importance for either cortisol or lipoyl formation, suggesting that the FDX1 interaction sites with CYP11B1 and LIAS are not identical.

#### Discussion

In this work, we have expanded the knowledge on the physiological roles of the mitochondrial ferredoxins FDX1 and FDX2 in human cells by identifying new targets of their electron transfer function and by dissecting the molecular basis of their target specificity (Fig. 6f). A major finding of our study was the identification of the so far unknown molecular function of FDX1 in lipoyl cofactor biosynthesis, half a century after the discovery of its (i.e. adrenodoxin's) crucial role in steroidogenesis<sup>53</sup>. Strikingly, both FDX1 and FDX2 are involved in lipoylation, yet perform distinct, non-overlapping roles. While FDX2 as a member of the core mitochondrial ISC machinery assists the assembly of the [4Fe-4S] protein lipoyl synthase (LIAS)<sup>22</sup>, also *FDX1* knockout cells showed a severe lipoylation defect. This was surprising, because FDX1 had no detectable role in Fe/S protein maturation (Fig. 1). To elucidate the molecular basis of this finding, we adapted an *in vitro* reconstitution system of bacterial lipoyl synthesis for the human pathway<sup>40</sup>, and show that FDX1 serves as a dedicated electron donor to kickstart the multistep radical SAM-dependent LIAS reaction (Fig. 3b,c). Frequently, the electron donors of members of the large radical SAM enzyme family are ill-defined<sup>41</sup>, or the roles of electron donors in either Fe/S cluster assembly or SAM reduction were not dissected <sup>54</sup>. *Thermotoga* 

maritima [4Fe-4S] FDXs reduce MiaB, and *E. coli* LipA employs a flavodoxin and its reductase<sup>55,56</sup>, clearly distinguishing mitochondrial and bacterial lipoylation pathways despite the close evolutionary connection of mitochondria and bacteria<sup>10</sup>. During *in vitro* reconstitution of lipoylation, FDX1 was more potent than the artificial reductant DT, yet could not efficiently be replaced by FDX2. The physiological relevance of the FDX specificity was further verified by a human LIAS-expressing yeast model in which endogenous Yah1 was depleted and replaced by FDX1 and/or FDX2. FDX1 but not FDX2 was essential for efficient lipoylation (Fig. 3d,e). Structural modeling using Alphafold showed a trimeric complex between LIAS, GCSH (H-protein of the glycine cleavage system;<sup>39</sup>) with the octanoyl-carrying loop reaching into the substrate tunnel of LIAS, and FDX1 with its [2Fe-2S] cluster being close to the catalytic cluster of LIAS consistent with direct electron transfer through a tunnel in LIAS (for details see Suppl. Results; Extended data Fig. 10). In contrast, FDX2 could not be modeled in a physiologically relevant position in keeping with its low activity in lipoylation.

FDX1 was further characterized to play a decisive role in COX maturation presumably by facilitating heme *a* synthesis (Fig. 6f), similar to Yah1 in yeast or FdxA in *Trypanosomes*<sup>4,24</sup>. This function became only evident upon *FDX1* gene knockout, again suggesting that rather low levels of FDX1 satisfy the cellular needs of heme *a* production (see Suppl. Discussion). In part, the low FDX1 requirement may be due to a minor activity of FDX2 in this process<sup>6</sup>, a notion supported by residual COX activity (33%) in human FDX1 knockout cells (Fig. 2b) and our humanized COX15 yeast model expressing FDX1 and/or FDX2 (Fig. 2d). Collectively, FDX1, besides its well-established role in steroidogenesis, shows a functional plasticity to cooperate with multiple target electron acceptors. Even in steroidogenesis, FDX1 is known to interact with multiple mitochondrial cytochrome P450 (CYP) enzymes<sup>5</sup>. The array of possible CYP partners of FDX1 might even be extended under certain (sometimes pathological) conditions<sup>57,58</sup>. We conclude that mammalian FDX1 has evolved to a remarkably versatile enzyme donating electrons to multiple acceptors in different physiological pathways.

In contrast, FDX2 mainly functions in Fe/S protein biogenesis. Given the importance of cellular Fe/S protein biogenesis for life, this FDX2 function is essential for virtually all eukaryotic cells and tissues<sup>11</sup>, and is even required at two stages within the mitochondrial ISC machinery (see Introduction). In contrast to earlier reports<sup>8,30</sup>, we did not find any activity of FDX1 in mitochondrial Fe/S protein maturation, neither *in vivo* in cells lacking FDX1 nor *in vitro* during enzymatic [2Fe-2S] cluster reconstitution on ISCU2 (Fig. 1). This notion was further supported by our yeast complementation experiments and the mutual interconversion of FDX1 and FDX2 functions (see below). The explanation for these contradictory findings remains unclear, yet a possible reason may be the indirect consequences of both lipoylation and heme *a* synthesis defects in FDX1-deficient cells on mitochondrial metabolism. Collectively, our study shows a high specialization of each FDX for electron transfer to distinct redox partners.

The high target specificity of the two human FDXs raised the question of what structural or other characteristics these enzymes utilize to discriminate their targets. The reduction potentials of FDX1 and FDX2 at -267 and -342 mV, respectively, cannot readily explain why FDX2 cannot cooperate with typical FDX1 substrates, fitting to a study with bacterial FDXs<sup>6,59</sup>. To explore structural criteria, we performed mutational studies to swap conspicuous regions between the two FDXs, thereby gaining Fe/S protein biogenesis function of FDX1 or lipoyl and cortisol synthesis activity of FDX2. In each case, only few selected regions showed a substantial activity increase over the low residual activity of each FDX, yet full activity was not reached showing the complexity of substrate selection. A prominent, up to 50-fold increased cortisol formation activity was observed by replacing a positive by a negative residue in FDX2 (mutant R135E; Fig. 6b). While specific ion pair interactions might explain the FDX2 activity gain, the charge inversion also changes the electronic surface potential above the [2Fe-2S] cluster binding site to better resemble that of FDX1-type proteins (Suppl. Fig. 5). In a study of bacterial Fdx-CYP interactions, a similar region was found critical for interaction with a large number of CYP partners<sup>59</sup>. Strongly negative surfaces can also be found for fungal Yah1 and Etp1<sup>fd</sup> (containing Asp at position 135) which primarily function in Fe/S protein and heme a biogenesis<sup>7,24,27</sup>, yet in vitro can perform CYP-dependent catalysis despite the absence of endogenous mitochondrial CYPs in fungi (Fig. 6c)<sup>50</sup>. Overall, negative ionic interactions and surface potentials may contribute to the specificity of FDX1-type proteins in steroidogenesis. Interestingly, a different structural determinant was critical for FDX1 specificity in lipoylation. Deletion of the conserved C terminus (FDX2 mutant ΔC12) created substantially increased (up to tenfold) lipoylation activity, while mutant R135E was not improved (Fig. 6d,e). This indicates different specificity determinants for FDX1 binding to its dedicated targets CYPs and LIAS. Conversely, FDX1 obtained a gain in FDX2 functionality (e.g., partial growth recovery of Yah1depleted yeast cells) upon transfer of the conserved C terminus of FDX2 (Fig. 5d-f). A minor growth improvement was obtained by (additionally) exchanging various small segments (M7 with M3, M6) discriminating the two FDXs. This shows that a combination of several regions is crucial to define FDX2 specificity in its major function, i.e. Fe/S protein biogenesis.

Here, we have studied known and novel physiological functions of the two human FDXs and have defined the molecular basis of their specificities. The findings may open avenues for engineering FDXs to function with diverse redox partners or as redox gates in synthetic biology approaches<sup>60</sup>. An interesting open question concerns the existence of additional FDX targets. Prime candidates are other mitochondrial radical SAM enzymes such as CDK5RAP involved in tRNA modification or RSAD1 with a still unclear function<sup>41,61</sup>. Future studies may therefore further expand the broad spectrum of FDX targets.

468

433

434

435

436

437

438

439

440441

442

443

444

445

446

447

448

449

450

451

452

453

454 455

456

457

458

459

460 461

462

463

464

465

466

#### Acknowledgments

- We thank Ralf Rösser and Sahra Hanschke for excellent technical assistance, Dr. Uwe Linne
- and Jan Bamberger from the Core Facility 'Mass spectrometry and Elemental analysis' of
- 473 Philipps-Universität Marburg for mass spectrometry, and Dr. Frank Hannemann and Rita
- 474 Bernhardt (Saarbrücken) for help with cortisol formation assays. We acknowledge the
- contribution of the Core Facility 'Protein Biochemistry and Spectroscopy' of the Philipps-
- 476 Universität Marburg. RL received generous financial support from Deutsche
- 477 Forschungsgemeinschaft (SPP 1927) and COST Action FeSBioNet (Contract CA15133). SJB
- 478 acknowledges support from the National Science Foundation (MCB-1716686) and the Eberly
- 479 Family Distinguished Chair in Science. SJB is an Investigator of the Howard Hughes Medical
- 480 Institute.

481

483

470

482

#### References

- Campbell, I.J., Bennett, G.N. & Silberg, J.J. Evolutionary Relationships Between Low
   Potential Ferredoxin and Flavodoxin Electron Carriers. *Frontiers in Energy Research* 7(2019).
- 487 2. Hanke, G. & Mulo, P. Plant type ferredoxins and ferredoxin-dependent metabolism. *Plant Cell Environ* **36**, 1071-84 (2013).
- 489 3. Miotto, O. et al. Genetic architecture of artemisinin-resistant Plasmodium falciparum. *Nat* 490 *Genet* 47, 226-34 (2015).
- 491 4. Changmai, P. et al. Both human ferredoxins equally efficiently rescue ferredoxin deficiency in Trypanosoma brucei. *Mol Microbiol* **89**, 135-51 (2013).
- 5. Ewen, K.M., Ringle, M. & Bernhardt, R. Adrenodoxin--a versatile ferredoxin. *IUBMB Life* **64**, 506-12 (2012).
- 495 6. Sheftel, A.D. et al. Humans possess two mitochondrial ferredoxins, Fdx1 and Fdx2, with 496 distinct roles in steroidogenesis, heme, and Fe/S cluster biosynthesis. *Proceedings of* 497 *the National Academy of Sciences of the United States of America* **107**, 11775-80 498 (2010).
- Lange, H., Kaut, A., Kispal, G. & Lill, R. A mitochondrial ferredoxin is essential for
   biogenesis of cellular iron-sulfur proteins. *Proc Natl Acad Sci U S A* 97, 1050-5 (2000).
- 501 8. Shi, Y., Ghosh, M., Kovtunovych, G., Crooks, D.R. & Rouault, T.A. Both human ferredoxins 1 and 2 and ferredoxin reductase are important for iron-sulfur cluster biogenesis. *Biochimica et biophysica acta* **1823**, 484-92 (2012).
- 9. Webert, H. et al. Functional reconstitution of mitochondrial Fe/S cluster synthesis on Isu1 reveals the involvement of ferredoxin. *Nat. Commun.* **5**, 5013 (2014).
- 506 10. Freibert, S.A. et al. Evolutionary conservation and in vitro reconstitution of microsporidian iron-sulfur cluster biosynthesis. *Nat Commun* **8**, 13932 (2017).
- Braymer, J.J., Freibert, S.A., Rakwalska-Bange, M. & Lill, R. Mechanistic concepts of iron-sulfur protein biogenesis in Biology. *Biochim Biophys Acta Mol Cell Res* 1868,
   118863 (2021).

- 12. Kispal, G., Csere, P., Prohl, C. & Lill, R. The mitochondrial proteins Atm1p and Nfs1p are essential for biogenesis of cytosolic Fe/S proteins. *EMBO J* **18**, 3981-9 (1999).
- 13. Boniecki, M.T., Freibert, S.A., Muhlenhoff, U., Lill, R. & Cygler, M. Structure and
   functional dynamics of the mitochondrial Fe/S cluster synthesis complex. *Nat Commun* 8, 1287 (2017).
- 14. Van Vranken, J.G. et al. The mitochondrial acyl carrier protein (ACP) coordinates
   mitochondrial fatty acid synthesis with iron sulfur cluster biogenesis. *Elife* 5, e17828
   (2016).
- 519 15. Kim, J.H., Frederick, R.O., Reinen, N.M., Troupis, A.T. & Markley, J.L. [2Fe-2S]520 Ferredoxin binds directly to cysteine desulfurase and supplies an electron for iron-sulfur
  521 cluster assembly but is displaced by the scaffold protein or bacterial frataxin. *Journal of*522 *the American Chemical Society* **135**, 8117-20 (2013).
- 16. Gervason, S. et al. Physiologically relevant reconstitution of iron-sulfur cluster biosynthesis uncovers persulfide-processing functions of ferredoxin-2 and frataxin. *Nat Commun* **10**, 3566 (2019).
- 17. Freibert, S.A. et al. N-terminal tyrosine of ISCU2 triggers [2Fe-2S] cluster synthesis by ISCU2 dimerization. *Nat Commun* **12**, 6902 (2021).
- Weiler, B.D. et al. Mitochondrial [4Fe-4S] protein assembly involves reductive [2Fe-2S]
   cluster fusion on ISCA1-ISCA2 by electron flow from ferredoxin FDX2. *Proc Natl Acad Sci U S A* 117, 20555-20565 (2020).
- 531 19. Spiegel, R. et al. Deleterious mutation in FDX1L gene is associated with a novel mitochondrial muscle myopathy. *Eur J Hum Genet* **22**, 902-6 (2014).
- 533 20. Paul, A. et al. FDXR Mutations Cause Sensorial Neuropathies and Expand the Spectrum of Mitochondrial Fe-S-Synthesis Diseases. *Am J Hum Genet* **101**, 630-637 (2017).
- 535 21. Gurgel-Giannetti, J. et al. A novel complex neurological phenotype due to a homozygous mutation in FDX2. *Brain* **141**, 2289-2298 (2018).
- 22. Lill, R. & Freibert, S.A. Mechanisms of Mitochondrial Iron-Sulfur Protein Biogenesis.
   Annu Rev Biochem 89, 471-499 (2020).
- Zhang, Y. et al. Ferredoxin reductase is critical for p53-dependent tumor suppression via
   iron regulatory protein 2. *Genes Dev* 31, 1243-1256 (2017).
- 541 24. Barros, M.H., Carlson, C.G., Glerum, D.M. & Tzagoloff, A. Involvement of mitochondrial ferredoxin and Cox15p in hydroxylation of heme O. *FEBS Lett* **492**, 133-8 (2001).
- 543 25. Bareth, B. et al. The heme a synthase Cox15 associates with cytochrome c oxidase assembly intermediates during Cox1 maturation. *Mol Cell Biol* **33**, 4128-37 (2013).
- 545 26. Swenson, S.A. et al. From Synthesis to Utilization: The Ins and Outs of Mitochondrial Heme. *Cells* **9**(2020).
- 547 27. Pierrel, F. et al. Involvement of mitochondrial ferredoxin and para-aminobenzoic acid in yeast coenzyme Q biosynthesis. *Chem Biol* **17**, 449-59 (2010).
- 549 28. Ozeir, M. et al. Coenzyme Q biosynthesis: Coq6 is required for the C5-hydroxylation 550 reaction and substrate analogs rescue Coq6 deficiency. *Chemistry & biology* **18**, 1134-551 42 (2011).
- 552 29. Yan, R., Adinolfi, S. & Pastore, A. Ferredoxin, in conjunction with NADPH and 553 ferredoxin-NADP reductase, transfers electrons to the IscS/IscU complex to promote 554 iron-sulfur cluster assembly. *Biochim Biophys Acta* **1854**, 1113-7 (2015).
- 555 30. Cai, K., Tonelli, M., Frederick, R.O. & Markley, J.L. Human Mitochondrial Ferredoxin 1 (FDX1) and Ferredoxin 2 (FDX2) Both Bind Cysteine Desulfurase and Donate Electrons for Iron-Sulfur Cluster Biosynthesis. *Biochemistry* **56**, 487-499 (2017).

- 31. Zhu, J. & Thompson, C.B. Metabolic regulation of cell growth and proliferation. *Nat Rev Mol Cell Biol* **20**, 436-450 (2019).
- 32. Tsvetkov, P. et al. Mitochondrial metabolism promotes adaptation to proteotoxic stress.

  Nat Chem Biol 15, 681-689 (2019).
- 33. Tsvetkov, P. et al. Copper induces cell death by targeting lipoylated TCA cycle proteins.
   Science 375, 1254-1261 (2022).
- 34. Campbell, I.J. et al. Recombination of 2Fe-2S Ferredoxins Reveals Differences in the Inheritance of Thermostability and Midpoint Potential. *ACS Synth Biol* **9**, 3245-3253 (2020).
- 567 35. Brown, K.R., Allan, B.M., Do, P. & Hegg, E.L. Identification of novel hemes generated by heme A synthase: evidence for two successive monooxygenase reactions. *Biochemistry* 569 **41**, 10906-13 (2002).
- 36. Moraes, C.T., Diaz, F. & Barrientos, A. Defects in the biosynthesis of mitochondrial heme c and heme a in yeast and mammals. *Biochim Biophys Acta* **1659**, 153-9 (2004).
- 572 37. Antonicka, H. et al. Mutations in COX15 produce a defect in the mitochondrial heme 573 biosynthetic pathway, causing early-onset fatal hypertrophic cardiomyopathy. *Am J Hum* 574 *Genet* **72**, 101-14 (2003).
- 575 38. Sheftel, A.D. et al. The human mitochondrial ISCA1, ISCA2, and IBA57 proteins are required for [4Fe-4S] protein maturation. *Mol Biol Cell* **23**, 1157-66 (2012).
- 577 39. Cronan, J.E. Assembly of Lipoic Acid on Its Cognate Enzymes: an Extraordinary and Essential Biosynthetic Pathway. *Microbiol Mol Biol Rev* **80**, 429-50 (2016).
- 40. McCarthy, E.L. & Booker, S.J. Destruction and reformation of an iron-sulfur cluster during catalysis by lipoyl synthase. *Science* **358**, 373-377 (2017).
- 41. Landgraf, B.J., McCarthy, E.L. & Booker, S.J. Radical S-Adenosylmethionine Enzymes in Human Health and Disease. *Annu Rev Biochem* **85**, 485-514 (2016).
- 583 42. Nagai, M. et al. The oncology drug elesclomol selectively transports copper to the 584 mitochondria to induce oxidative stress in cancer cells. *Free Radic Biol Med* **52**, 2142-50 585 (2012).
- 586 43. Soma, S. et al. Elesclomol restores mitochondrial function in genetic models of copper deficiency. *Proc Natl Acad Sci U S A* **115**, 8161-8166 (2018).
- 44. Hasinoff, B.B., Yadav, A.A., Patel, D. & Wu, X. The cytotoxicity of the anticancer drug
   elesclomol is due to oxidative stress indirectly mediated through its complex with Cu(II).
   *J Inorg Biochem* 137, 22-30 (2014).
- 45. Modica-Napolitano, J.S., Bharath, L.P., Hanlon, A.J. & Hurley, L.D. The Anticancer
   Agent Elesclomol Has Direct Effects on Mitochondrial Bioenergetic Function in Isolated
   Mammalian Mitochondria. *Biomolecules* 9(2019).
- 594 46. Yadav, A.A., Patel, D., Wu, X. & Hasinoff, B.B. Molecular mechanisms of the biological activity of the anticancer drug elesclomol and its complexes with Cu(II), Ni(II) and Pt(II). *J Inorg Biochem* **126**, 1-6 (2013).
- 597 47. Vallieres, C., Holland, S.L. & Avery, S.V. Mitochondrial Ferredoxin Determines 598 Vulnerability of Cells to Copper Excess. *Cell Chem Biol* **24**, 1228-1237 e3 (2017).
- 48. Mellor, S.B., Vavitsas, K., Nielsen, A.Z. & Jensen, P.E. Photosynthetic fuel for
   heterologous enzymes: the role of electron carrier proteins. *Photosynth Res* 134, 329-342 (2017).
- 49. Mühlenhoff, U. et al. Cytosolic monothiol glutaredoxins function in intracellular iron sensing and trafficking via their bound iron-sulfur cluster. *Cell Metab* **12**, 373-85 (2010).
- 50. Schiffler, B. et al. The adrenodoxin-like ferredoxin of Schizosaccharomyces pombe mitochondria. *J Inorg Biochem* **98**, 1229-37 (2004).

- 606 51. Muller, J.J. et al. Structural and thermodynamic characterization of the adrenodoxin-like 607 domain of the electron-transfer protein Etp1 from Schizosaccharomyces pombe. *J Inorg* 608 *Biochem* **105**, 957-65 (2011).
- 52. Omura, T. & Gotoh, O. Evolutionary origin of mitochondrial cytochrome P450. *J Biochem* **161**, 399-407 (2017).
- Kimura, T. & Suzuki, K. Components of the electron transport system in adrenal steroid hydroxylase. Isolation and properties of non-heme iron protein (adrenodoxin). *J Biol Chem* 242, 485-91 (1967).
- 54. Swift, R.P., Rajaram, K., Elahi, R., Liu, H.B. & Prigge, S.T. Roles of Ferredoxin-Dependent Proteins in the Apicoplast of Plasmodium falciparum Parasites. *mBio*, e0302321 (2022).
- 55. Arcinas, A.J., Maiocco, S.J., Elliott, S.J., Silakov, A. & Booker, S.J. Ferredoxins as
   interchangeable redox components in support of MiaB, a radical S-adenosylmethionine
   methylthiotransferase. *Protein Sci* 28, 267-282 (2019).
- 56. Cicchillo, R.M. et al. Lipoyl synthase requires two equivalents of S-adenosyl-L methionine to synthesize one equivalent of lipoic acid. *Biochemistry* 43, 6378-86 (2004).
- 57. Lehnerer, M., Schulze, J., Bernhardt, R. & Hlavica, P. Some properties of mitochondrial adrenodoxin associated with its nonconventional electron donor function toward rabbit liver microsomal cytochrome P450 2B4. *Biochem Biophys Res Commun* **254**, 83-7 (1999).
- 58. Liao, W.L., Dodder, N.G., Mast, N., Pikuleva, I.A. & Turko, I.V. Steroid and protein ligand binding to cytochrome P450 46A1 as assessed by hydrogen-deuterium exchange and mass spectrometry. *Biochemistry* **48**, 4150-8 (2009).
- 59. Zhang, W. et al. Mechanistic Insights into Interactions between Bacterial Class I P450 Enzymes and Redox Partners. *ACS Catalysis* **8**, 9992-10003 (2018).
- 631 60. Atkinson, J.T. et al. Metalloprotein switches that display chemical-dependent electron transfer in cells. *Nat Chem Biol* **15**, 189-195 (2019).
- 63. Wei, F.Y. et al. Cdk5rap1-mediated 2-methylthio modification of mitochondrial tRNAs governs protein translation and contributes to myopathy in mice and humans. *Cell Metab* 21, 428-42 (2015).
- 636 62. Heigwer, F., Kerr, G. & Boutros, M. E-CRISP: fast CRISPR target site identification. *Nat Methods* **11**, 122-3 (2014).
- 638 63. Ran, F.A. et al. Genome engineering using the CRISPR-Cas9 system. *Nat Protoc* **8**, 2281-2308 (2013).
- 64. Sherman, F. Getting started with yeast. *Methods Enzymol.* **350**, 3-41 (2002).
- 65. Gietz, R.D. & Woods, R.A. Transformation of yeast by lithium acetate/single-stranded carrier DNA/polyethylene glycol method. *Methods Enzymol* **350**, 87-96 (2002).
- 66. Diekert, K., deKroon, A.I.P.M., Kispal, G. & Lill, R. Isolation and sub-fractionation of mitochondria from the yeast *Saccharomyces cerevisiae*. *Methods Cell Biol.* **65**, 37-51 (2001).
- 67. McCarthy, E.L. & Booker, S.J. Biochemical Approaches for Understanding Iron-Sulfur
   Cluster Regeneration in Escherichia coli Lipoyl Synthase During Catalysis. *Methods Enzymol* 606, 217-239 (2018).
- 68. Harlow, E. & Lane, D. *Using Antibodies: A Laboratory Manual*, (Cold Spring Harbor Laboratory, Cold Spring Harbor, NY, 1998).
- 69. Biederbick, A. et al. Role of human mitochondrial Nfs1 in cytosolic iron-sulfur protein biogenesis and iron regulation. *Mol. Cell. Biol.* **26**, 5675-5687 (2006).

- 70. Stehling, O. et al. Investigation of iron-sulfur protein maturation in eukaryotes. in *Methods in Molecular Biology*, Vol. 372 (eds. Leister, D. & Herrmann, J.M.) 325-342. (Humana Press Inc., Totowa, NJ, 2007).
- 71. Stehling, O., Sheftel, A.D. & Lill, R. Chapter 12 Controlled expression of iron-sulfur cluster assembly components for respiratory chain complexes in mammalian cells.
   Methods Enzymol 456, 209-31 (2009).
- 72. Sambrook, J. & Russell, D.W. *Molecular cloning: A laboratory manual*, (Cold Spring Harbor Press, Cold Spring Harbor, NY, 2001).
- 73. Gueldener, U., Heinisch, J., Koehler, G.J., Voss, D. & Hegemann, J.H. A second set of loxP marker cassettes for Cre-mediated multiple gene knockouts in budding yeast.
   *Nucleic Acids Res* 30, e23 (2002).
- 664 74. Mühlenhoff, U., Richhardt, N., Ristow, M., Kispal, G. & Lill, R. The yeast frataxin 665 homolog Yfh1p plays a specific role in the maturation of cellular Fe/S proteins. *Hum Mol* 666 *Genet* 11, 2025-36 (2002).
- 75. Molik, S., Lill, R. & Mühlenhoff, U. Methods for studying iron metabolism in yeast mitochondria. *Methods Cell. Biol.* **80**, 261-280 (2007).

#### **Materials and Methods**

#### Small interfering RNAs and guide RNAs

- Sets of three Silencer Select small interfering RNAs (siRNAs) directed against the mRNA of
- 674 FDX1 or FDX2<sup>6</sup> were purchased from ThermoFisher Scientific (Waltham, USA). FDX1- and
- 675 FDX2-directed guide RNA sequences for CRISPR-Cas9-mediated gene knockout (Suppl.
- Table 1) were designed using E-CRISP<sup>62</sup> and cloned into plasmid PX459 (Addgene,
- 677 Watertown, MA, USA) according to Ref. 63.

#### Tissue culture and cell transfection

- Human embryonic kidney (HEK) 293 cells were cultured in high glucose DMEM with standard
- supplements and transfected with siRNA by electroporation<sup>6</sup> as specified in Supplementary
- Materials and Methods. PX459-based plasmids allowing for simultaneous expression of gRNA,
- 683 Cas9, and the puromycin resistance marker were chemically transfected into HEK293 cells
- 684 using the JetPrime transfection reagent (Polyplus, Illkirch, France) according to the
- 685 manufacturer's instructions. In order to facilitate chemical transfection, cells were grown in
- collagenized flasks, and transfectants were selected by puromycin (10 µg/mL) for two to three
- days. The day of puromycin removal was considered as day zero of gene knockout, and cells
- were cultured as lines until use for up to 17 days.

669

670

671

672

678

#### Yeast strains, cell growth and plasmids

Yeast strains and plasmids used in this study are listed in Suppl. Table 4 and 5. Cells were cultivated either in minimal medium containing all recommended supplements (SC) or in rich medium (YP) plus the following carbon sources: 2% w/v glucose (SD/YPD), 2% w/v galactose (SGal/YPGal), 3% w/v glycerol (SGly/YPGly), 2% w/v lactate plus 0.05% w/v glucose (SLac/YPLac) or 2% w/v raffinose plus 0.2% w/v galactose (SRaff + Gal)<sup>64</sup>. Yeast cells were transformed using the lithium acetate method<sup>65</sup>.

#### Yeast complementation assays with human genes

For FDX1/2 interconversion experiments, Gal-YAH1 cells<sup>7</sup> were transformed with plasmids encoding yeast or human FDXs (p426-FDX1, p426-FDX2, p416-Yah1 and corresponding FDX1/2 mutant plasmids). Single colonies were grown on SGal plates and resuspended in water to OD<sub>600</sub> 0.5. Serial dilutions (1:5) were spotted onto plates containing different growth media and incubated at 30°C for three days. Enzyme activity measurements of isolated yeast mitochondria were performed as described previously<sup>66</sup>.

For *in vivo* lipoyl and heme *a* formation experiments, Gal-YAH1-lip5 $\Delta$  and Gal-YAH1-cox15 $\Delta$  cells were transformed with plasmids p416-FDX1, p415-FDX2, p414-LIAS and p414-COX15. Transformants were grown overnight in SD medium, centrifuged, and cell pellets diluted in water to OD<sub>600</sub> 0.1. Serial dilutions (1:5) were spotted onto plates containing different growth media and incubated at 30°C for three days.

#### Reconstitution of de novo Fe/S cluster synthesis on ISCU2

*In vitro* enzymatic reconstitution of [2Fe-2S] cluster formation on ISCU2 was performed as described<sup>9,10</sup>. Ferredoxin titration reactions were prepared in an anaerobic chamber and contained 0.5 mM NADPH, 0.8 mM sodium-ascorbate, 0.3 mM FeCl<sub>2</sub>, 0.2 mM MgCl<sub>2</sub>, 5 mM GSH, 75 μM ISCU2, 7.5 μM NIA, 7.5 μM FXN, 1 μM FDXR and FDX1 or FDX2 as indicated at a final volume of 300 μL in degassed reconstitution buffer (50 mM Tris/HCl pH 8.0, 150 mM NaCl). Reactions were transferred to a CD-spectrometer (Jasco J-815) in a tightly sealed cuvette containing a magnetic stirring bar, and the CD-signal at 431 nm was monitored at 20°C. After 30 s, Fe/S cluster synthesis was initiated by injecting 0.5 mM cysteine into the sealed cuvette and a time course recorded for 10 min. Time courses were normalized to the signal intensity before cysteine addition.

#### Chemical Fe/S cluster reconstitution on LIAS

Chemical reconstitution of LIAS was done under strictly anaerobic conditions. His-affinity chromatography purified LIAS was diluted to 0.1 mM in degassed LIAS buffer (50 mM HEPES pH 7.5, 300 mM KCl and 20% w/v glycerol) on ice. 10 mM DTT was added, and the mixture was incubated for 1 h. Subsequent addition of 0.8 mM ferric ammonium citrate (FAC) and 0.8 mM Li<sub>2</sub>S, both added slowly whilst mixing gently, led to a deep brown-yellowish color. Spectroscopic analysis at different time points after reconstitution revealed that the cluster content of LIAS reaches its maximum within 30 min. LIAS was re-purified after 30 min reconstitution by size exclusion chromatography using a HiLoad® 16/600 Superdex® 75 pg column. The holoprotein was characterized as described previously<sup>67</sup> by UV/Vis-spectroscopy (Jasco V-550), Bradford assay, amino acid analysis, SDS-PAGE, and iron and sulfide determination.

#### Lipoyl formation assay

Experiments were done under strictly anaerobic conditions  $^{40}$ . Degassed reaction buffer (50 mM HEPES pH 7.5, 300 mM KCl, 10% w/v glycerol) was supplied with 10 mM MgCl<sub>2</sub>, 2 mM NADPH and 0.5 mM octanoyl peptide (Glu-Ser-Val-[ $N^6$ -octanoyl]Lys-Ala-Ala-Ser-Asp). Optionally, up to 2 mM CuCl<sub>2</sub> and/or elesclomol (Ele) were added. Ele:Cu inhibition assays contained 2% v/v DMSO. Control reactions showed LIAS activity not being altered at concentrations of 0–4% v/v DMSO. 20  $\mu$ M FDXR, 140  $\mu$ M FDX and 1 mM S-adenosylmethionine (SAM) were added subsequently. The reaction was started by adding 35  $\mu$ M reconstituted LIAS to a final volume of 25  $\mu$ L and incubated at 23°C for 2.5 h, if not noted otherwise. Reactions were quenched by adding 100 mM H<sub>2</sub>SO<sub>4</sub>, 4 mM TCEP and 40  $\mu$ M of an internal peptide standard (Pro-Met-Ser-Ala-Pro-Ala-Arg-Ser-Met). The amounts of octanoyl-, 6-thiooctanoyl- and lipoyl-peptide were quantified by HPLC-MS as described previously  $^{67}$ .

#### Miscellaneous methods

Specific rabbit antisera against human FDX1 and FDX2 were raised using recombinant full-length proteins  $^{6,68}$ . For other primary antibodies see Suppl. Table 6. Peroxidase- (Biorad, Germany) or biotin- (Vector Laboratories, Burlingame, USA) conjugated goat anti-rabbit and anti-mouse antibodies as well as the ABC system (Vector Laboratories, Burlingame, USA) were used as secondary reagents. The following published methods were used: Digitonin-based fractionation of HEK293 cells, activity measurements for aconitase, succinate dehydrogenase, cytochrome c reductase; cytochrome c oxidase, citrate synthase, and lactate and malate dehydrogenase c manipulation of DNA and PCR72; gene disruptions and

promoter exchanges in yeast $^{73,74}$ ; preparation of yeast mitochondria and cell extracts $^{66}$ ; determination of enzyme activities in yeast extracts $^{75}$ ; immunological techniques $^{68}$ ; *in vitro* cytochrome c reduction by FDXs $^{18}$ . Measurements of replicates were performed using distinct samples. Statistical analyses were performed via ordinary one-way analyses of variance (ANOVA) with multiple comparisons using Prism software.

#### Figure legends

766767

768

769770

771

772773

774

775

776

777

778

779

780

781 782

783

784

Fig. 1 FDX1 is not involved in mitochondrial Fe/S protein assembly. a HEK293 cells were transfected without (control) or with scrambled (SCR) non-targeting siRNA, or with pools of FDX1- or FDX2-directed siRNAs (si) at a three-day interval<sup>6</sup>. Cells were harvested 9 days after the first transfection. Cell extracts were analyzed by immunostaining for the indicated mitochondrial proteins. Observed molecular masses (kDa) for proteins are given in parentheses. C-I, C-II, C-III, respiratory complexes I, II, and III; C-V, F<sub>1</sub>F<sub>0</sub> ATP synthase. **b** HEK293 cells were chemically transfected with the empty plasmid PX459 (control) or with plasmids containing three different FDX1-directed gRNAs (CC1 to CC3). Transfected cells were selected by puromycin for 3 days. Samples harvested 8 days after antibiotic removal were subjected to immunostaining of the indicated mitochondrial proteins. For quantitation see Extended data Fig. 1b. c Total aconitase (Aco) and succinate dehydrogenase (SDH) enzyme activities were determined in extracts from cells described in (b). Results were expressed as a ratio to citrate synthase (CS) activity, and presented relative to the respective values of control cells (set to 100%, dashed line;  $n \ge 6$ ). **d** Enzymatic reconstitution of [2Fe-2S] cluster formation on ISCU2 in the presence of indicated amounts of FDX1 or FDX2 was measured by CD spectroscopy. Initial rates were determined by linear fitting of the kinetic traces (Extended data Fig. 2; n = 3; one-way ANOVA for control without versus with FDX reactions, \*p < 0.05, \*\*\*p < 0.001). Error bars indicate the SEM. Representative blots are shown.

785 786 787

788

789 790

791

792

793794

795

796 797

798

799 800

801

802

Fig. 2 The role of human ferredoxins in heme a and CoQ<sub>10</sub> biosynthesis. a HEK293 cell extracts from Fig. 1b were subjected to immunostaining of indicated cytochrome c oxidase (complex IV, C-IV) subunits. VDAC1 served as loading control (see Fig. 1b). Observed molecular masses (kDa) for proteins are given in parentheses. Representative blots are shown. **b** COX activity (relative to CS activity) was analyzed in total membrane fractions derived from cells treated as in Fig. 1c ( $n \ge 3$ ; one-way ANOVA for control versus FDX1-CC1-3, \*\*\*p < 0.001). **c** Gal-YAH1-cox15 $\Delta$  yeast cells were transformed with plasmids encoding human COX15 and additionally FDX1, FDX2 or no FDX (-) as indicated. Subsequently, cells initially grown in liquid SC glucose medium were plated as a 1:5 dilution series, and grown for 3 days at 30°C on the indicated minimal media. d COX activities (relative to malate dehydrogenase, MDH) were determined in extracts from cells of part (c) grown for 3 days in liquid SD medium ( $n \ge 4$ ; one-way ANOVA for empty vector control versus FDX-complemented cells, \*\*\*p < 0.001). **e** HEK293 cells transfected as in Fig. 1b were harvested within the indicated time intervals after puromycin selection. Total cellular coenzyme Q<sub>10</sub> (CoQ10) content per total cellular protein was determined and presented relative to the value of control cells ( $n \ge 4$ ). f HEK293 cells were chemically transfected with the FDX1-directed gRNA-

encoding plasmid CC2 or with the PX459 control plasmid. Six to seven days after puromycin selection cells were repeatedly transfected by electroporation at a three-day interval with a pool of FDX2-directed siRNAs, and harvested up to 9 days after the first transfection similar to Fig. 1a. At each transfection round cell samples were removed for the analysis of total cellular  $CoQ_{10}$  content as in (e) ( $n \ge 3$ ).  $CoQ_{10}$  levels were normalized to amounts before starting RNAi depletion. Error bars show the SEM.

Fig. 3 FDX1 starts the radical chain reaction of lipoyl biosynthesis. a HEK293 cell samples from Fig. 1b were immunostained for the indicated proteins or the lipoyl cofactor. VDAC1 served as loading control (see Fig. 1b). Observed molecular masses (kDa) for proteins are given in parentheses. Representative blots are shown. **b**, **c** Formation of the (**b**) 6-thiooctanoyl and (c) lipoyl peptide from a peptide substrate analogue [Glu-Ser-Val-(N6-octanoyl)Lys-Ala-Ala-Ser-Asp] by LIAS. Samples contained 0.5 mM peptide substrate, 35 µM LIAS, 2 mM NADPH, 20 µM FDXR, 140 µM FDX1, and 1 mM SAM, unless indicated otherwise. Dithionite (DT) samples lacked FDX1, FDXR, and NADPH. Reactions were incubated at 23°C, quenched with acid after 2.5 h, and products quantified by HPLC-MS using peptide standards ( $n \ge 3$ ; oneway ANOVA for FDX1 reactions versus all other conditions). d Gal-YAH1-lip5∆ yeast cells harboring plasmids encoding human LIAS, FDX1 and/or FDX2 as indicated were grown in minimal medium with glucose (Glc) or galactose (Gal) as indicated for 3 days. Mitochondria were isolated and analyzed for the indicated proteins or lipoyl cofactor in PDH and KGDH by immunostaining. Porin (Por1) was used as loading control. e Mitochondrial extracts were analyzed for aconitase (Aco1) and KGDH activities, and results were normalized to MDH activity. Wild-type (WT) and  $lip5\Delta$  cells served as controls ( $n \ge 4$ ; one-way ANOVA, LIAScomplemented Gal-YAH1-lip5∆ cells versus all other Gal-YAH1-lip5∆ cells). \*p < 0.05, \*\*\*p < 0.001. Error bars indicate the SEM. n.d., not detectable.

**Fig. 4 Inhibitory effect of elesclomol-copper on lipoyl synthesis** *in vitro.* **a,b** Formation and quantitation of the 6-thiooctanoyl- (**a**) and lipoyl- (**b**) peptide was as in Fig. 3b,c in the presence of the indicated concentrations of  $CuCl_2$  and/or elesclomol (Ele) (n = 2; one-way ANOVA for control versus Ele/Cu titrations, \*\*p < 0.01, \*\*\*p < 0.001). n.d., not detectable. **c** Reduction of cytochrome c (80 μM) by 1 mM NADPH, 2 nM FDXR, and 0.1 μM FDX1 in samples containing  $CuCl_2$  and/or Ele as indicated. Cytochrome c reduction was monitored at 550 nm for 60 s. Error bars indicate the SEM ( $n \ge 3$ ; one-way ANOVA, \*\*\*p < 0.001). **d,e** CD spectra of FDX1 (**d**) and FDX2 (**e**) recorded after incubation with the indicated amounts of  $CuCl_2$  and/or Ele (see also Suppl. Fig. 3). **f** HEK293 cells were grown in the presence of the indicated amounts of Ele and/or Cu for 72 h before harvesting and immunostaining of the

indicated proteins or lipoyl cofactor. Observed molecular masses (kDa) for proteins are given in parentheses. Representative blots are shown.

840841842

843

844 845

846847

848

849

850

851

852 853

854

855

856

857

858

859

839

Fig. 5 Identification of structural elements crucial for functional specificity of FDX2. a Superposition of crystal structures of human FDX1 (gold, PDB code: 3P1M, residues 65–170) and FDX2 (green, PDB code: 2Y5C, residues 69-174). The PheGly insertion in FDX1 (FG loop) is shown in magenta, and the orientation of helix C is indicated by rods. The C terminus is not resolved in the FDX2 structure and corresponding FDX1 residues are not shown. b Electrostatic surface potential calculated by the **APBS** server (https://server.poissonboltzmann.org) mapped to human ferredoxin surfaces (orientation as in a; color bar covers the range from -10 kT/e to +10 kT/e). The Fe/S cluster binding sites are marked by yellow circles. Red, negative charges; blue, positive charges. c Structure of FDX1 (PDB code: 3P1M, residues 65–184) highlighting regions exchanged with the respective FDX2 sequences. The bottom table provides the residues introduced from FDX2 into FDX1 for functional interconversion. **d** Complementation of *Gal-YAH1* yeast with plasmids encoding FDX2, FDX1 variants depicted in c or no FDX (-). Cells were grown for 3 days on minimal medium (S) with glucose (Glc) or galactose (Gal) using a dilution series of resuspended cells initially grown on SGal plates. Dashed lines separate different agar plates. **e** Aconitase (Aco) and f catalase (Cat) activities were determined in extracts from Gal-YAH1 cells complemented with the indicated constructs. Cells were grown for 40 h in liquid SGIc medium prior to analysis. Error bars indicate the SEM (n = 3; one-way ANOVA for FDX1-complemented yeast versus all other conditions, \*p < 0.05, \*\*\*p < 0.001).

860 861

862

863

864

865

866

867

868

869

870

871

872

873 874

875

**Fig. 6 Conversion of FDX2 to generate FDX1 functionality. a** Structure of FDX2 (PDB code: 2Y5C, residues: 69–174) highlighting regions exchanged with the respective FDX1 sequences. The bottom table provides the residues introduced from FDX1 into FDX2 for functional interconversion. The site of the C-terminal truncation (ΔC12) is marked by an arrow because the C terminus is not resolved in the crystal structure. **b, c** Cortisol formation by different FDXs (**b**) or the indicated FDX2 variants (**c**) for 10 min at 37°C. Reactions contained 11-deoxycortisol, human CYP11B1, and the electron transfer chain NADPH, FDXR, and ferredoxin. Cortisol content was quantified by HPLC and normalized to FDX1 reactions. (Yah1, Etp1(fd), FDX2 R135E mutants: n = 2, Adx: n = 3, all other reactions: n = 4). **d, e** Synthesis of 6-thiooctanoyl (**d**) and lipoyl (**e**) by LIAS in the presence of different FDXs or indicated FDX2 variants. Formation and quantitation was as in Fig. 3b,c. Values were normalized to FDX1 reactions (n = 3). Error bars indicate the SEM. One-way ANOVA for FDX2 reactions versus all other conditions was conducted in **b, c, d, e** (\*\*p < 0.01, \*\*\*p < 0.001). **f** Model showing the distinct functions of human FDX1 and FDX2 in mitochondrial metabolism. FDX2 performs a

specific function in both *de novo* [2Fe-2S] cluster assembly by the core ISC complex and the IBA57-ISCA1-ISCA2-dependent reductive fusion of two glutaredoxin GLRX5-derived [2Fe-2S] to [4Fe-4S] clusters<sup>18,22</sup>. FDX1 cannot replace FDX2 in these functions, yet is shown here to perform two crucial functions in addition to the long-known mitochondrial cytochrome P450 (CYP)-dependent steroid transformation<sup>5</sup>. First, FDX1 serves as an electron donor to initiate the radical SAM-dependent biosynthesis of the lipoyl cofactor by the [4Fe-4S] protein lipoyl synthase (LIAS). Lipoyl is a cofactor in, e.g., pyruvate and 2-ketoglutarate dehydrogenase (PDH, KGDH) complexes. The LIAS reaction is a sensitive target of the toxic elesclomol-copper (Ele:Cu) anti-cancer drug. Second, FDX1 is involved in cytochrome oxidase (COX) heme *a* formation by the COX15 enzyme, yet FDX2 can partially replace this FDX1 function. Heme *a* is exclusively present in cytochrome *c* oxidase. Different from yeast mitochondria, a non-FDX oxidoreductase (oxred) is required for the biosynthesis of coenzyme Q (CoQ) by the ubiquinone (UBI) complex.

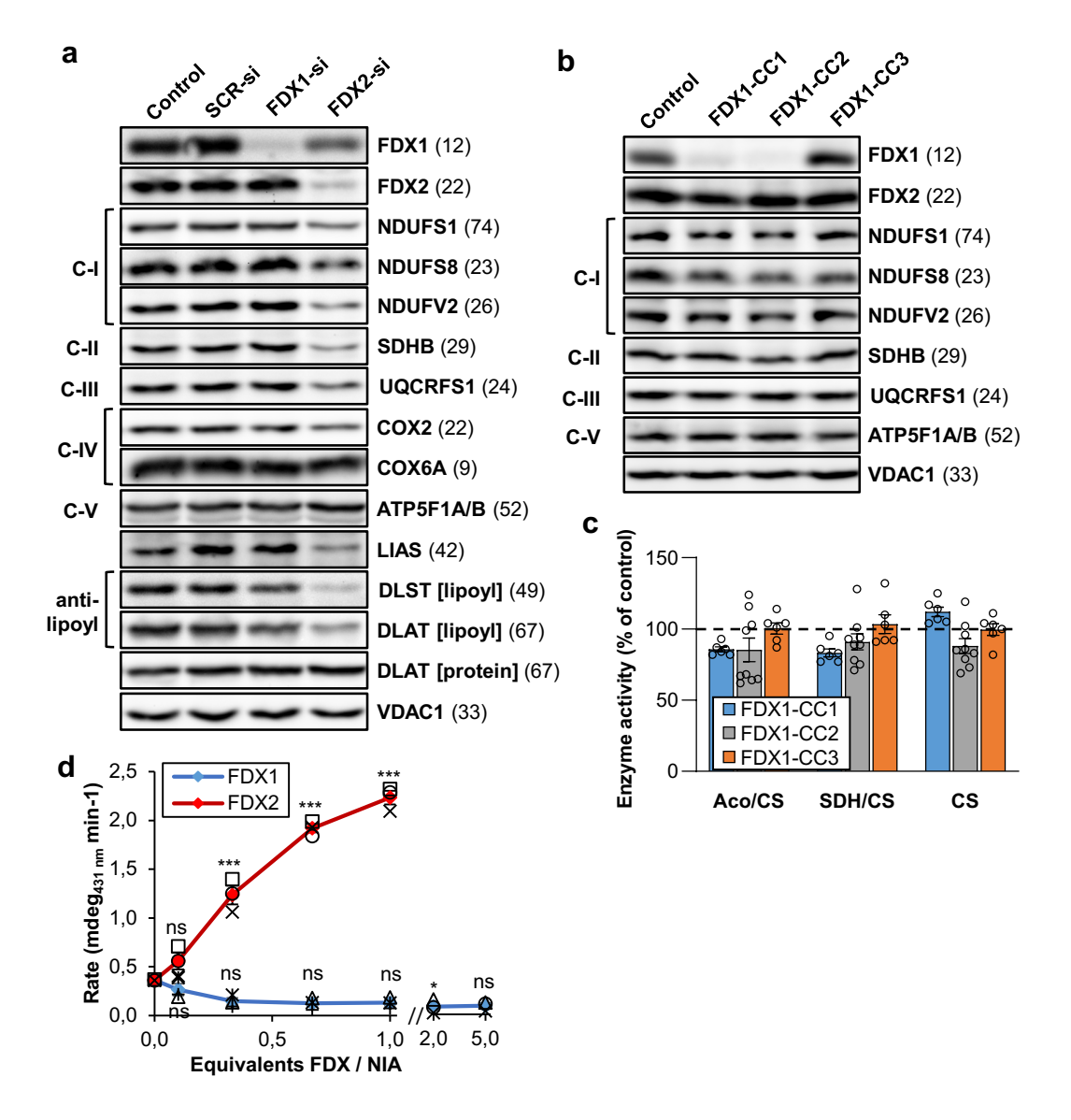
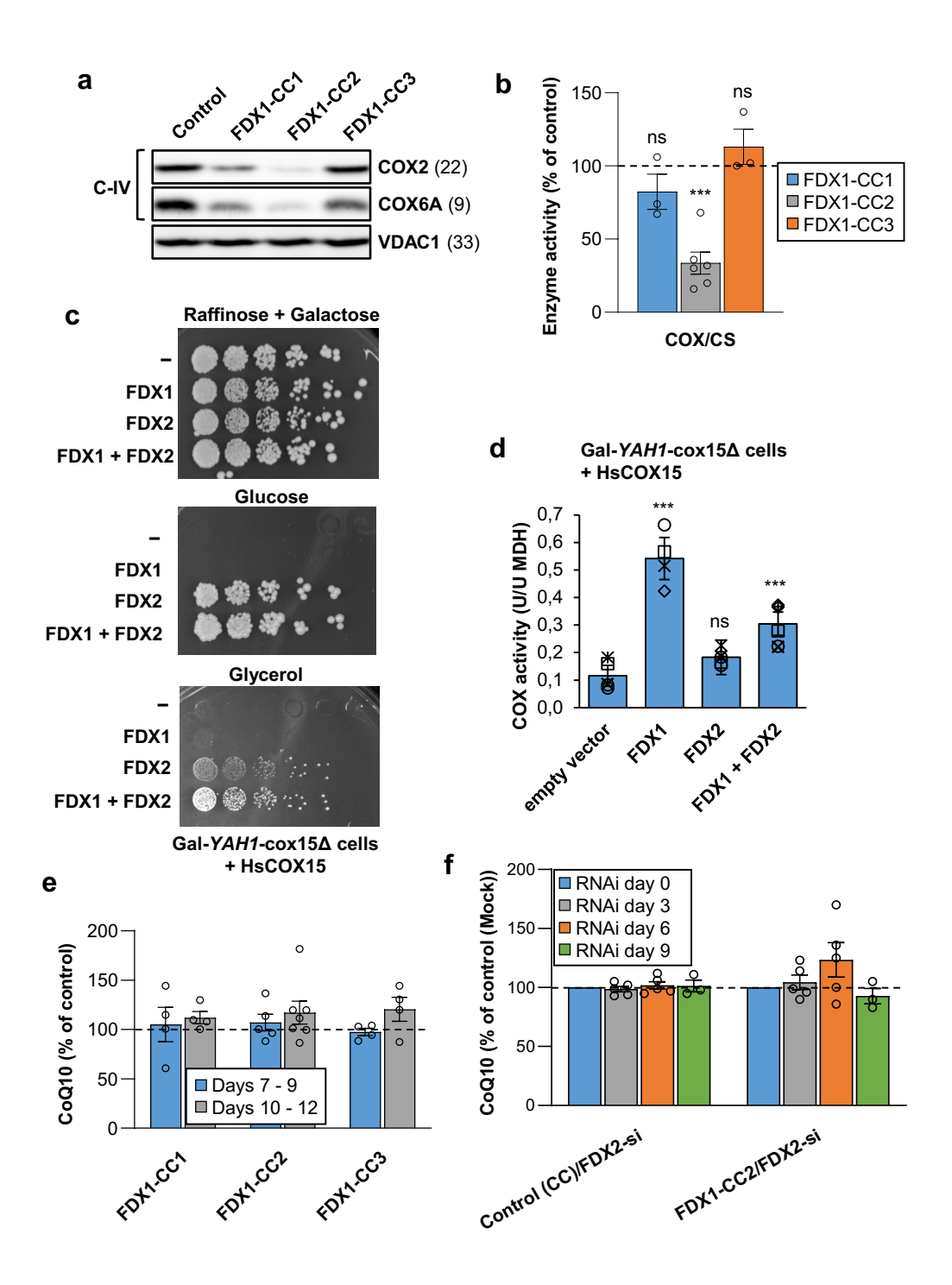
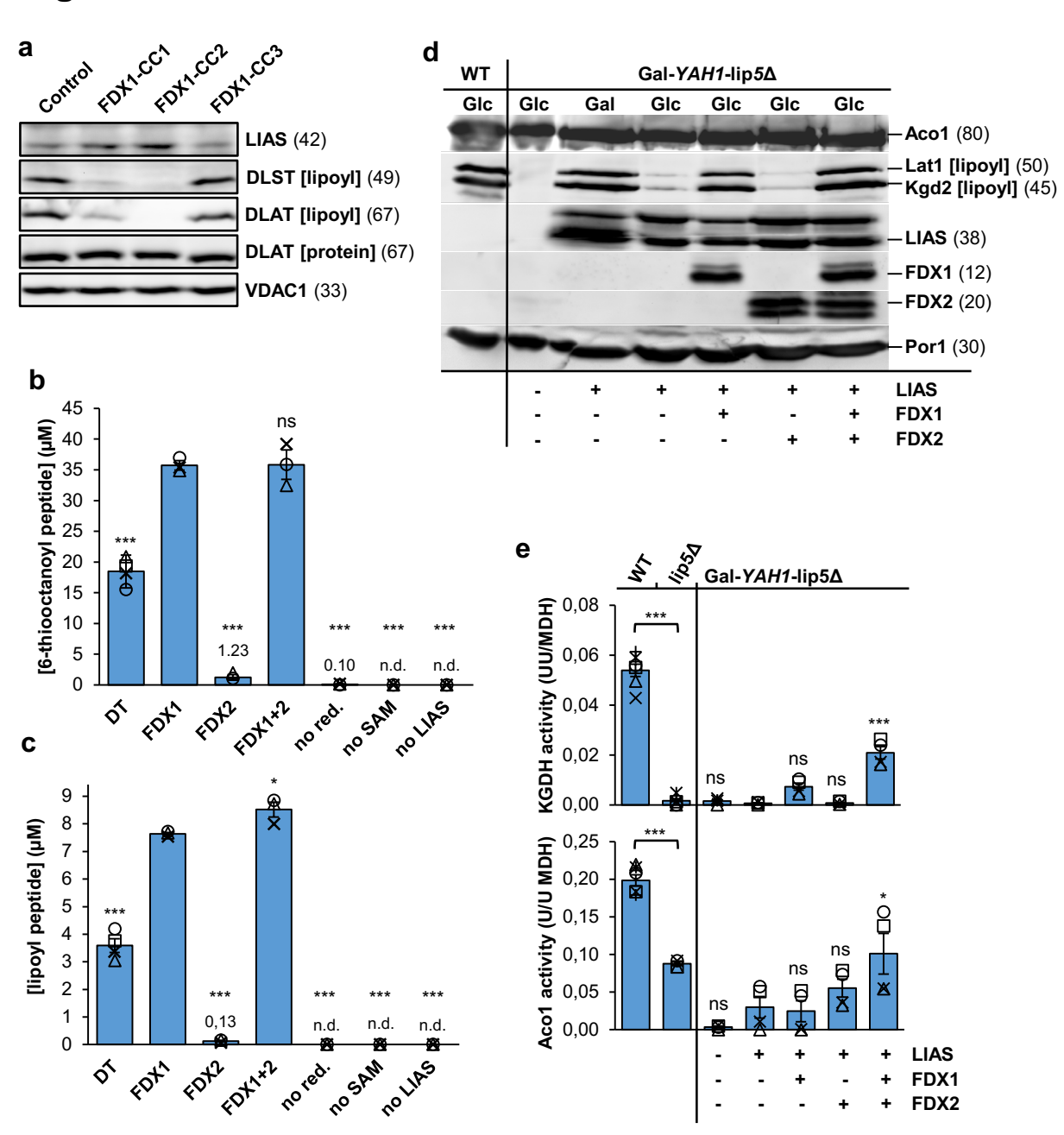
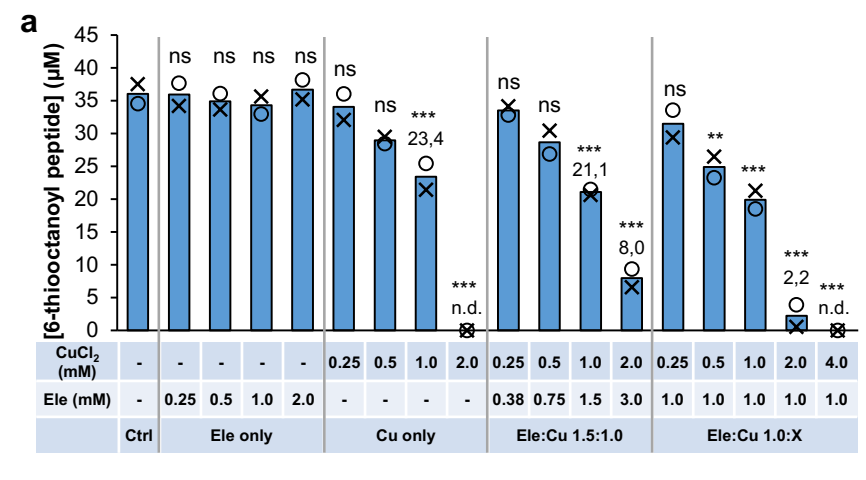
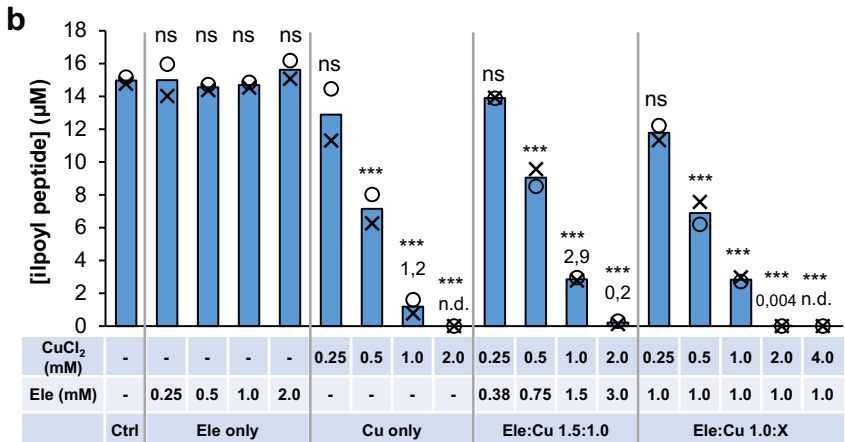


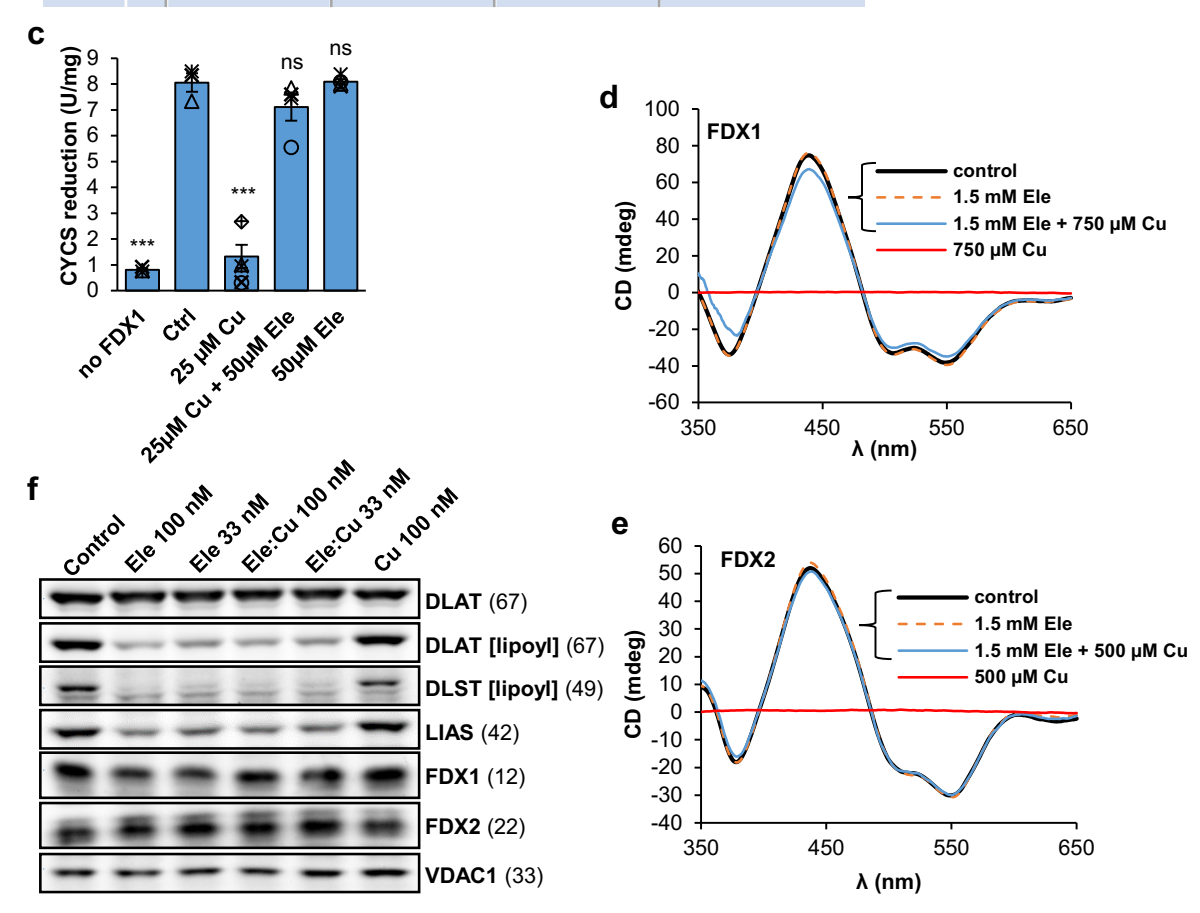
Figure 2











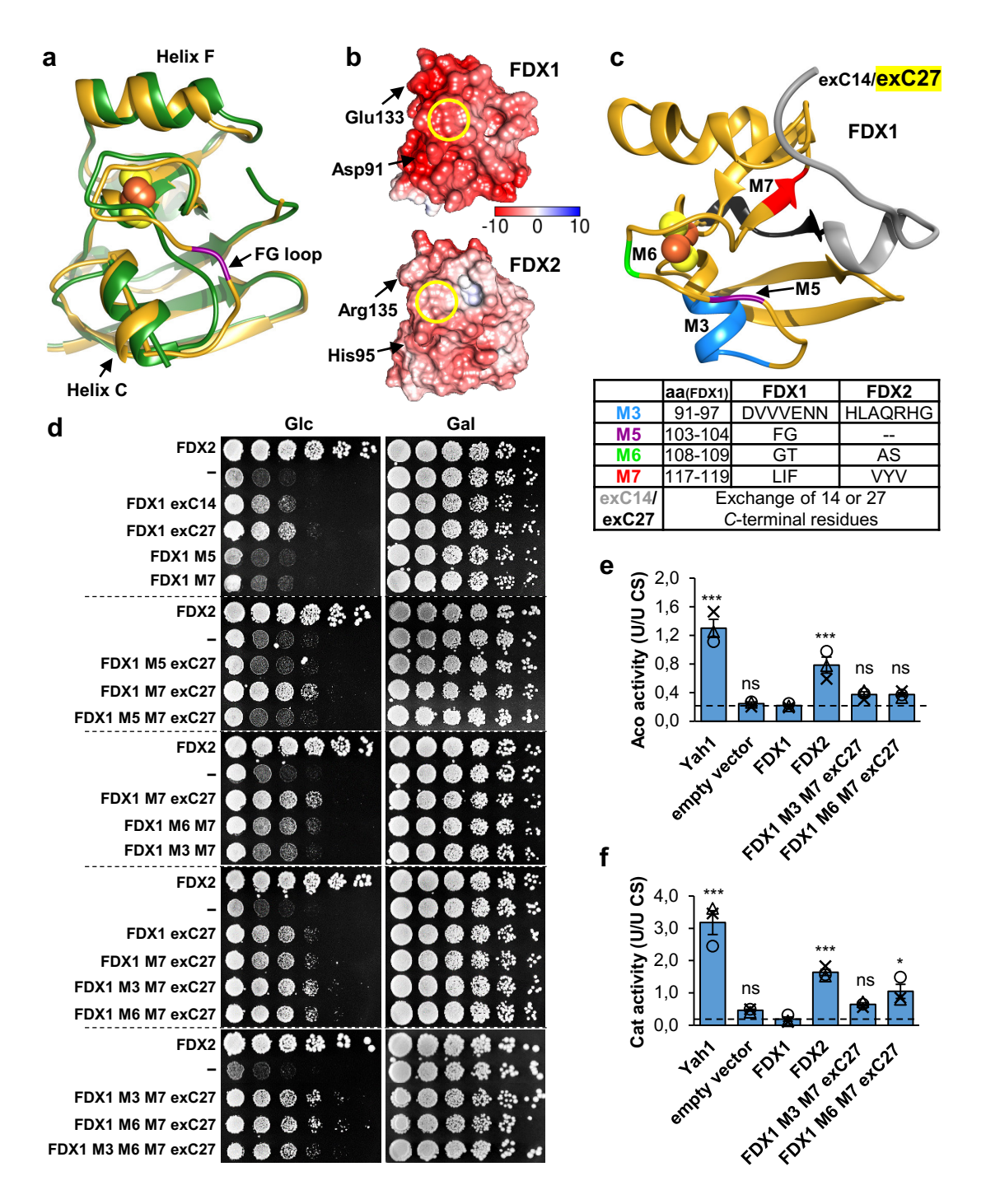
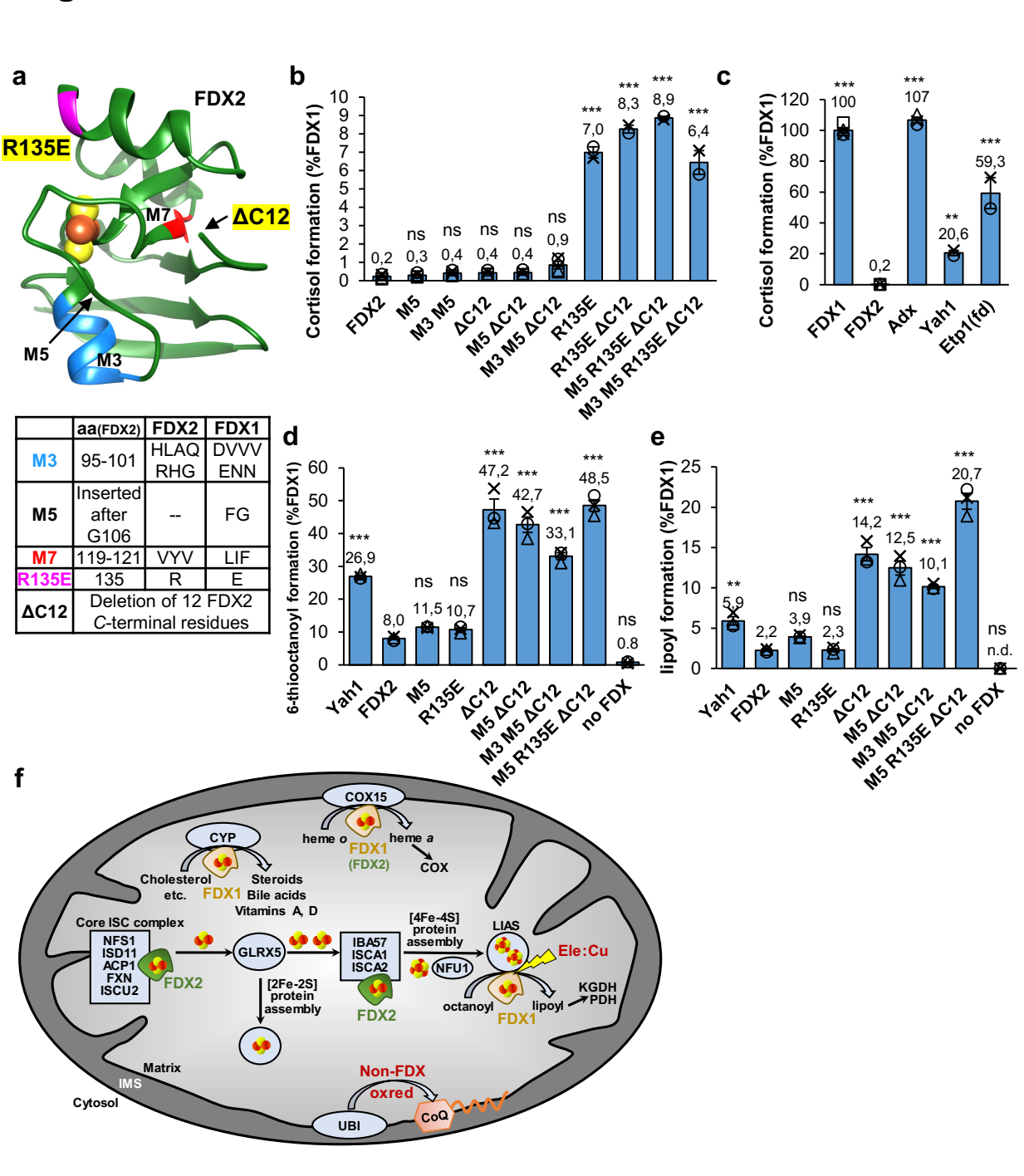


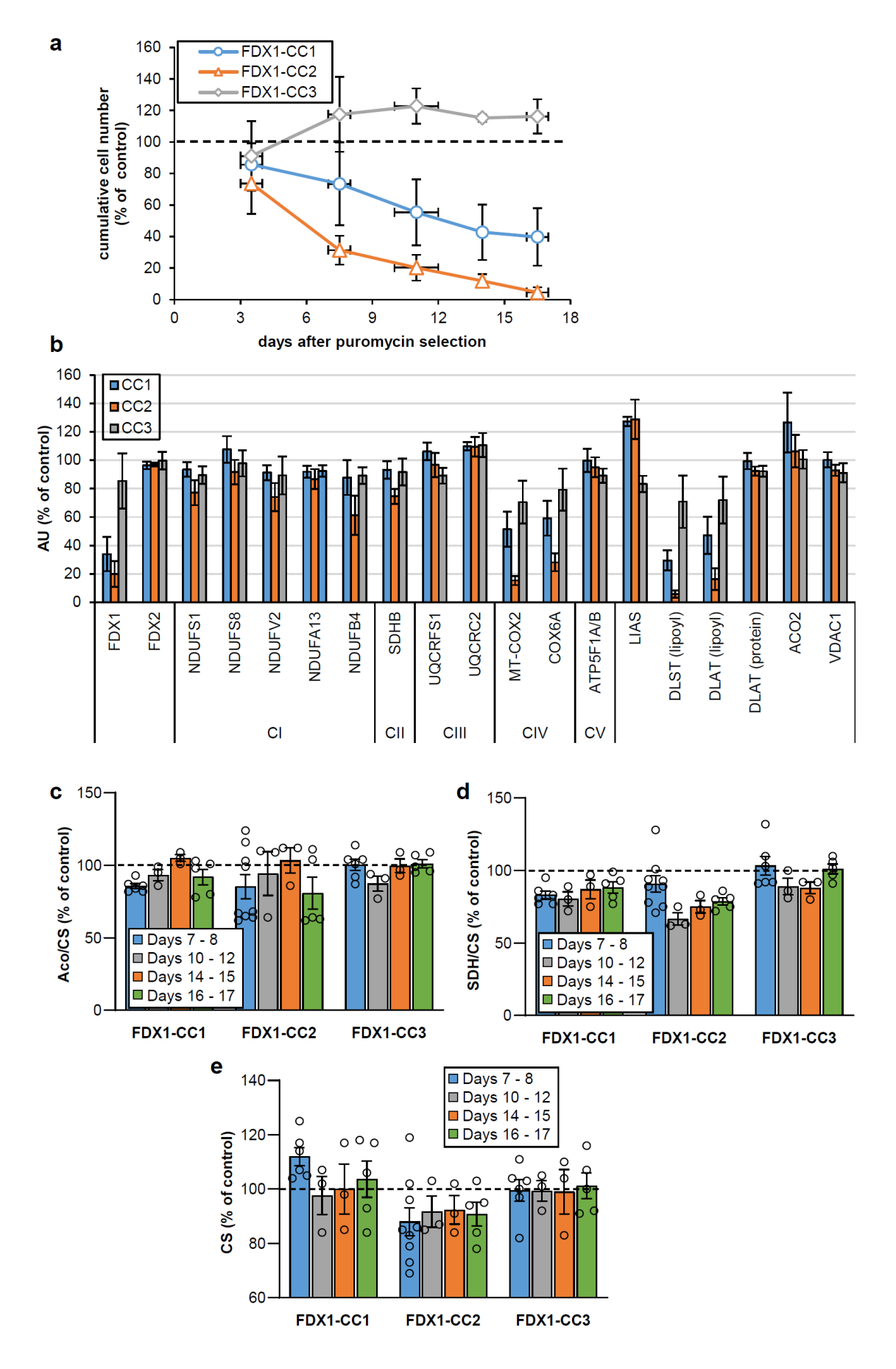
Figure 6



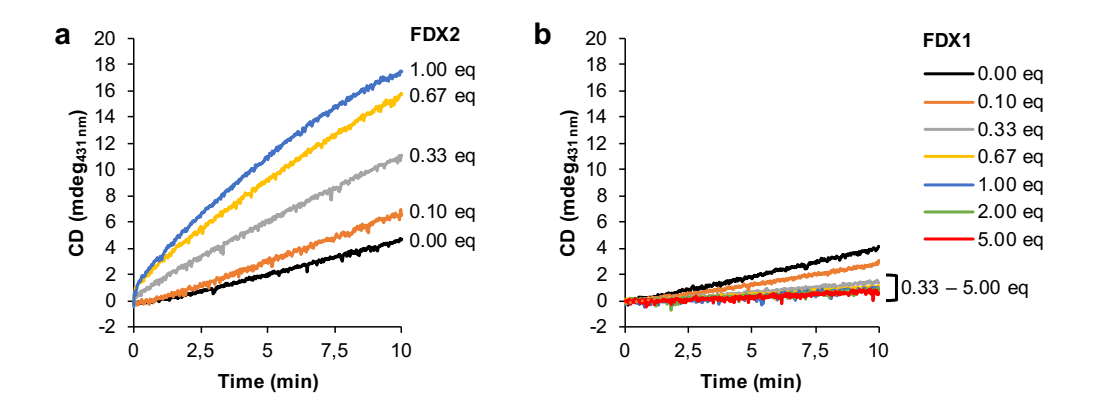
#### **Extended data for**

## Functional spectrum and structural specificity of mitochondrial ferredoxins FDX1 and FDX2

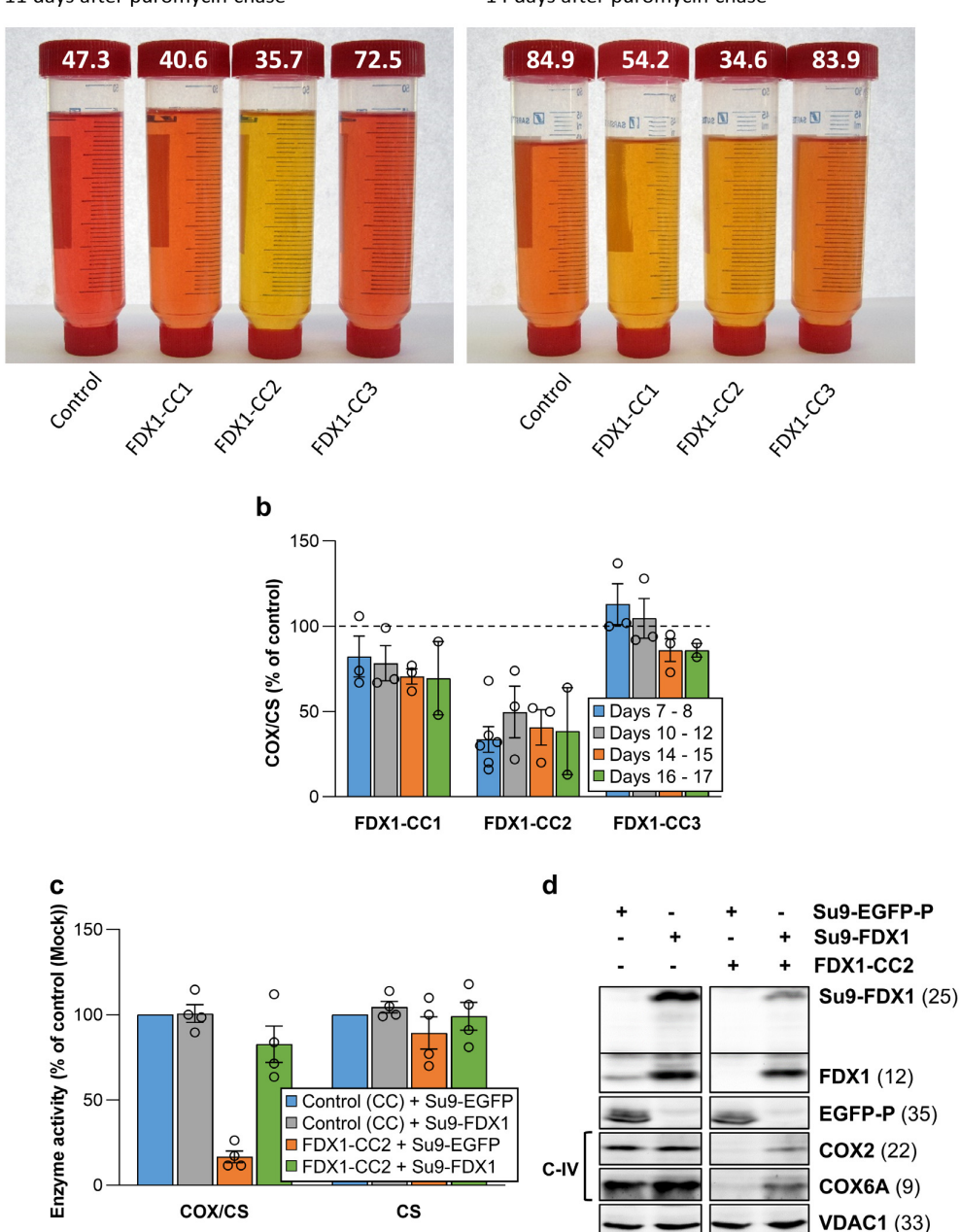
Vinzent Schulz, Somsuvro Basu, Sven-A. Freibert, Holger Webert, Linda Boß,
Ulrich Mühlenhoff, Fabien Pierrel, Lars-O. Essen, Douglas M. Warui, Squire Booker,
Oliver Stehling, and Roland Lill



Extended data Figure 1 | Growth phenotypes and mitochondrial Fe/S protein status of FDX1 knockout cells. a HEK293 cell lines were subjected to CRISPR-Cas9 FDX1 gene knockout using CC1-CC3 guide RNAs. Cumulative growth of cells treated as in Fig. 1b was calculated from cell counts at various harvesting time points after puromycin removal. In detail, individual cell lines were sub-cultured by harvesting an entire culture vessel and subsequent re-seeding of a defined cell number into a new culture device. Remaining cells were collected, and the total protein content of this sample was determined. This protein amount was then used as a denominator for the calculation of the specific (i.e. total protein-related) enzymes activities measured in the respective sample. This tissue culture regime involving the re-seeding of aliquots of harvested cells produced sufficient cell material to conduct multiple analyses, even in case of an experimentally elicited growth retardation. Based on the cell counting performed at each harvest, the cumulative growth was calculated for each cell line from the total cell yield as well as the portion of cells needed for re-seeding during subculturing. Values are presented relative to those of control cells (set to 100%, dashed line;  $n \ge 4$ ; mean ± SEM). **b** Densitometric quantification of immunostains from cells treated as in Fig. 1b. 2a. and 3a (i.e. harvested 7 or 8 days after puromycin removal) using Image studio lite 5.2. Error bars indicate SEM ( $n \ge 4$ ). **c-e** Total aconitase (Aco), succinate dehydrogenase (SDH) and citrate synthase (CS) activities were determined in cell samples obtained at the indicated time points after puromycin removal as in Fig. 1c. Values were presented relative to those of control cells (set to 100%, dashed line;  $n \ge 3$ ; mean  $\pm$  SEM).



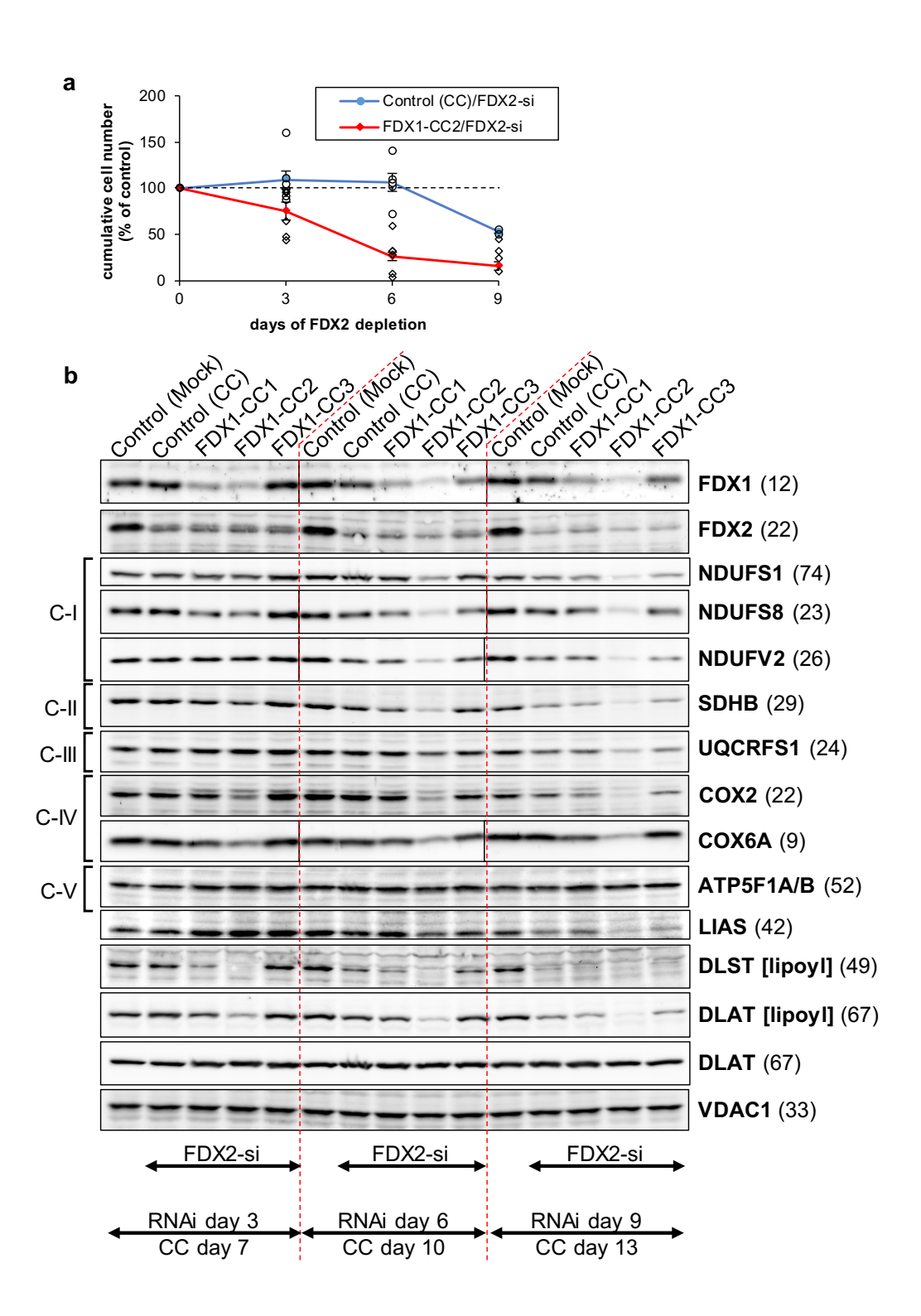
**Extended data Figure 2 | Even high excess of FDX1 does not support enzymatic [2Fe-2S] cluster reconstitution on ISCU2.** Enzymatic synthesis of [2Fe-2S] clusters on ISCU2 *in vitro* was monitored by the CD signal at 431 nm for 10 min. Reactions included NIA, FXN, FDXR and the indicated equivalent amounts (eq.) of (a) FDX2 or (b) FDX1 relative to NIA. Representative experiments are shown and initial rates are presented in Fig. 1d.



#### Extended data Figure 3 | FDX1 knockout cells are deficient in cytochrome oxidase activity. a

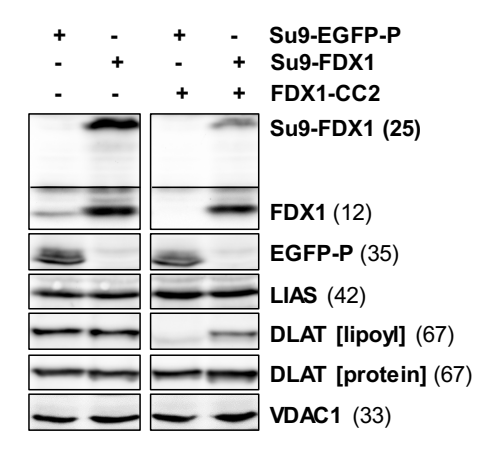
Tissue culture media of HEK293 control and *FDX1* knockout cells (cf. Figs. 2a and Extended data Fig. 1a) were collected at the indicated time points. Cells were harvested, counted, and processed as required. The color change of the pH indicator phenol red in the culture medium from reddish toward yellowish, particularly for *FDX1*-CC1 and -CC2 knockout cells, revealed a pH drop despite lower cell numbers in these cultures (given at the top; in millions). **b** Cytochrome *c* oxidase (COX) activities were determined in total membrane fractions from cells harvested at the indicated time points after puromycin removal (cf. Fig. 2b). COX activities were expressed relative to citrate

synthase (CS) activities (Extended data Fig. 1e), and values are presented relative to those of control cells (set to 100%, dashed line;  $n \ge 3$ ; mean  $\pm$  SEM). **c** HEK293 cells (see Fig. 2f) were chemically transfected with control plasmid PX459 or the PX459-derived plasmid FDX1-CC2 and selected by puromycin for 3 days as in Fig. 2a. 10 to 15 days after selection cells were transiently transfected by electroporation with plasmids coding for either a PEST-destabilized EGFP or FDX1, each fused to the N-terminal mitochondrial Su9 targeting sequence (from *Neurospora crassa* subunit 9 of mitochondrial F<sub>1</sub>F<sub>0</sub> ATP synthase). Three days after transfection cells were harvested and analyzed for COX and CS activities. Data are presented relative to the values for Su9-EGFP control cells (n = 4; SEM). **d** Cell samples from (**c**) were subjected to immunostaining against the indicated proteins. Observed molecular masses (kDa) for proteins are given in parentheses. Representative blots are shown.

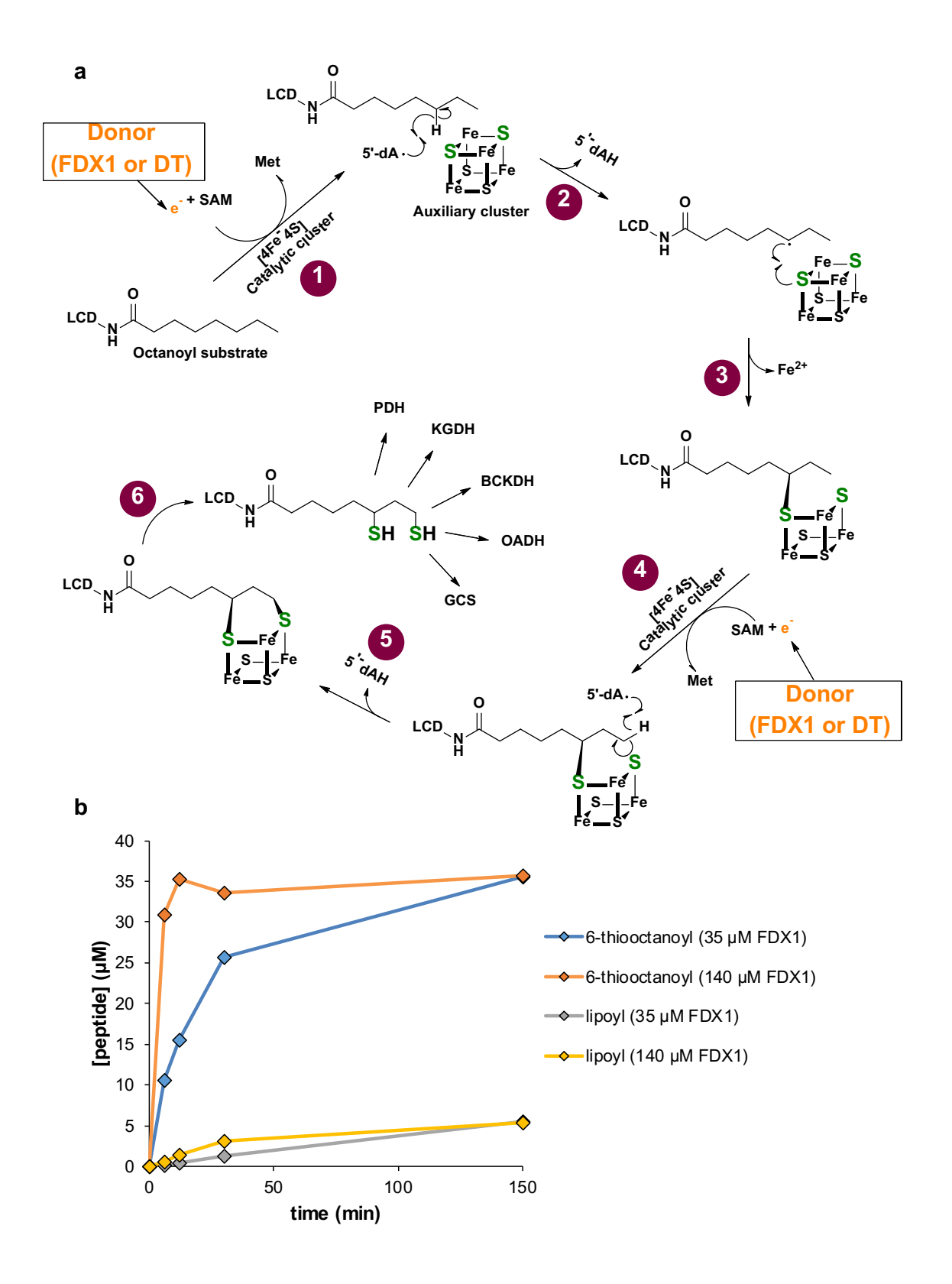


Extended data Figure 4 | Combined *FDX1* deletion and FDX2 depletion elicits severe defects in growth and mitochondrial Fe/S proteins. a Cumulative growth of HEK293 cells from Fig. 2f was calculated from cell counts at the three harvests on days 3, 6 ( $n \ge 4$  each), and 9 (n = 2) after the first electroporation. Values were presented relative to those of mock control cells (no CRISPR, no RNAi treatment; set to 100%, dashed line; mean  $\pm$  SEM). b HEK293 cells were transfected with *FDX1*-directed gRNA-encoding plasmids (CC1 to CC3) and subsequently with *FDX2*-directed

siRNAs similar to Fig. 2f. Cell samples were obtained at the specified time points and subjected to immunostaining of the indicated mitochondrial proteins or lipoyl cofactor. The observed molecular weights are given in parentheses. C-I, C-III, C-III, respiratory complexes I, II, and III. C-V, F<sub>1</sub>F<sub>0</sub> ATP synthase. The immunoblot signals from cell samples with combined FDX1-CC2 and FDX2-si deficiency are representative for at least three independent experiments, and are here presented conjointly with FDX1-CC1 / FDX2-si and FDX1-CC1 / FDX2-si treated cells, respectively.

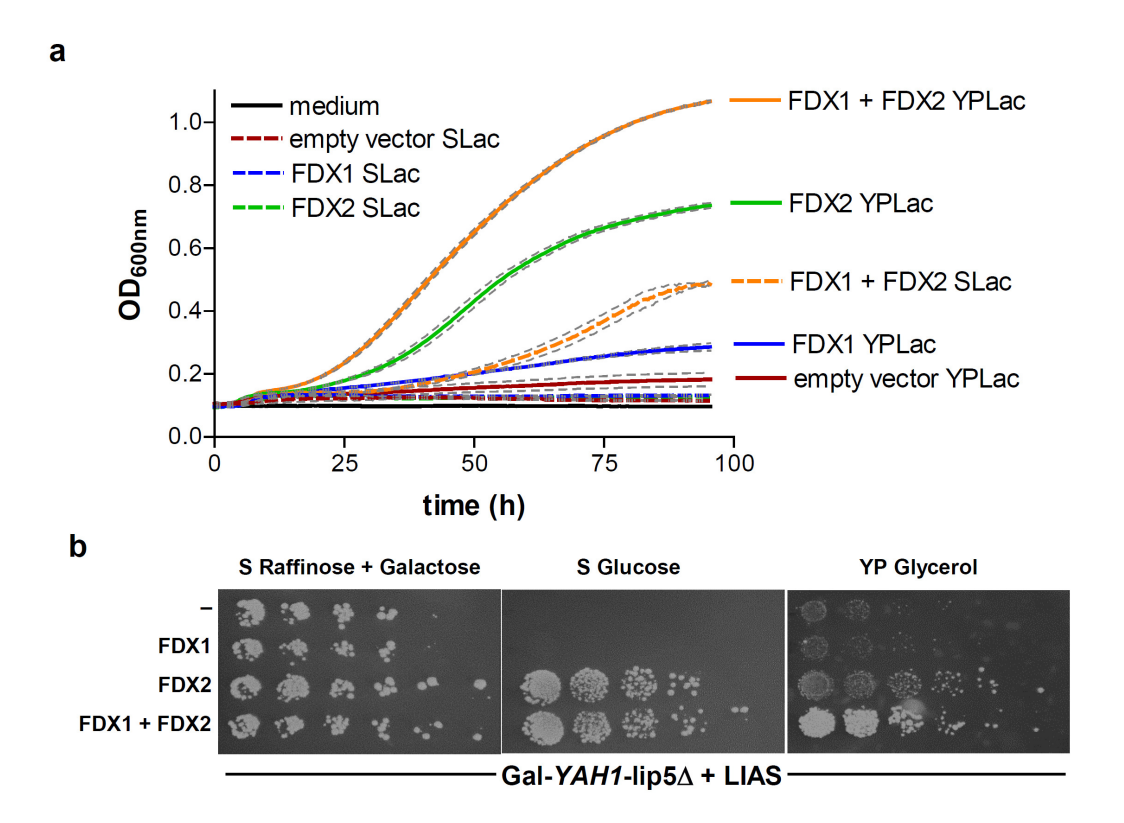


**Extended data Figure 5 | The lipoylation defect in** *FDX1* **knockout cells can be complemented by FDX1**. HEK293 cells from Extended data Fig. 3c,d knocked out for *FDX1* (by FDX1-CC2 gRNA) and complemented with Su9-EGFP-PEST or Su9-FDX1 plasmids were subjected to immunostaining against the indicated proteins or lipoyl cofactor. Observed molecular masses (kDa) for proteins are given in parentheses. Representative blots are shown.

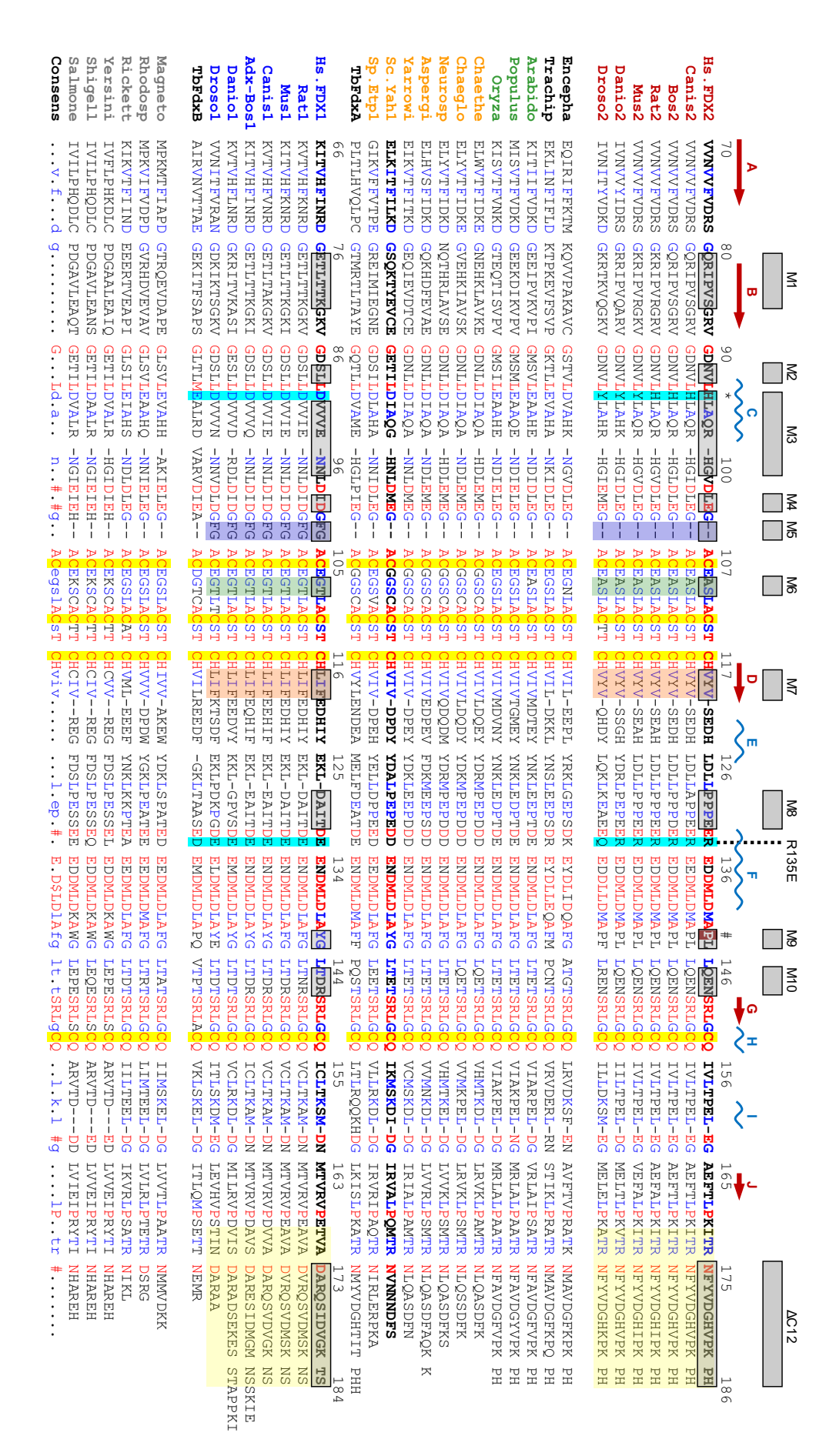


Extended data Figure 6 | *In vitro* synthesis of 6-thiooctanoyl intermediate and lipoyl product by human lipoyl synthase LIAS requires ferredoxin FDX1 as an electron donor. a Model of the multi-step reaction mechanism of lipoyl formation by human lipoyl synthase (LIAS) based on bacterial LipA<sup>1</sup>. The LIAS enzyme contains two [4Fe-4S] clusters, the catalytic and auxiliary cluster,

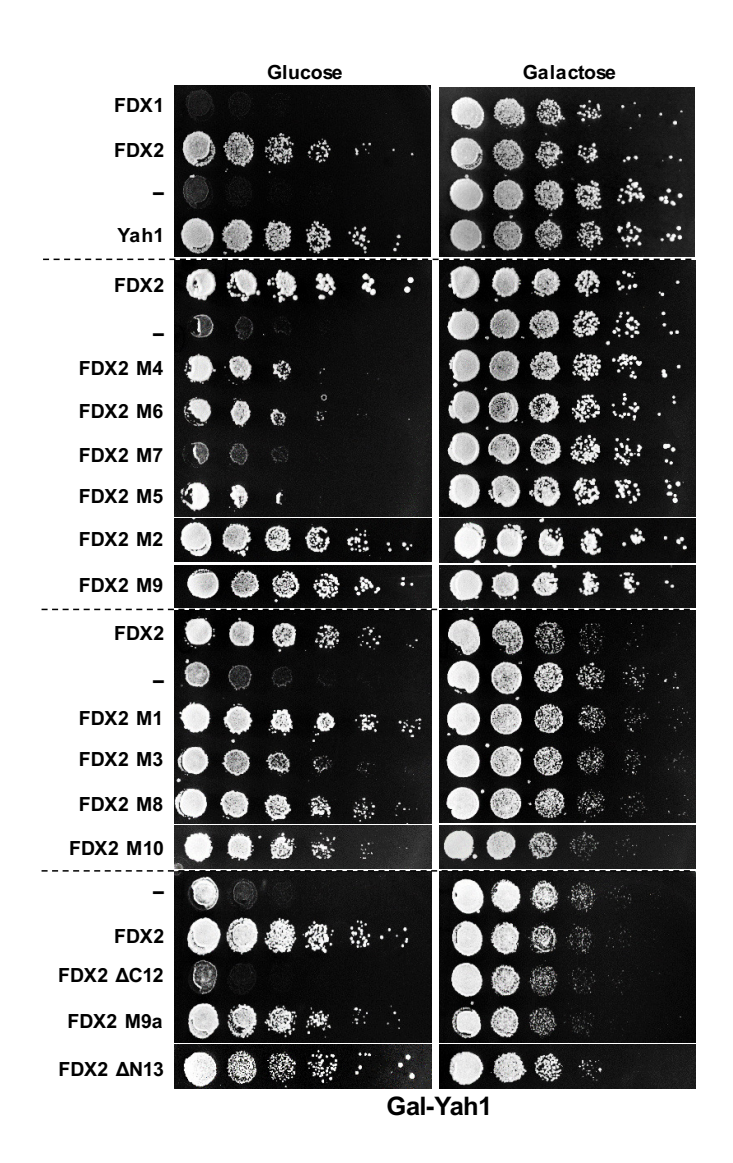
needed for reductive cleavage of S-adenosylmethionine (SAM) and as a source for sulfur insertion into the octanoyl precursor, respectively. (1) The reaction starts with the binding of SAM and the octanovl substrate which is covalently attached to a lysinyl residue of a lipoyl carrier domain (LCD) of the H protein of the glycine cleavage system (GCS)<sup>1,2</sup>. An electron donor (orange) transfers a single electron to the catalytic cluster which mediates reductive cleavage of SAM to methionine and a 5'-deoxyadenosyl radical (5'-dA'). This work identified human FDX1 as the physiological electron donor, efficiently replacing dithionite that typically is used as an artificial electron donor<sup>1</sup>. (2) The radical abstracts a hydrogen atom from the octanoyl C6 carbon, forming 5'-deoxyadenosine (5'dAH). (3) The octanoyl C6 carbon in turn forms a covalent bond with a sulfur atom of the auxiliary cluster, concomitant with partial degradation of the cluster. (4) A second SAM molecule binds to LIAS, and upon electron supply from FDX1 (or DT) again leads to 5'-dA' radical formation by the catalytic cluster and abstraction of a proton from the terminal C8 carbon of the octanoyl moiety. (5) A second sulfur atom is covalently attached to the thiooctanoyl molecule, (6) leading to formation of the mature lipoyl cofactor and further degradation of the Fe/S cluster. To enable multiple reaction cycles, the auxiliary cluster must be regenerated by a still unclear mechanism. In humans, the mature lipoyl cofactor is finally transferred to the target proteins, e.g., the E2 subunits of pyruvate (PDH) and α-ketoglutarate (KGDH) dehydrogenase complexes. BCKDH, branched-chain ketoacid dehydrogenase; OADH, 2-oxoadipate dehydrogenase<sup>3</sup>. **b** Time courses of 6-thiooctanoyl intermediate and lipoyl product formation in FDX1-catalyzed reactions (see Fig. 3b,c). Samples included 0.5 mM peptide substrate, 35 µM LIAS, 2 mM NADPH, 20 µM FDXR, FDX1 as indicated and 1 mM SAM. Formation of the 6-thiooctanoyl intermediate proceeded significantly faster than lipoyl formation, indicating the second sulfur insertion step to be rate-limiting under the experimental conditions. The result suggested to record the data of other experiments after 150 min incubation.



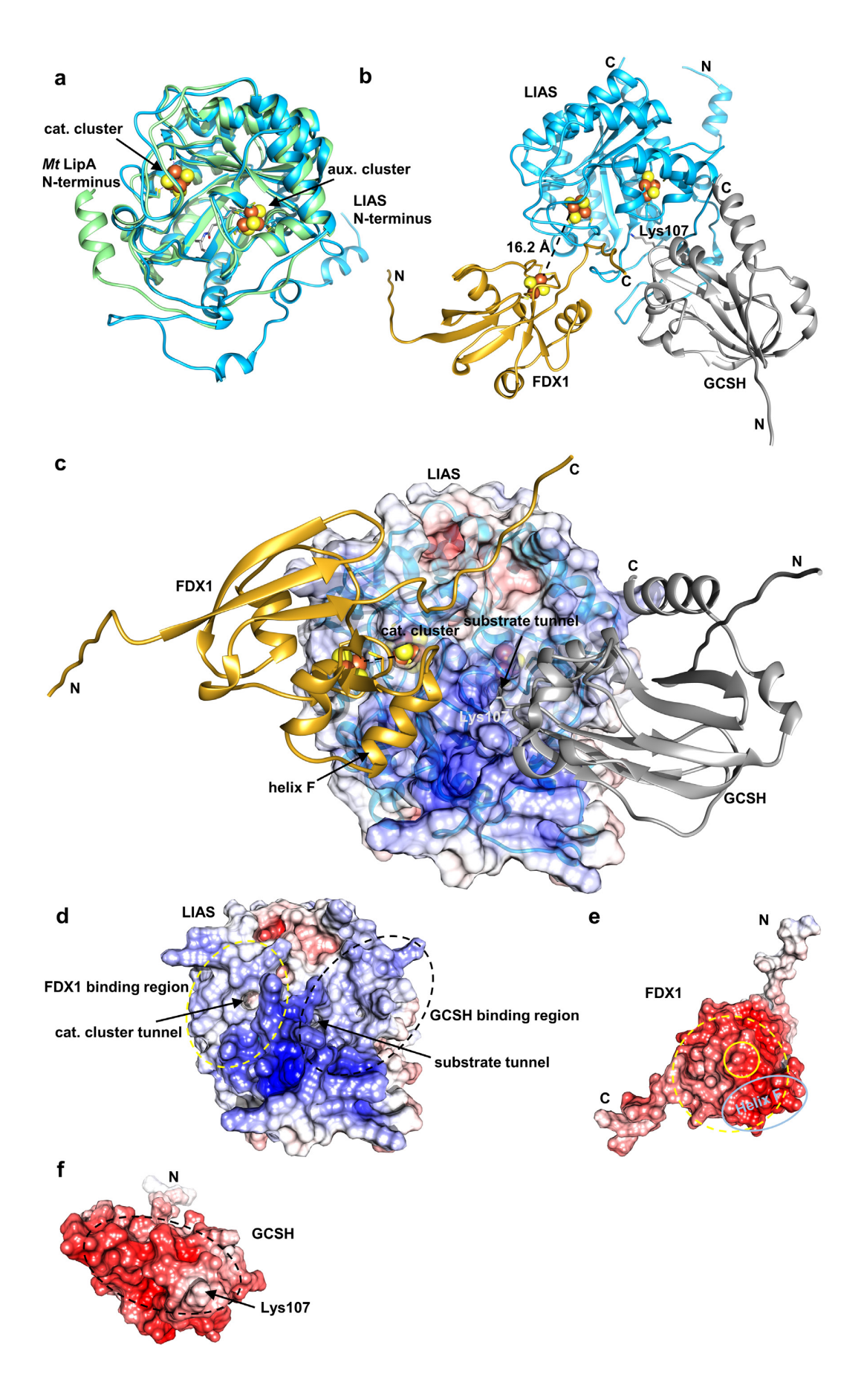
Extended data Figure 7 | Differential growth complementation of human LIAS-containing Gal-YAH1-lip5Δ cells by human FDX1 and FDX2 reflects their distinct functions. Gal-YAH1-lip5Δ yeast cells were transformed with a plasmid encoding human LIAS plus vectors containing no gene (-), FDX1 and/or FDX2 as indicated. a Cells were grown in liquid media for 4 days. Optical density (OD) at 600 nm was measured every 30 min. Growth in minimal lactate medium (SLac) is indicated by dashed lines, in rich yeast peptone lactate (YPLac) medium by solid lines. Grey dashed lines indicate standard errors (n = 4) using a microplate reader. **b** Serial dilutions of the indicated yeast strains were spotted onto agar plates containing minimal (S) or yeast peptone rich (YP) medium plus the indicated carbon sources. Plates were incubated at 30°C for 3 days. The growth results fit to distinct functions of human FDX1 and FDX2 in lipoylation/heme a synthesis and Fe/S protein biogenesis, respectively. Complementation of the LIAS-expressing Gal-YAH1-lip5Δ cells with FDX2 but not FDX1 supported growth due to Fe/S protein biogenesis restoration. The residual growth on non-fermentable carbon sources (lactate or glycerol) was due to the leaky GAL promoter allowing residual amounts of Yah1, and hence lipoate/heme a, being produced. Growth under these conditions was increased to normal levels by the combined expression of both human FDXs because FDX1 regenerated synthesis of both lipoate and heme a, and FDX2 supported Fe/S protein biogenesis.



Extended data Figure 8 | Multi-sequence alignment of mitochondrial ferredoxins. The multisequence alignment was generated by Multalin<sup>4</sup>. Secondary structure elements of the human FDX2 structure are shown above the alignment according to PROMOTIF<sup>5</sup>. Numbering is according to the full-length sequences of human (Hs) FDX1 and FDX2 retrieved from Uniprot (https://www.uniprot.org). The Fe/S cluster-coordinating cysteine residues are highlighted in yellow. Altered residues/regions of human FDX1 and FDX2 are highlighted in grey (see also Suppl. Table S3), Residues/regions mutated for interconversion of FDX1 and FDX2 functions (mutants M3, M5, M6, M7, R135E and C-terminal deletion/exchange) are additionally highlighted by colored boxes for animal FDX1/2-type sequences. Names of organisms are colored according to FDX-type: animal FDX2 (red), mitosomal (black), plant (green), fungal (orange), animal FDX1 (blue) and bacterial (grey). Two Trypanosoma brucei (Tb) FDXs best align between fungal and FDX1-type (FdxA) proteins or between FDX1-type and bacterial (FdxB) proteins<sup>6</sup>. FDXs from the following organisms were used (sequence identifiers in brackets): Homo sapiens (NP 001026904.2, NP 004100.1), Canis Iupus familiaris (XP 038284595.1, XP 038367022.1), Bos taurus (NP 001073695.1, Rattus norvegicus (NP\_001101472.1, NP 851354.1), NP 058822.2), Mus (NP 001034913.1, NP 032022.1), Danio rerio (NP 001070132.1, XP 001922722.2), Drosophila melanogaster (NP 001189075.1, NP 647889.2), Encephalitozoon cuniculi GB-M1 (NP 585988.1), Trachipleistophora hominis OX=72359 GN=THOM\_0371 PE=4 SV=1 (L7K0F4\_TRAHO), Arabidopsis thaliana (NP 001329852.1), Populus alba (XP\_034922198.1), Oryza sativa Japonica (XP 015647182.1). Chaetomium thermophilum var. thermophilum DSM (XP 006692961.1), Chaetomium globosum CBS 148.51 (XP 001225251.1), Neurospora crassa OR74A (XP 958085.1), Aspergillus fumigatus Af293 (XP\_747954.1), Yarrowia lipolytica CLIB122 (XP 500417.1), Saccharomyces cerevisiae S288C (NP 015071.1), Schizosaccharomyces pombe Etp1<sup>fd</sup> (2WLB A), Trypanosoma brucei brucei (XP 845713.1 and XP 844647.1), Magnetospirillum magnetotacticum (WP 009867486.1), Rhodospirillum rubrum (WP 200292119.1), Rickettsia (WP 004595967.1), pestis (WP 015683702.1), prowazekii Yersinia Shigella flexneri (EHF1065008.1), Salmonella enterica (WP 001124473.1).



**Extended data Figure 9 | Site-directed mutagenesis identifies FDX2 regions that functionally distinguish from FDX1.** Gal-YAH1 yeast cells were transformed with vectors expressing the indicated FDXs and variants (see Supplementary Table 5). Growth of serial cell dilutions on minimal medium (S) agar plates containing glucose or galactose was at 30°C for 3 days. FDX1-FDX2-discriminating regions critical for the *in vivo* function of human FDX2 were identified using FDX2 variants in which amino acids where exchanged to those of FDX1. A loss of cell growth identified the respective altered region as being important for FDX2 function. The broken lines separate independent plates.



Extended data Figure 10 | Alphafold2 predicts a functionally meaningful structure for the trimeric LIAS-GCSH-FDX1 complex. Structures of human LIAS, GCSH, and FDX1, and of complexes were predicted with Google Colab and the top-scoring prediction is displayed (https://colab.research.google.com/github/sokrypton/ColabFold/blob/main/beta/AlphaFold2 advance ed.ipynb). a Overlay of the predicted LIAS structure (blue, residues: 29-372) with Mycobacterium tuberculosis LipA (PDB code: 5EXK, green). The Mt LipA catalytic (cat.) and auxiliary (aux.) cluster are displayed as spheres and its bound 6-thiooctanoyllysyl (thiooct) moiety as grey sticks. b-c Modeling of the LIAS-GCSH-FDX1 complex (residues: LIAS, 29-372; GCSH, 41-173; FDX1, 54-184) predicted a functionally meaningful complex, where GCSH inserts its lipoyl-carrying residue Lys107 into the octanoyl substrate entry tunnel of LIAS. The position of the [2Fe-2S] cluster of FDX1 is consistent with electron transfer to the catalytic [4Fe-4S] cluster of LIAS. Fe/S cluster-coordinating residues and GCSH Lys107 are shown as sticks. Positions of Fe/S clusters are modelled based on crystal structures of FDX1 (PDB code: 3P1M) and Mt LipA (PDB code: 5EXK). LIAS, blue; GCSH, grey; FDX1, gold. In (c) the electrostatic surface potential is mapped onto the half transparent surface of LIAS. When we instead modeled a trimeric LIAS-GCSH-FDX2 complex, binding of FDX2 was predicted at the substrate tunnel of LIAS. This would block substrate-product delivery by GCSH. GCSH interacted with FDX2, but hardly with LIAS in this case. Overall, no physiologically relevant complex could be modeled in presence of FDX2. d-f Electrostatic surfaces mapped onto LIAS (d), FDX1 (e) and GCSH (f). LIAS-FDX1 and LIAS-GCSH interacting regions are encircled by yellow and black dashed lines, respectively. The location of the FDX1 [2Fe-2S] cluster and helix F are encircled by yellow and light blue solid lines, respectively. Surface potentials were calculated using the APBS server (https://server.poissonboltzmann.org). Negative charges are colored in red, positive charges in blue. The color bar covers the range from -10 kT/e to +10 kT/e. N and C termini are indicated.

#### **Extended data References**

- 1. McCarthy, E.L. & Booker, S.J. Destruction and reformation of an iron-sulfur cluster during catalysis by lipoyl synthase. *Science* **358**, 373-377 (2017).
- 2. Landgraf, B.J., McCarthy, E.L. & Booker, S.J. Radical S-Adenosylmethionine Enzymes in Human Health and Disease. *Annu Rev Biochem* **85**, 485-514 (2016).
- 3. Solmonson, A. & DeBerardinis, R.J. Lipoic acid metabolism and mitochondrial redox regulation. *J Biol Chem* **293**, 7522-7530 (2018).
- 4. Corpet, F. Multiple sequence alignment with hierarchical clustering. *Nucleic Acids Res.* **16**, 10881-10890. (1988).
- 5. Hutchinson, E.G. & Thornton, J.M. PROMOTIF--a program to identify and analyze structural motifs in proteins. *Protein Sci* **5**, 212-20 (1996).
- 6. Changmai, P. et al. Both human ferredoxins equally efficiently rescue ferredoxin deficiency in Trypanosoma brucei. *Mol Microbiol* **89**, 135-51 (2013).

# **Supplementary information for**

# Functional spectrum and structural specificity of mitochondrial ferredoxins FDX1 and FDX2

Vinzent Schulz, Somsuvro Basu, Sven-A. Freibert, Holger Webert, Linda Boß, Ulrich Mühlenhoff, Fabien Pierrel, Lars-O. Essen, Douglas M. Warui, Squire Booker, Oliver Stehling, and Roland Lill

#### Content:

Supplementary Results
Supplementary Discussion
Supplementary Figures 1-7
Supplementary Materials and Methods
Supplementary Tables 1-6
Supplementary References

#### **Supplementary Results**

#### Crystal structure of FDX1 and 3D structural features discriminating it from FDX2

The 3D structure of mature FDX2 (residues 66-171; PDB ID: 2Y5C) was solved a priori by single-wavelength anomalous diffraction (SAD) phasing using the anomalous scattering of the [2Fe-2S] iron ions (Suppl. Table 2). Consistent with other [2Fe-2S] FDXs, only a C-terminally truncated protein formed crystals diffracting to 1.7 Å. FDX2 displays a compact ( $\alpha+\beta$ ) fold typical for vertebrate-type mitochondrial FDXs (Fig. 5a). Significant structural differences between the known FDX1 structure (PDB ID: 3P1M) and that of FDX2 were observed only for the FDX2 loop between helix C and the Fe/S cluster binding site, with the Phe-Gly (FG) dipeptide of FDX1 missing in FDX2 (Fig. 5a; Extended data Fig. 8; Suppl. Fig. 4). The lack of FG leads to a distortion of helix C by 15° compared to FDX1, resulting in a more compact structure and different surface shape around the helix-loop region. These subtle differences alone were unlikely to provide a satisfactory explanation for the striking specificity of the two human FDXs. We therefore compared the surface potentials<sup>1</sup> of both FDXs and found that FDX2 possesses a less negatively charged area around the Fe/S cluster binding site, including helix F, which is known to participate in partner protein recognition<sup>2-4</sup> (Fig. 5b; Suppl. Fig. 5). Most conspicuously, exchanges of Asp91FDX1 by His95FDX2 in helix C and Glu133FDX1 by Arg135<sup>FDX2</sup> in helix F are the major contributions to the altered surface potential at the redoxactive site of these human FDXs. However, since these positively charged residues of FDX2 are not fully conserved in organisms with two FDXs, there may be other specificitydiscriminating structural factors (Extended data Fig. 8). In conclusion, the 3D structures of FDX1 and FDX2 display only minor differences in backbone geometry and partner interaction surfaces, with a different surface potential as a discriminating feature.

#### Structural prediction of the trimeric LIAS-GCSH-FDX1 complex

The structure of LIAS in a catalytic heterotrimeric complex with the physiological octanoyl-substrate carrier GCSH (H protein of glycine cleavage system<sup>5</sup>) and the electron donor FDX1 was modelled using Google Colab, a software based on AlphaFold<sup>6,7</sup>. Predicted folds of GCSH and FDX1 are almost identical to published crystal structures of bovine GCSH (PDB code: 3KLR) and human FDX1 (PDB code: 3P1M), excluding the disordered N- and C-terminal regions. Apart from the N terminus, the predicted fold of LIAS and positioning of its Fe/S cluster-coordinating residues are similar to published crystal structures of *Mycobacterium tuberculosis* (*Mt*) and *Thermosynechococcus elongatus* (*Te*) LipA (PDB codes: 5EXJ, 5EXK, 5U0O, 5U0P)<sup>8,9</sup>. Similarity is highest to a crystallographic snapshot of lipoyl synthesis showing *Mt* LipA with a 6-thiooctanoyl intermediate bound at the auxiliary cluster site (Extended data Fig. 10a).

Intriguingly, the predicted trimeric LIAS-GCSH-FDX1 complex exhibits GCSH and FDX1 suitably positioned to fulfil their respective functions (Extended data Fig. 10b). The side chain of Lys104<sup>GCSH</sup> functioning as octanoyl-carrier is inserted into the substrate binding tunnel of LIAS, resembling the positioning of the 6-thiooctanoyllysyl intermediate as observed in *Mt* LipA; the respective Lys ε-amino moieties of both structures are displaced by 1.9 Å<sup>8</sup>. FDX1 binds LIAS via its cluster-coordinating loop and helix F, as reported previously for complexes of FDX1 with FDXR, CYP11A1 and CYP11B2<sup>2,3,10</sup>. The Fe/S cluster is located above a LIAS tunnel potentially involved in electron transfer to the catalytic Fe/S cluster of LIAS (Extended data Fig. 10c). The predicted distance between the Fe ions of the FDX1 and LIAS clusters of 16.2 Å might allow for direct electron transfer<sup>11</sup>. Notably, both *Mt* and *Te* LipA crystal structures exhibit a similar tunnel (see PDB codes: 5EXK and 5U0P), yet other structures of the same two proteins show the tunnel entrance being blocked by rearrangement of residues of the catalytic cluster-coordinating loop (PDB codes: 5EXJ and 5U0O). It is currently unknown whether the opening or closing of the tunnel might represent a means of regulating the electron flow.

In the predicted trimeric LIAS-GCSH-FDX1 complex, LIAS-binding regions of both GCSH and FDX1 are strongly negatively charged (red) and contact positively charged regions (blue) of LIAS, suggesting that electrostatic interactions may be crucial for binding (Extended data Fig. 10d-f). The region between both aforementioned LIAS tunnels exhibits the most positive surface potential of the protein.

Removal of the FDX2 C terminus was shown in this work to enable lipoylation to some extent (14.2% of FDX1 reactions, Fig. 6e). As this may suggest the FDX2 C terminus to interfere with LIAS interaction, it is interesting to note that the FDX1 C terminus makes slight contact to LIAS in the predicted structure. Modelling the trimeric complex with FDX2 WT or the FDX2ΔC12 variant instead of FDX1 did not yield any physiologically relevant quaternary structure, in line with FDX1 being the dedicated redox partner of LIAS. In summary, the predicted structure of the trimeric LIAS-GCSH-FDX1 complex is compatible with the experimental data presented in this work and may support future investigation of the biosynthetic mechanism of lipoyl formation.

#### **Supplementary Discussion**

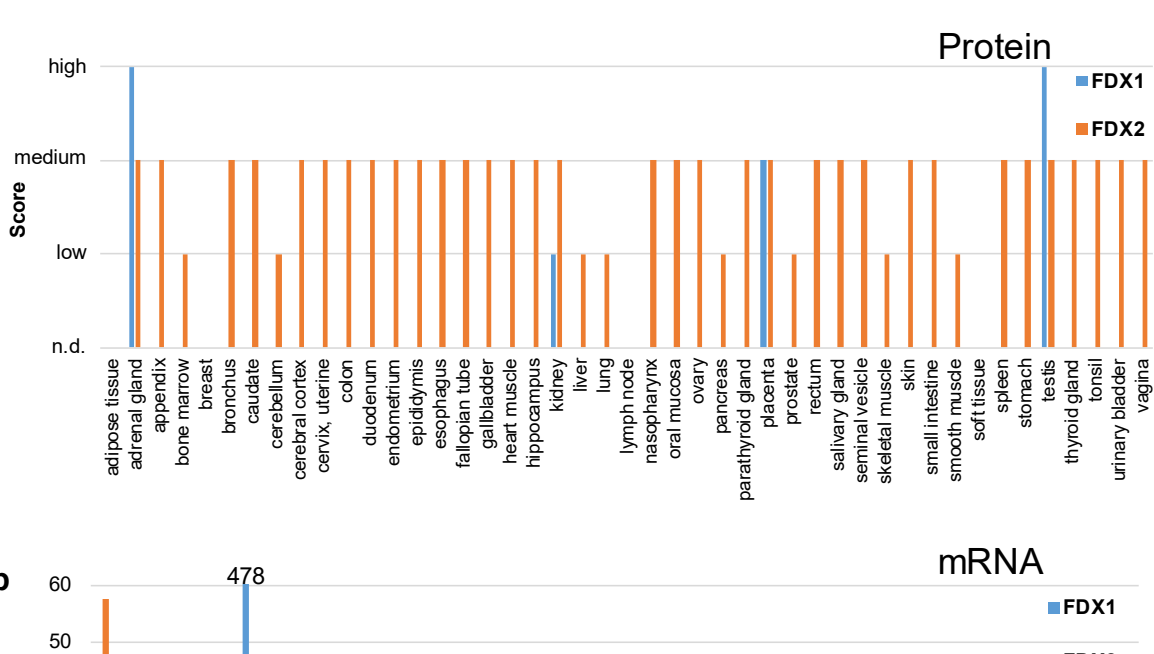
The results from both the RNAi-based *FDX1* knockdown and the humanized yeast system also resolve the old conundrum of conflicting *FDX1* expression levels in mammalian cells. Transcriptomics data suggest that *FDX1* is expressed in virtually all cell types, yet the FDX1 protein was detectable by immunostaining solely in tissues associated with high steroid production such as adrenal gland, testis, and placenta (Suppl. Fig. 1)<sup>12</sup>. The importance of

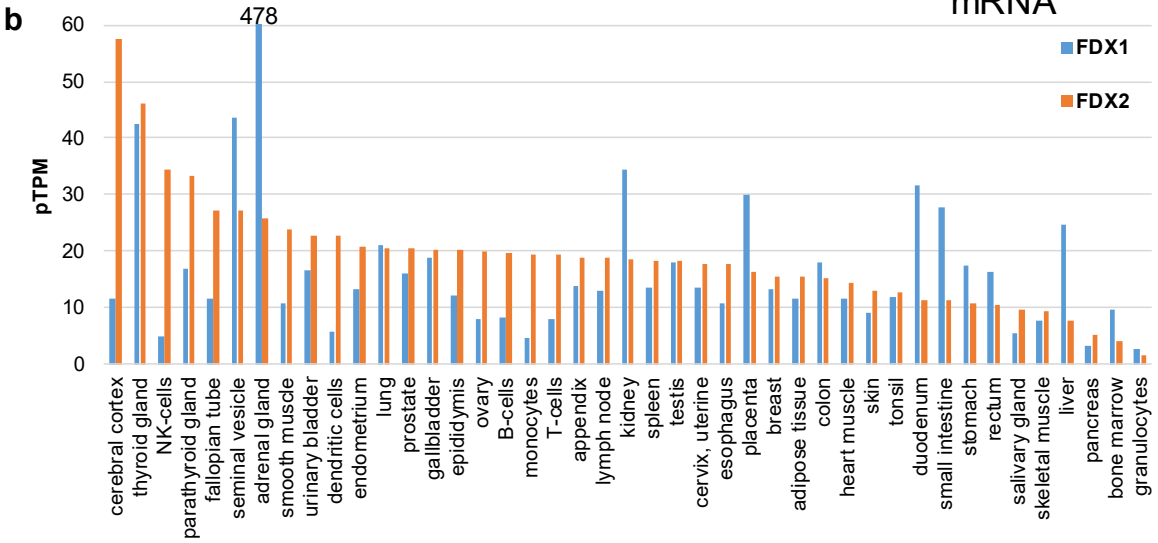
lipoylation in virtually all cell types necessitates and explains the global expression of *FDX1*, yet low lipoyl synthesis capacity, i.e. low FDX1 or LIAS, suffices to satisfy the needs for normal mitochondrial metabolism. In keeping with this idea, low levels of FDX1 remaining after RNAi-based knockdown maintained lipoylation in human cells (Fig. 1a). Likewise, small residual amounts of yeast Yah1 were sufficient to produce enough ectopic LIAS for normal lipoylation by FDX1 (Fig. 3d).

FDX1 has been identified in a systematic study to be a target of the tight complex of the Cu ionophore Ele with Cu, leading to the proposal that the role of FDX1 in Fe/S protein maturation might explain the Ele:Cu toxicity<sup>13-15</sup>. This view has been revised and extended by work published during review of our study to show that both FDX1 and lipoylation might be the target of Ele:Cu toxicity, yet a molecular explanation was not provided 16. Our definition of the physiological FDX1 functions, particularly in lipoylation and not in Fe/S protein maturation, renders it unlikely that FDX1 is the primary target of Ele:Cu toxicity in vivo, because FDX1 is sensitive to high Cu but not Ele:Cu (Fig. 4c-e). However, FDX1 could be damaged by the Cu accumulated in cells and mitochondria in the presence of Ele<sup>14</sup>. This seems unlikely though, because FDX1 and FDX2 show similar Cu sensitivity, yet their Fe/S protein biogenesis is unaffected by Ele (Fig. 4d-f; Suppl. Fig. 3). Here, we provide in vitro and in vivo evidence that the complex process of lipoylation, most prominently the final step of lipoyl formation by LIAS. is severely affected by both Ele:Cu and Cu (Fig. 4a,b,f). The lipoyl-dependence of the mitochondrial enzymes PDH and KGDH satisfactorily explains why particularly cells critically relying on mitochondrial metabolism are most sensitive to Ele treatment<sup>15</sup>. An interesting future question will be the deeper mechanistic dissection of how Ele:Cu affects the biochemical function of LIAS. Overall, our findings identify lipoylation as a highly Cu-sensitive pathway in human cells, distinguishing these cells from both fungi hosting highly Cu-sensitive Fe/S proteins and bacteria containing Cu-sensitive hydratases with solvent-exposed [4Fe-4S] clusters<sup>17,18</sup>.

#### **Supplementary Figures**

а



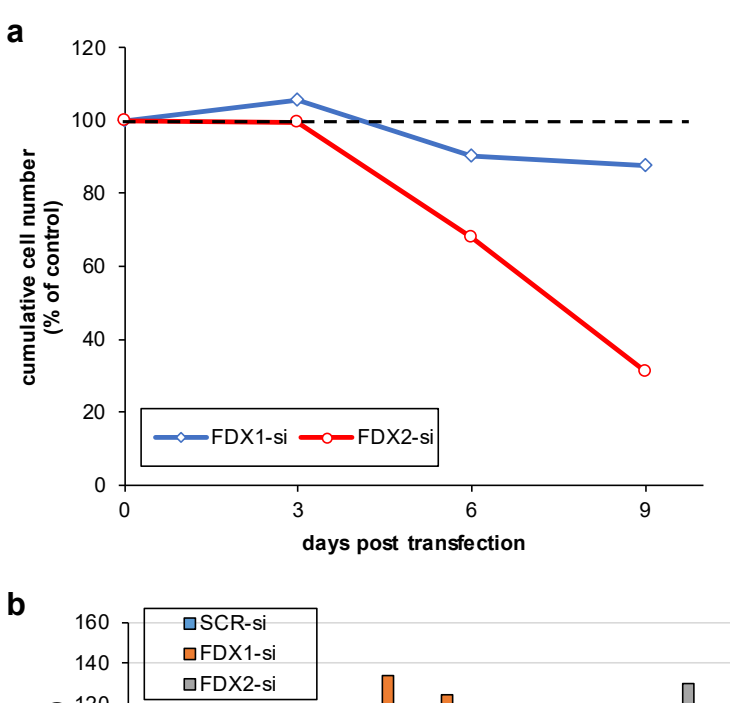


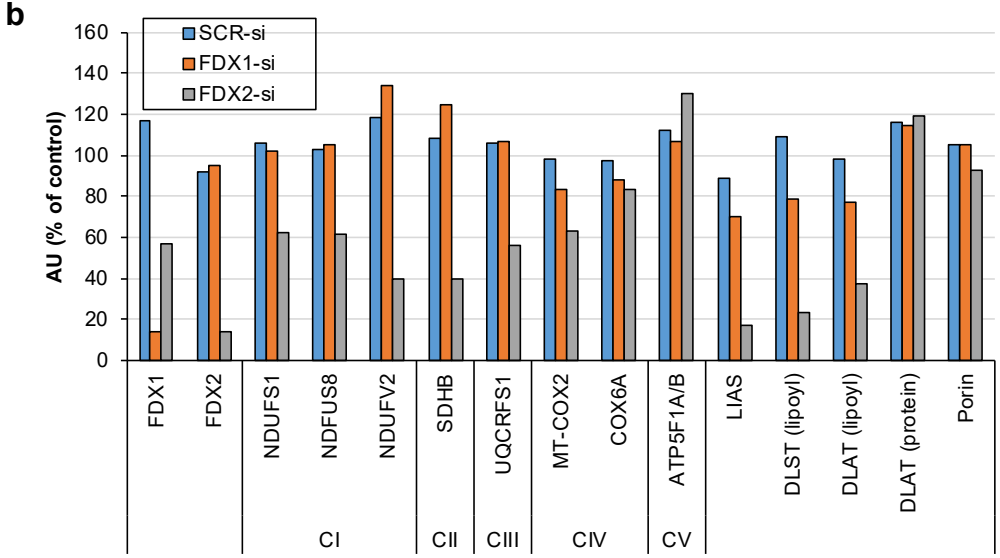
**Supplementary Figure 1** | **Tissue-specific protein and mRNA levels for human mitochondrial FDX1 and FDX2.** Expression analyses for the two human FDXs by either specific protein immunostaining or transcript measurements within the Human Protein Atlas project (HPA; see below)<sup>19</sup> provide contradictory results for FDX1. The high expression of FDX1 RNA and protein in testis, placenta, adrenal gland and kidney is well explained by its long-known role in steroid conversion. The findings of our work now satisfactorily explain the general expression of the *FDX1* gene in all tissues as judged by transcript analyses. The newly described function of FDX1 in lipoylation represents a central biosynthetic reaction that is needed in virtually all tissues.

**a** Semi-quantitative estimation of FDX1 and FDX2 protein levels by immunostaining using commercially obtained tissue lysates (see Fig. S1 in Ref. <sup>12</sup>) or a systematic tissue distribution

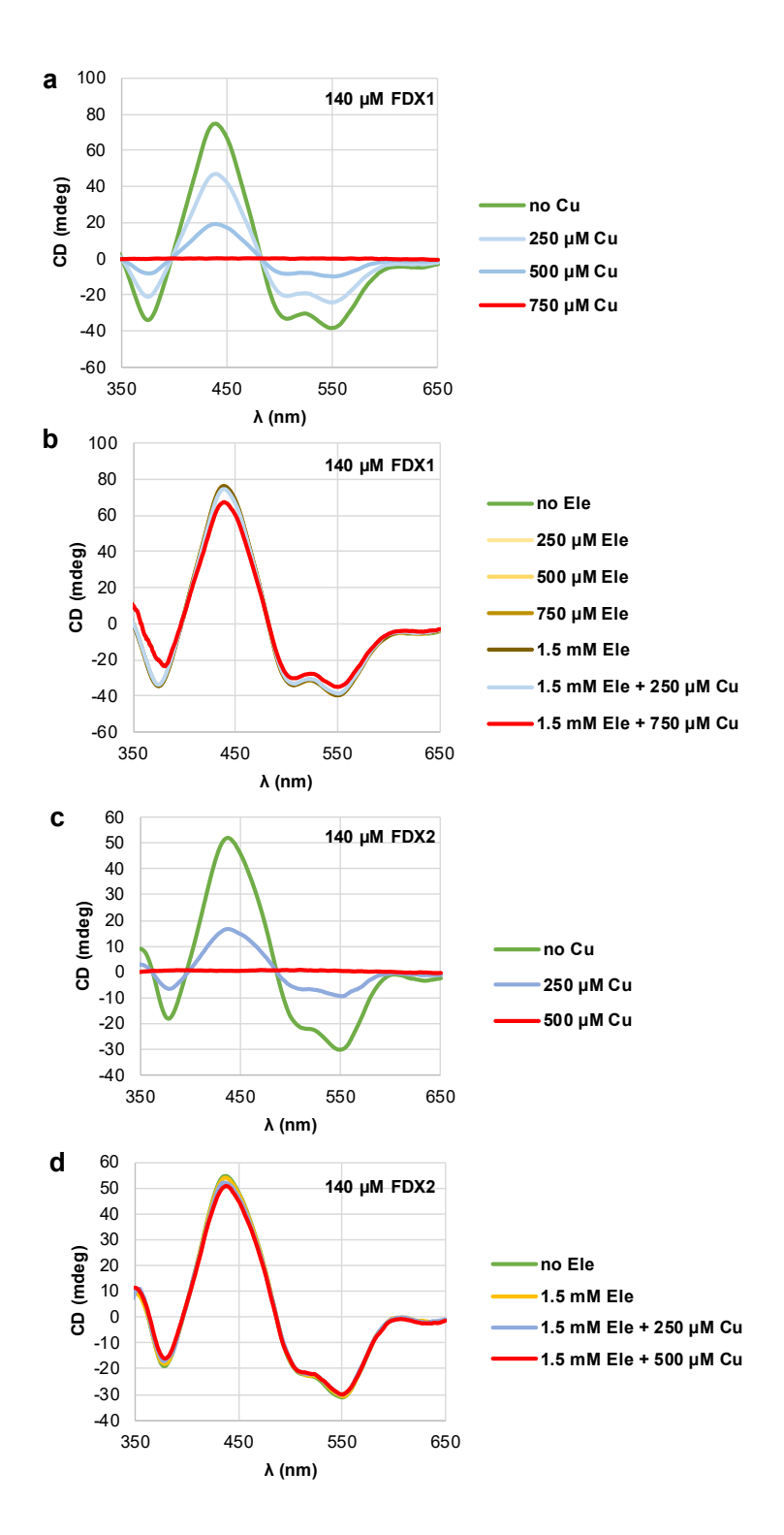
analysis within the HPA project showed detectable levels of FDX2 in almost all analyzed tissues, whereas FDX1 was found only in testis, placenta, adrenal gland and kidney.

**b** On the contrary, significant amounts of both *FDX1* and *FDX2* mRNAs were detected within the HPA project across numerous tissues, with FDX2 levels normally being higher than those of FDX1. The latter expectedly is expressed most strongly in steroid-transforming organs. Quantitation of FDX1 and FDX2 mRNA levels is presented as protein-coding transcripts per million (pTPM) across 43 tissues/cell types. Credit: **HPA** project (https://www.proteinatlas.org/ENSG00000137714-FDX1/tissue and https://www.proteinatlas.org/ENSG00000267673-FDX2/tissue, release 01.10.2020). Notably, the transcript results are not fully consistent with independent datasets for tissue-specific RNA levels obtained in projects Genotype-Tissue Expression (GTEx) and Functional Annotation Of The Mammalian Genome (FANTOM5; see above websites for details).

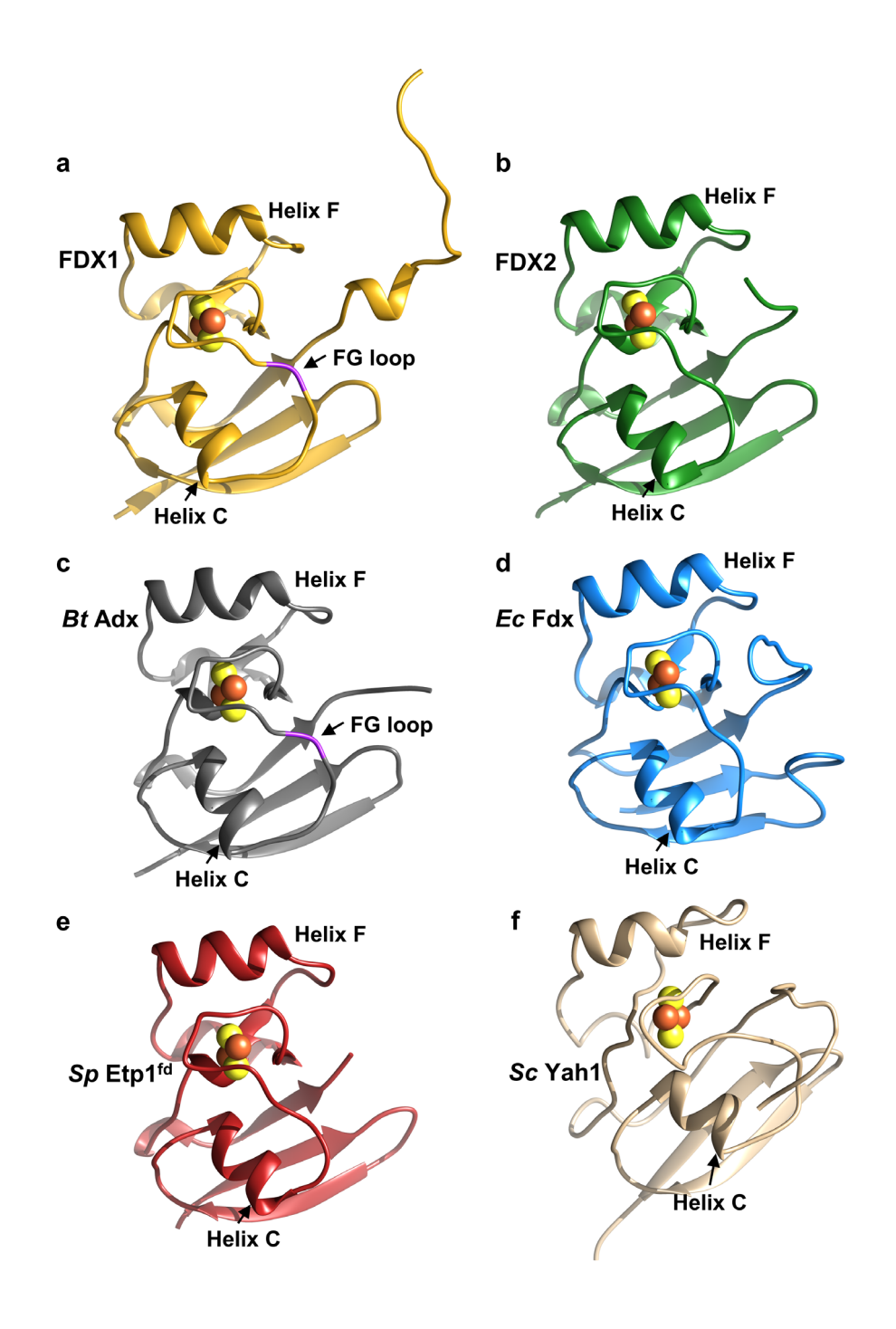




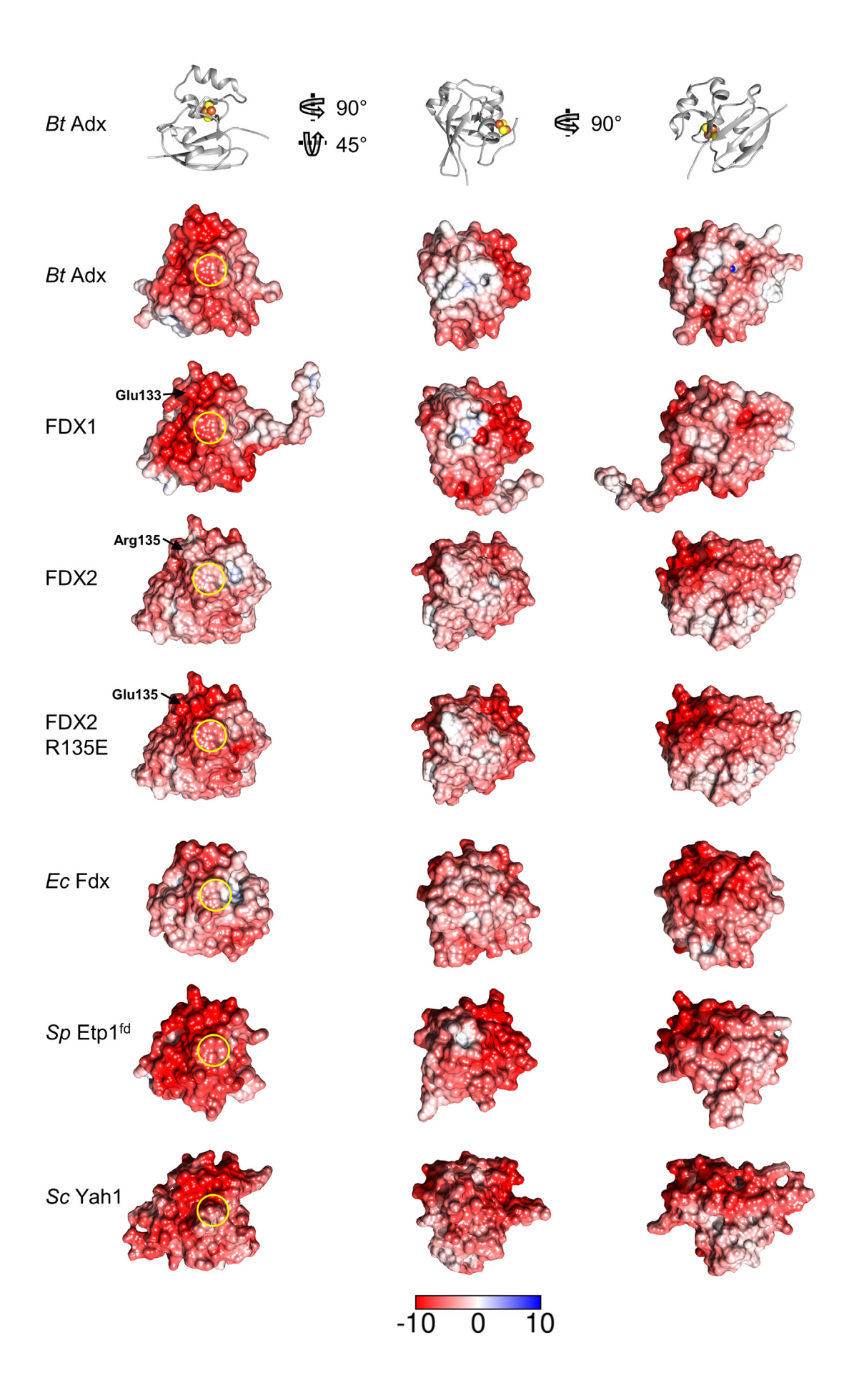
Supplementary Figure 2 | RNAi-mediated *FDX1* and *FDX2* knockdown phenotypes. a Cumulative growth of control, FDX1-depleted (FDX1-si), and FDX2-depleted cells treated as in Fig. 1a was calculated from cell counts at the three harvests on days 3, 6, and 9 after the first transfection. **b** Densitometric quantitation of immunoblots of Fig. 1a using Image studio lite 5.2. Values were presented relative to those of control cells (set to 100%, dashed line in a).



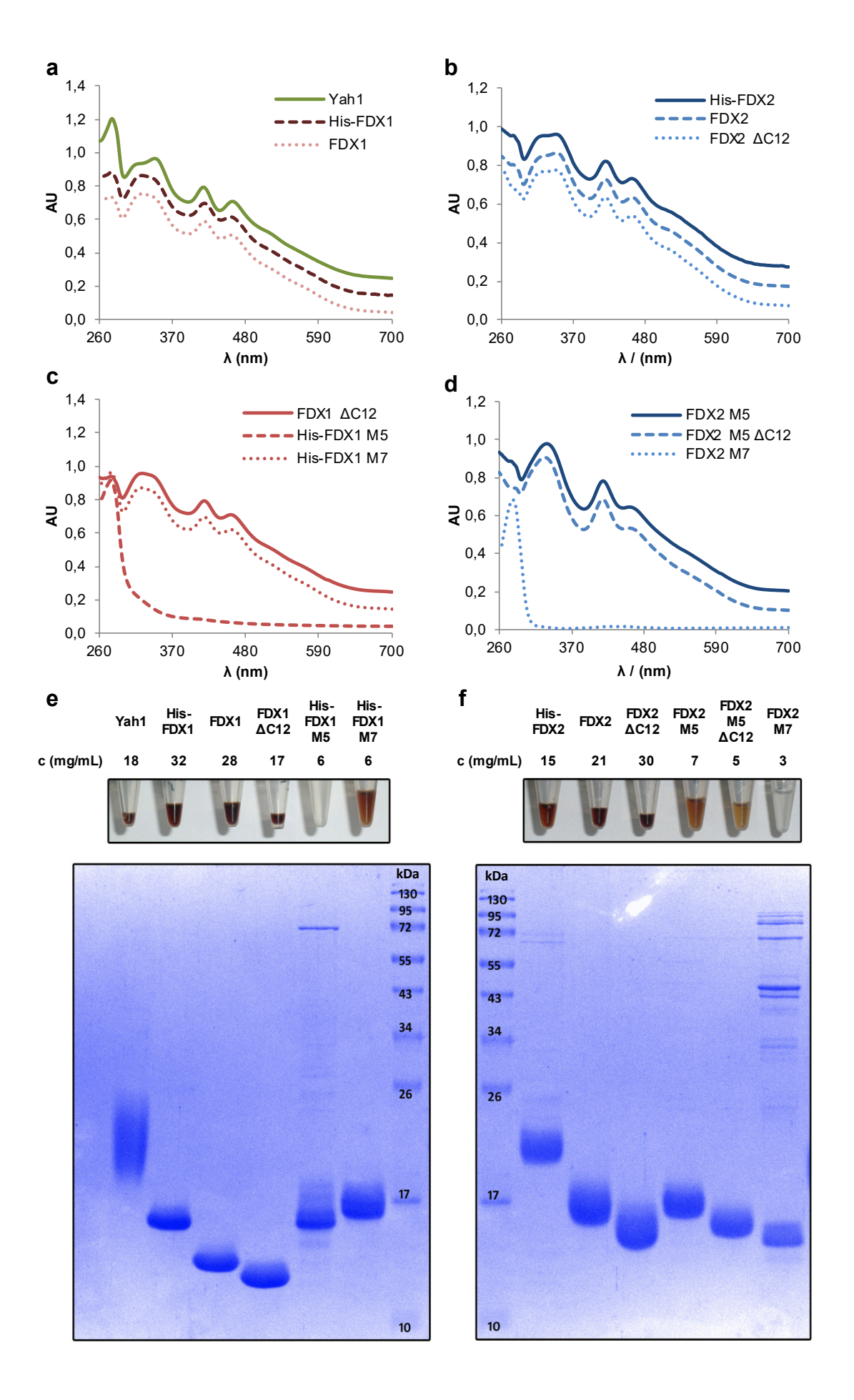
Supplementary Figure 3 | Elesclomol prevents copper-mediated Fe/S cluster destruction on FDX1 and FDX2. Samples containing 140 µM FDX1 or FDX2 were titrated with CuCl<sub>2</sub> or elesclomol (Ele) under anaerobic conditions, and CD spectra of the [2Fe-2S] clusters were recorded after each titration step. Samples containing 1.5 mM Ele were subsequently titrated with CuCl<sub>2</sub>. Excess of Ele prevented Cu-mediated destruction of Fe/S clusters on FDX1 and FDX2 by Ele:Cu complex formation (see also Fig. 4d,e). Representative data of two independent experiments per condition.

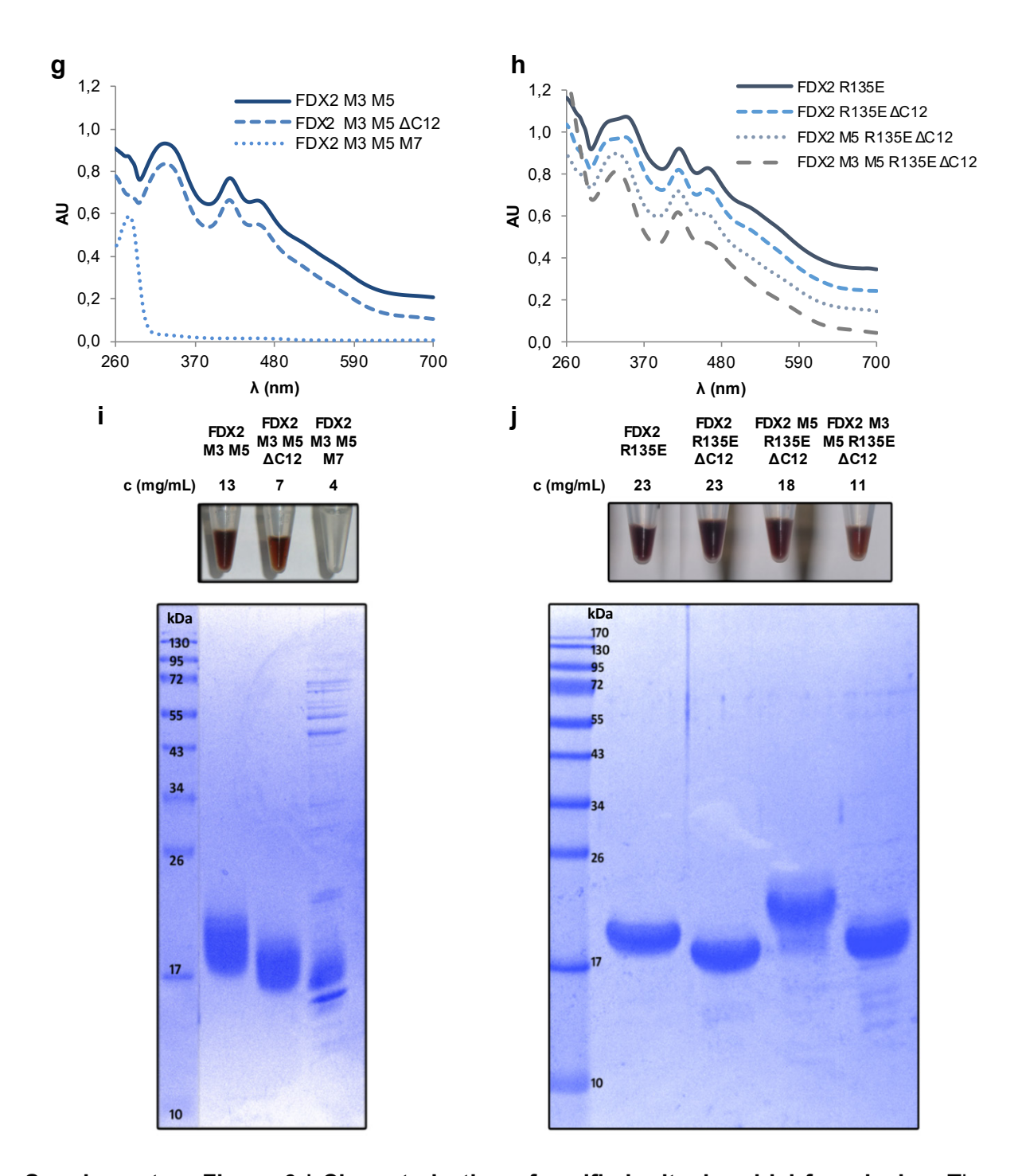


Supplementary Figure 4 | Comparison of the 3D structures of different ferredoxins. Depicted are the crystal structures of a FDX1 (PDB code: 3P1M, residues 65 - 184), b FDX2 (2Y5C, 69 - 174), c Bt Adx (1CJE, 63 - 169), d Ec Fdx (1I7H, 2 - 110), and e Sp Etp<sup>fd</sup> (2WLB, 518 - 603), as well as f the NMR solution structure of Sc Yah1 (2MJD, 58 - 172). For the crystal structures, C-terminal residues are resolved only for FDX1. The PheGly dipeptide present in FDX1-like proteins (FG loop) is depicted in magenta.



Supplementary Figure 5 | The electrostatic surface potential of FDX2 is less negatively charged. Depicted are Bt Adx (PDB code: 1CJE, residues 63-169), FDX1 (3P1M, 65-184), FDX2 (2Y5C, 69-174), Ec Fdx (1I7H, 2-110), Sp Etpfd (2WLB, 518-603) and Sc Yah1 (2MJD, Surface potentials were calculated using the APBS 58-160). server (https://server.poissonboltzmann.org). Negative charges are colored in red, positive charges in blue. The color bar covers the range from -10 kT/e to +10 kT/e. All proteins are shown in three different orientations, defined on top by the ribbon presentations of Bt Adx (grey). In the left column the position of the Fe/S cluster binding site is marked by yellow circles. For Sc Yah1, the NMR structure was employed, as no crystal structure was available. The C-terminal residues are only shown for FDX1. The structure of FDX2 R135E variant was modelled using UCSF Chimera<sup>20</sup>. The exchanged residue is indicated by an arrow.





Supplementary Figure 6 | Characterization of purified mitochondrial ferredoxins. The indicated mitochondrial FDXs were purified after recombinant expression in *E. coli.* a-d, g, h UV/VIS spectra were recorded and normalized to 62 μM. Spectra were shifted by 0.1 AU<sub>700nm</sub> along the y-axis for better visualization. e, f, i, j Photographs were taken for FDX solutions at the indicated protein concentrations (top). Purified proteins (5 μg each) were analyzed for purity by SDS-PAGE (bottom). Typically, apoproteins lacking a Fe/S cluster showed poorer purity. Where indicated, proteins possessed an N-terminal His<sub>6</sub>-tag. All other proteins were devoid of tags.

# Supplementary Figure 7 | Reaction scheme for cortisol formation by cytochrome P450 CYP11B1. The monooxygenase CYP11B1 (also named $\beta$ -hydroxylase) introduces a hydroxyl group into 11-deoxycortisol in the final step of cortisol formation. The required reduction of molecular oxygen is enabled by delivery of two electrons from FDX1<sup>21</sup>.

#### **Supplementary Materials and Methods**

#### Transfection of HEK293 cells by electroporation

HEK293 cells were harvested by trypsination, and 9 x  $10^6$  cells were resuspended in 250 µL of electroporation buffer<sup>22</sup>. 250 pmol of each of three individual siRNA were added, yielding a total of 750 pmol or 3 µM siRNA, and transfection by electroporation was performed by a Xcell Gene Pulser device (Biorad, München, Germany) using a pulse of 262 V and 525 µF with exponential decay. Cell recovery was improved by addition of up to 5 µg of the pVA-I plasmid to the transfection<sup>23,24</sup>. Immediately after electroporation cells were transferred into 20 mL of high-glucose DMEM supplemented with 7.5% FCS, penicillin/streptomycin, and glutamine, and seeded into collagenized 75 cm² flasks. In order to prolong the time period of RNAi-mediated mRNA depletion, cells were re-transfected twice at a three-day interval, resulting in a total depletion time of 9 days.

#### Coenzyme Q extraction and HPLC analysis

Cell pellets (~1mg protein) were processed and analyzed essentially as described<sup>25</sup>. Briefly, we added to the cell pellets 0.3 mL of 150 mM KCl, 200 µL glass beads, 10 µL of a 5 µM CoQ8 standard solution and 3 mL methanol. The tubes were vortexed for 1 min, 2 mL petroleum ether (40 - 60 °C boiling range) was added, and vortex was repeated for 1 min. After centrifugation at 700 rpm for 1 min, the upper phase was collected, and the methanol phase was extracted again with 2 mL petroleum ether. Both petroleum ether phases were combined, dried under a nitrogen flow and the lipid extracts were resuspended in 100 µL ethanol. Samples corresponding to 0.2 mg protein were injected onto the C18 column, and separation was obtained at a flow rate of 1 mL/min with a mobile phase composed of 25% isopropanol, 45% methanol, 20% ethanol, and 10% of a solution composed of 90% (v/v) isopropanol, 10% (v/v) 1 M ammonium acetate, and 0.1% (v/v) formic acid. A precolumn electrode (5020 Guard Cell, Thermo) was set at +650 mV and electrochemical detection (ECD) was performed with a Coulochem III equipped with a 5011A analytical cell (E1, -650 mV; E2, +650 mV). Standard solutions of CoQ<sub>8</sub> and CoQ<sub>10</sub> were injected in the same conditions to generate standard curves that were used to quantify CoQ<sub>10</sub> in the samples and to correct for sample loss during the organic extraction (based on the recovery of CoQ<sub>8</sub>).

#### Expression and purification of recombinant proteins

An overview of the plasmid constructs used for heterologous protein expression is given in Supplementary Table 5. CYP11B1<sup>26</sup>, FDXR<sup>27</sup> and LIAS<sup>28</sup> were expressed and purified as described before, with the exception that LIAS was overproduced in terrific broth instead of M9

medium. For all other proteins, plasmids were introduced into E. coli BL21 (DE3) cells and overproduced in terrific broth medium using appropriate antibiotics (100 µg/mL ampicillin or 30 µg/mL kanamycin). Cultures were inoculated from bacterial overnight suspensions and shaken at 37°C and 160 rpm until OD<sub>600</sub> ~0.8. pASK-IBA43(+) constructs were induced with 0.2 mg/L anhydrotetracycline and pET-vectors with 1 mM isopropyl-β-D-thiogalactoside (IPTG). For NIA production, two constructs encoding NFS1-ISD11 and ACP were coexpressed. Additional supplements were added for production of all FDXs (50 µM Fe(NH<sub>4</sub>)<sub>2</sub>(SO<sub>4</sub>)<sub>2</sub>) and NIA (2 mM pyridoxine hydrochloride). Subsequently, cultures were shaken at 22°C overnight and cell pellets harvested by centrifugation. Purification was done aerobically at 4°C or on ice. His-tagged constructs were purified by His-affinity and non-tagged constructs by anion exchange chromatography (AEC). Pellets were resuspended in His-buffer (35 mM Tris/HCl pH 7.4, 300 mM NaCl, 5% w/v glycerol) or AEC-buffer (35 mM Tris/HCl pH 7.5, 50 mM NaCl, 5% w/v glycerol), respectively. Subsequent to the addition of proteinase inhibitor (cOmplete™ Protease Inhibitor Cocktail) and optionally lysozyme and/or DNAse I, cells were lysed by sonication. The lysate was cleared by centrifugation and the cell extract loaded onto either a His-binding (NiNTA-Agarose) or an anion exchange column (Source 30Q) pre-equilibrated with His- or AEC-buffer. His-binding columns were washed using His-buffer plus 10 mM (NIA) or 70 mM (ISCU2, FXN) imidazole and proteins eluted in His-buffer plus 250 mM imidazole. Anion exchange columns were washed with AEC-buffer and proteins eluted using a gradient from AEC- to high salt buffer (35 mM Tris/HCl pH 7.5, 1 M NaCl, 5% w/v glycerol). Eluates were concentrated to a volume of 2 mL and further purified by size exclusion chromatography using HiLoad® 16/600 Superdex® columns. Desired fractions were combined, concentrated to ~1 mL and checked for purity by SDS-PAGE. Protein concentration was determined using the Bradford assay. A correction factor for concentrations determined by the Bradford assay was determined for FDX1, FDX2, LIAS, ISCU2, FXN and NIA by amino acid analysis (Leibniz-Institut für Analytische Wissenschaften, Dortmund, Germany). Iron and sulfide content of Fe/S cluster proteins were estimated by colorimetric methods<sup>29,30</sup>.

#### In vitro Fe/S cluster stability assay of ferredoxins

FDX1 or FDX2 were diluted to a final volume of 300  $\mu$ L in CD-buffer (50 mM Tris/HCl pH 7.5, 150 mM NaCl, 5% w/v glycerol) in an anaerobic chamber and transferred to a CD-cuvette which was sealed tightly. CD-spectra (300 – 650 nm) were recorded at 20°C and the proteins subsequently titrated with elesclomol and/or CuCl<sub>2</sub>. For each addition of the reagents, the cuvette was transferred back to the anaerobic chamber to sustain anaerobicity.

As the full length FDX2 did not yield crystals even without a His<sub>6</sub>-tag, we designed a *C*-terminally truncated construct assuming that flexibility of the *C*-terminus is precluding crystal formation. We also found that the first *N*-terminal residues of FDX2 are not important for *in vivo* function (Extended data Fig. 9), hence for crystallization we *N*-terminally truncated the human FDX2 protein to the same length as the crystallized bovine Adx<sup>31,32</sup>. The truncated FDX2 protein covered residues 66 – 171 and yielded crystals after one day. Crystals diffracted to 1.7 Å and the structure could be solved *a priori* by single-wavelength anomalous diffraction (SAD) phasing using the anomalous scattering of the iron atoms of the [2Fe-2S] cluster. Data collection and refinement statistics are summarized in Supplementary Table 2. The final model of FDX2 covered two *holo*-proteins within one asymmetric unit with all residues visible except the most likely cleaved start methionine.

Initial crystallization screening was done with the His-tagged version, the untagged full length and the untagged C-terminal truncated version of human FDX2 using commercially available screens (QIAGEN) with a Cartesian 4000 dispensing system (Genomic Solutions). Only the untagged C-terminal truncated human FDX2 protein yielded crystals in different conditions with either ammonium sulfate or sodium citrate as precipitant within one to a few days. Optimized crystals were grown by mixing 300 nL of purified protein solution (30 mg/ mL) with 300 nL reservoir solution and incubation against 80 µL reservoir solution at 4°C in the sitting drop setup. The optimized reservoir solution contained solely 1.6 M sodium citrate. For data collection, a single red-brown crystal of the *holo*-protein was flash-frozen in liquid nitrogen with 20% w/v glycerol as cryo protectant. Native data set from this single crystal was collected at 100 K at the European Synchrotron Radiation Facility (ESRF, Grenoble), beamline ID14-4, on a MAR CCD detector to a resolution of 1.70 Å. The data were processed using XDS and the CCP4 package<sup>33</sup>. The crystal belonged to be the primitive monoclinic space group P2<sub>1</sub> and contained two molecules in the asymmetric unit with molecular masses of 11937 Da resulting in an apparent V<sub>m</sub> of 2.79 Å<sup>3</sup>/ Da and a solvent content of 55.9% <sup>34</sup>.

The crystal structure of the human FDX2 protein was determined by the Single-wavelength Anomalous Diffraction (SAD) technique using the anomalous signal of the iron from the Fe/S cluster. Initial phasing with SHELX-CDE<sup>35</sup> clearly showed four anomalous sites as expected for two FDX2 *holo*-proteins per asymmetric unit each containing a [2Fe-2S] cluster. Automated model building using ARP/wARP<sup>36</sup> yielded a model containing 202 of the 216 amino acids of the two molecules. Missing residues could be manually added into additional electron density using COOT<sup>37</sup> and refinement with REFMAC<sup>38</sup>. Several rounds of refinement provided a final model covering residues 3 to 109 in both chains, 220 water molecules, two [2Fe-2S] cluster and two sulfate ions (R<sub>cryst</sub> = 17.28%, R<sub>free</sub> = 20.05%). In the final model the residues E40 in chain A and Q16 in chain B were modeled in alternative conformations. The side chains of some charged residues (E58, D62, E83, K106, R109) were flexible and could only be modeled

with lower or zero occupancy due to missing electron density. The model quality was analyzed with PROCHECK<sup>39</sup> and PROMOTIF<sup>40</sup>. The quality of the final model is summarized in Supplementary Table 2. The structure factors have been deposited in the Protein Data Bank, www.PDB.org (PDB code: 2Y5C).

The human FDX1 structure was generated by homology modeling using the bovine adrenodoxin structure (PDB code: 1CJE\_B) as template with SWISS MODEL<sup>41</sup>. Figures were generated using UCSF Chimera.

#### In vitro cortisol formation assay

In vitro hydroxylation of 11-deoxycortisol to cortisol was performed using human mitochondrial CYP11B1 as described previously  $^{26}$ . The reaction mixture contained 0.5  $\mu$ M FDXR, 0.5  $\mu$ M CYP11B1, 400  $\mu$ M 11-deoxycortisol, 20  $\mu$ M FDX and a NADPH regenerating system consisting of 1 mM MgCl2, 5 mM glucose-6-phosphate and 1 U glucose-6-phosphate dehydrogenase. The reaction was started by the addition of 1 mM NADPH and incubated at 37°C for 10 min. The reaction was stopped and the steroid compounds were organically extracted and analyzed by reversed phase HPLC.

# **Supplementary Tables**

# Supplementary Table 1: Guide RNA sequences used in this study

gRNA	cDNA sequence
FDX1-CC1	GCGGCCTGCTGAGGAACCGG
FDX1-CC2	GTGACAGGTTGAACAAGCCA
FDX1-CC3	GATGGCTTTGGTGCATGTGA
FDX2-CC1	GGTCTTCACTCACATACACA
FDX2-CC2	GCTGGAGAGGAGGACGCGGG
FDX2-CC3	GGCCAGCGGATCCCAGTGAG

## Supplementary Table 2: Crystal structure of human FDX2 – data collection and refinement statistics

Data collection	
Wavelength, Å	1.319
Space group	P 1 2 1
Cell dimensions	54 00 05 45 <b>7</b> 5 54
a, b, c, Å	51.38, 35.45, 75.51
β, ° Passilution range Å	105.12
Resolution range, Å	49.6 – 1.70 (1.79 – 1.70) 5.7 (45.7)
R <sub>merge</sub> , %	, ,
I/σ(I)	22.0 (5.2)
Completeness, %	97.9 (96.5)
Multiplicity Number of reflections	7.1 (7.2)
Overall	202987 (29635)
Unique	28713 (4094)
B factor <sup>a</sup> , Å <sup>2</sup>	18.0
Anomalous Completeness	96.9 (95.6)
Anomalous Multiplicity	3.7 (3.7)
Phasing statistics	,
No. of Fe sites	4
CC for solutions <sup>b</sup>	>20
Refinement statistics	
$R_{\text{cryst}}/R_{\text{free}}$ (%)	17.31/ 20.17
No. nonhydrogen-atoms	
Protein <sup>°</sup>	1688
Water	222
<i>B</i> factors, Å <sup>2</sup>	
Protein <sup>c</sup>	14.8
Water	27.0
Rmsd bonds length (Å)	0.012
Rmsd bonds angle (°)	1.55
Ramachandran plot	
Allowed regions (%)	91.8
Additional allowed regions (%)	8.2
Generously allowed regions (%)	0
Disallowed regions (%)	0

Values in parentheses are for the highest resolution shell.

<sup>&</sup>lt;sup>a</sup> *B* factor as defined from Wilson plot.
<sup>b</sup> correlation coefficient CC as defined by SHELXD

<sup>°</sup> including two [2Fe-2S] clusters and two sulfate-ions

Supplementary Table 3: Overview of mutated regions in FDX1 and FDX2

Mutant name	Residues (FDX1)	Sequence (FDX1)	Residues (FDX2)	Sequence (FDX2)
ΔN13			56 – 68	AGEEDAGGPERPG
M1	77 – 82	ETLTTK	81 – 86	QRIPVS
M2	88 – 89	SL	92 – 93	NV
M3	91 – 97	DVVVEN	95 – 101	HLAQRH
M4	100 – 101	ID	104 – 105	LE
M5	103 – 104	FG		
M6	108 – 109	GT	110 – 111	AS
M7	117 – 119	LIF	119 – 121	VYV
M8	128 – 131	DAIT	130 – 133	PPPE
M9	142 – 143	YG	144 – 145	PL
М9а	142	Y	144	Р
M10	145 – 157	TDR	147 – 149	QEN
R135E	133	Е	135	R
exC14	171 – 184	VADARQSIDVGKTS	161 – 174	TRNFYVDGHVPKPH
exC27	158 – 184	KSMDNMTVRVPET	148 – 174	PELEGAEFTLPKITR
63027	130 - 104	VADARQSIDVGKTS		NFYVDGHVPKPH
ΔC12	173 – 184	DARQSIDVGKTS	163 – 174	NFYVDGHVPKPH

The table shows the name of the mutations and the respective native sequences of human FDX1 and FDX2 as depicted in Extended data Fig. 8. For mutants M1 – M10, the FDX1 sequence was replaced with the respective FDX2 residues and vice versa. For mutants exC14 and exC27, the 14/27 C-terminal residues of FDX1 were exchanged with the respective FDX2 sequence. These mutations were only done with FDX1.  $\Delta$ N13 and  $\Delta$ C12 refer to deletions of the N- and C-terminal residues. The  $\Delta$ N13 and R135E mutations were only done with FDX2. Numbering according to sequence alignment in Extended data Fig. 8.

Supplementary Table 4: Yeast strains used in this study

Strain	Genotype	Method of Generation	Source/Reference	
W303-1A	MATa; ura3-1; ade2-1; trp1-		42	
	1; his3-11,15; leu2-3,112			
Gal-YAH1	W303-1A, <i>pYAH1::LEU2-</i>		43	
Gal-TATT	pGAL1-10			
BY4742	MATα;his3Δ1; leu2Δ0;	obtained from Euroscarf	44	
	met15Δ0; ura3Δ0	obtained from Edioscari		
lip5∆	BY4742, lip5::KanMX4	obtained from Euroscarf		
GalL-YAH1	lip5∆; trp1::hph1NT1;	PCR fragments (pFA6a-hph1NT1;	this work	
lip5∆	pYAH1:: GAL-L-natNT2	pYM-N27) <sup>45</sup>	uns work	
GalL-YAH1	W303-1A; cox15::HIS3;	PCR fragments (pFA6a-HIS3	this work	
cox15∆	pYAH1::GAL-L-natNT2	(Euroscarf); pYM-N27 <sup>45</sup> )		

Table 5: Plasmid constructs used in this study

Plasmid	ORF	Backbone	Use	Source/Reference
pVA-I	none	pHindB	Human cell recovery after electroporation	23
PX459	none	pSpCas9(BB)- 2A-Puro	gRNA expression	10.1038/nprot.2013.143
pEGFP-PEST	EGFP-PEST	pEGFP-N1	transfection control	this work
Su9-FDX1	Su9-FDX1	pDsRed2-C1	complementation	this work
p414- <i>LIAS</i>	F1β-LIAS (1- 35Δ)	p414- <i>TDH3</i>	complementation	this work
p414-COX15	F1β-COX15 (1- 67Δ)	p414 <i>-TDH3</i>	complementation	this work
p416- <i>FDX1</i>	F1β-FDX1 (1- 60Δ)	p416- <i>TDH3</i>	complementation	this work
p415- <i>FDX2</i>	F1β-FDX2 (1- 68Δ)	p415- <i>TDH</i> 3	complementation	this work
p426-TDH3	none	p426- <i>TDH3</i>	complementation	46
p426- <i>FDX1</i>	F1β-FDX1 (1- 61Δ)	p426- <i>TDH3</i>	complementation	this work
p426- <i>FDX</i> 2	F1β-FDX2 (1- 68Δ)	p426- <i>TDH</i> 3	complementation	this work
p416- <i>Yah1</i>	S.c. Yah1	p416- <i>MET25</i>	complementation	47
pETDuet1- FDX1	His <sub>6</sub> -FDX1 (1- 60Δ)	pETDuet1	protein purification	12
pETDuet1- FDX2	His <sub>6</sub> -FDX2 (1- 68Δ)	pETDuet1	protein purification	12
pASK-IBA43(+)- FDX1	FDX1 (1-62Δ)	pASK-IBA43(+)	protein purification	this work
pASK-IBA43(+)- FDX2	FDX2 (1-68Δ)	pASK-IBA43(+)	protein purification	this work
pASK-IBA43(+)- FDX2-ΔC12	FDX2 (1-68Δ, 175-186Δ)	pASK-IBA43(+)	protein purification, crystallization	this work
pET15b-Yah1	S.c. Yah1 (1- 57Δ)	pET15b	protein purification	this work
pET28a(+)-LIAS	His <sub>6</sub> -Thr-LIAS (1-35Δ)	pET28a(+)	protein purification	this work
pET24b(+)- ISCU2	ISCU2-His <sub>6</sub> (1- 34Δ)	pET24b(+)	protein purification	48
pETDuet1- NFS1-ISD11	NFS1 (1-55∆), His <sub>6</sub> -Tev-ISD11	pETDuet1	protein purification	48
pRSFDuet1- ACP	ACP (1-68Δ)	pRSFDuet1	protein purification	48
pMCSG7-FXN	His <sub>6</sub> -Tev-FXN (1-80Δ)	pMCSG7	protein purification	48
pETDuet1- FDXR	His <sub>6</sub> -FDXR (1- 32Δ)	pETDuet1	protein purification	12

Mutations of the human FDXs as described in the paper were introduced by mutagenesis PCR using p426-FDX1, p426-FDX2, pETDuet1-FDX1, pASK-IBA43(+)-FDX1 and pASK-IBA43(+)-FDX2 as the initial templates. Combinations of different mutations were achieved by employment of newly generated mutated plasmids as templates for further rounds of mutagenesis.

### Supplementary Table 6: Primary antibodies used in this study

Antibody	Source
rabbit anti-FDX1	12
rabbit anti-FDX2	12
rabbit anti-UQCRFS1	H. Schägger (Frankfurt, Germany)
rabbit anti-MT-COX2	H. Schägger (Frankfurt, Germany)
rabbit anti-COX6A	H. Schägger (Frankfurt, Germany)
rabbit anti-ATP5F1A/B	H. Schägger (Frankfurt, Germany)
mouse anti-SDHB	Abcam (Cambridge, UK)
rabbit anti-lipoic acid	Calbiochem (Merck, Darmstadt, Germany)
rabbit anti-LIAS	Protein Tech Group (Chicago, USA)
rabbit anti VDAC1	Protein Tech Group (Chicago, USA)
mouse anti-DLAT	Santa Cruz biotechnology (Dallas, USA)
mouse anti-NDUFS1	Santa Cruz biotechnology (Dallas, USA)
mouse anti-NDUFS8	Santa Cruz biotechnology (Dallas, USA)
mouse anti-NDUFV2	Santa Cruz biotechnology (Dallas, USA)
mouse anti-GFP	Takara Bio (Göteborg, Sweden)

#### **Supplementary References**

- Mellor, S.B., Vavitsas, K., Nielsen, A.Z. & Jensen, P.E. Photosynthetic fuel for heterologous enzymes: the role of electron carrier proteins. *Photosynth Res* 134, 329-342 (2017).
- 2. Strushkevich, N. et al. Structural basis for pregnenolone biosynthesis by the mitochondrial monooxygenase system. *Proc Natl Acad Sci U S A* **108**, 10139-43 (2011).
- 3. Muller, J.J., Lapko, A., Bourenkov, G., Ruckpaul, K. & Heinemann, U. Adrenodoxin reductase adrenodoxin complex structure suggests electron transfer path in steroid biosynthesis. *J. Biol. Chem.* **276**, 2786-2789. (2001).
- 4. Coghlan, V.M. & Vickery, L.E. Site-specific mutations in human ferredoxin that affect binding to ferredoxin reductase and cytochrome P450scc. *J Biol Chem* **266**, 18606-12 (1991).
- 5. Cronan, J.E. Assembly of Lipoic Acid on Its Cognate Enzymes: an Extraordinary and Essential Biosynthetic Pathway. *Microbiol Mol Biol Rev* **80**, 429-50 (2016).
- 6. Jumper, J. et al. Highly accurate protein structure prediction with AlphaFold. *Nature* **596**, 583-589 (2021).
- 7. Varadi, M. et al. AlphaFold Protein Structure Database: massively expanding the structural coverage of protein-sequence space with high-accuracy models. *Nucleic Acids Res* **50**, D439-D444 (2022).
- 8. McLaughlin, M.I. et al. Crystallographic snapshots of sulfur insertion by lipoyl synthase. *Proc Natl Acad Sci U S A* **113**, 9446-50 (2016).
- 9. Harmer, J.E. et al. Structures of lipoyl synthase reveal a compact active site for controlling sequential sulfur insertion reactions. *Biochem J* **464**, 123-33 (2014).
- 10. Brixius-Anderko, S. & Scott, E.E. Structural and functional insights into aldosterone synthase interaction with its redox partner protein adrenodoxin. *J Biol Chem* **296**, 100794 (2021).
- Chiliza, Z.E., Martinez-Oyanedel, J. & Syed, K. An overview of the factors playing a role in cytochrome P450 monooxygenase and ferredoxin interactions. *Biophys Rev* 12, 1217-1222 (2020).
- 12. Sheftel, A.D. et al. Humans possess two mitochondrial ferredoxins, Fdx1 and Fdx2, with distinct roles in steroidogenesis, heme, and Fe/S cluster biosynthesis. *Proceedings of the National Academy of Sciences of the United States of America* **107**, 11775-80 (2010).
- 13. Yadav, A.A., Patel, D., Wu, X. & Hasinoff, B.B. Molecular mechanisms of the biological activity of the anticancer drug elesclomol and its complexes with Cu(II), Ni(II) and Pt(II). *J Inorg Biochem* **126**, 1-6 (2013).
- Nagai, M. et al. The oncology drug elesclomol selectively transports copper to the mitochondria to induce oxidative stress in cancer cells. *Free Radic Biol Med* 52, 2142-50 (2012).
- 15. Tsvetkov, P. et al. Mitochondrial metabolism promotes adaptation to proteotoxic stress. *Nat Chem Biol* **15**, 681-689 (2019).
- 16. Tsvetkov, P. et al. Copper induces cell death by targeting lipoylated TCA cycle proteins. *Science* **375**, 1254-1261 (2022).
- 17. Vallieres, C., Holland, S.L. & Avery, S.V. Mitochondrial Ferredoxin Determines Vulnerability of Cells to Copper Excess. *Cell Chem Biol* **24**, 1228-1237 e3 (2017).
- 18. Macomber, L. & Imlay, J.A. The iron-sulfur clusters of dehydratases are primary intracellular targets of copper toxicity. *Proc Natl Acad Sci U S A* **106**, 8344-9 (2009).

- 19. Uhlen, M. et al. Proteomics. Tissue-based map of the human proteome. *Science* **347**, 1260419 (2015).
- 20. Pettersen, E.F. et al. UCSF Chimera--a visualization system for exploratory research and analysis. *J Comput Chem* **25**, 1605-12 (2004).
- 21. Ewen, K.M., Ringle, M. & Bernhardt, R. Adrenodoxin--a versatile ferredoxin. *IUBMB Life* **64**, 506-12 (2012).
- 22. Chu, G., Hayakawa, H. & Berg, P. Electroporation for the efficient transfection of mammalian cells with DNA. *Nucleic Acids Res* **15**, 1311-26 (1987).
- 23. Svensson, C. & Akusjarvi, G. Adenovirus VA RNAI: a positive regulator of mRNA translation. *Mol Cell Biol* **4**, 736-42 (1984).
- 24. Stehling, O. et al. Function and crystal structure of the dimeric P-loop ATPase CFD1 coordinating an exposed [4Fe-4S] cluster for transfer to apoproteins. *Proc Natl Acad Sci U S A* **115**, E9085-E9094 (2018).
- 25. Acosta Lopez, M.J. et al. Vanillic Acid Restores Coenzyme Q Biosynthesis and ATP Production in Human Cells Lacking COQ6. *Oxid Med Cell Longev* **2019**, 3904905 (2019).
- 26. Zollner, A. et al. Purification and functional characterization of human 11beta hydroxylase expressed in Escherichia coli. *FEBS J* **275**, 799-810 (2008).
- 27. Weiler, B.D. et al. Mitochondrial [4Fe-4S] protein assembly involves reductive [2Fe-2S] cluster fusion on ISCA1-ISCA2 by electron flow from ferredoxin FDX2. *Proc Natl Acad Sci U S A* **117**, 20555-20565 (2020).
- 28. McCarthy, E.L. & Booker, S.J. Biochemical Approaches for Understanding Iron-Sulfur Cluster Regeneration in Escherichia coli Lipoyl Synthase During Catalysis. *Methods Enzymol* **606**, 217-239 (2018).
- 29. Molik, S., Lill, R. & Mühlenhoff, U. Methods for studying iron metabolism in yeast mitochondria. *Methods Cell. Biol.* **80**, 261-280 (2007).
- 30. Rabinowitz, J.C. Analysis of acid-labile sulfide and sulfhydryl groups. *Methods Enzymol* **53**, 275-7 (1978).
- 31. Muller, A. et al. New aspects of electron transfer revealed by the crystal structure of a truncated bovine adrenodoxin, Adx(4-108). *Structure* **6**, 269-80 (1998).
- 32. Pikuleva, I.A., Tesh, K., Waterman, M.R. & Kim, Y. The tertiary structure of full-length bovine adrenodoxin suggests functional dimers. *Arch Biochem Biophys* **373**, 44-55 (2000).
- 33. Collaborative Computational Project, N. The CCP4 suite: programs for protein crystallography. *Acta Crystallogr D Biol Crystallogr* **50**, 760-3 (1994).
- 34. Matthews, B.W. Solvent content of protein crystals. *J Mol Biol* **33**, 491-7 (1968).
- 35. Sheldrick, G.M. A short history of SHELX. Acta Crystallogr A 64, 112-22 (2008).
- 36. Perrakis, A., Morris, R. & Lamzin, V.S. Automated protein model building combined with iterative structure refinement. *Nat Struct Biol* **6**, 458-63 (1999).
- 37. Emsley, P. & Cowtan, K. Coot: model-building tools for molecular graphics. *Acta Crystallogr D Biol Crystallogr* **60**, 2126-32 (2004).
- 38. Murshudov, G.N., Vagin, A.A. & Dodson, E.J. Refinement of macromolecular structures by the maximum-likelihood method. *Acta Crystallogr D Biol Crystallogr* **53**, 240-55 (1997).
- 39. Laskowski, R.A., MacArthur, M.W., Moss, D.S. & Thornton, J.M. PROCHECK: a program to check the stereochemical quality of protein structures. *Journal of Applied Crystallography* **26**, 283-291 (1993).
- 40. Hutchinson, E.G. & Thornton, J.M. PROMOTIF--a program to identify and analyze structural motifs in proteins. *Protein Sci* **5**, 212-20 (1996).

- 41. Arnold, K., Bordoli, L., Kopp, J. & Schwede, T. The SWISS-MODEL workspace: a web-based environment for protein structure homology modelling. *Bioinformatics* **22**, 195-201 (2006).
- 42. Mortimer, R.K. & Johnston, J.R. Genealogy of principal strains of the yeast genetic stock center. *Genetics* **113**, 35-43 (1986).
- 43. Lange, H., Kaut, A., Kispal, G. & Lill, R. A mitochondrial ferredoxin is essential for biogenesis of cellular iron-sulfur proteins. *Proc Natl Acad Sci U S A* **97**, 1050-5 (2000).
- 44. Brachmann, C.B. et al. Designer deletion strains derived from Saccharomyces cerevisiae S288C: a useful set of strains and plasmids for PCR-mediated gene disruption and other applications. *Yeast* **14**, 115-32 (1998).
- 45. Janke, C. et al. A versatile toolbox for PCR-based tagging of yeast genes: new fluorescent proteins, more markers and promoter substitution cassettes. *Yeast* **21**, 947-962 (2004).
- 46. Mumberg, D., Müller, R. & Funk, M. Yeast vectors for controlled expression of heterologous proteins in different genetic backgrounds. *Gene* **156**, 119-122. (1995).
- 47. Ozeir, M. et al. Coenzyme Q biosynthesis: Coq6 is required for the C5-hydroxylation reaction and substrate analogs rescue Coq6 deficiency. *Chemistry & biology* **18**, 1134-42 (2011).
- 48. Freibert, S.A. et al. N-terminal tyrosine of ISCU2 triggers [2Fe-2S] cluster synthesis by ISCU2 dimerization. *Nat Commun* **12**, 6902 (2021).

#### Response to Reviewers' comments

#### Manuscript NCHEMB-A220314618, Schulz et al.

We thank the Reviewers for their careful reading of our manuscript, the overall very positive evaluation, and the helpful suggestions for our work. We have addressed all mentioned issues in our revised version by introducing additional statistical information (including additional replicates), and by providing better explanations. The manuscript was further polished and small mistakes and typos were corrected. The entire text was shortened and formatted according to the requirements of *Nature Chemical Biology*. We hope that our manuscript will now be acceptable for publication in the *Nature Chemical Biology*.

**Note:** Reviewers' original text is in italics; our response is in plain text. The changes in our manuscript during revision are highlighted in the file <u>Schulz.revision-changes.pdf</u> to ease the reviewing process.

#### Referee #1 (Remarks to the Author):

.... (first two paragraphs deleted)

Overall, the manuscript was easy to read, albeit quite dense overall given the level of thorough and diverse experimental approaches pursued. Some minor comments. In the supplement, some figures appear to have rigorous replicate experiments, while others do not. For example, Figures S1, S2, S4, S8, S9, S10, etc lack a description of replicates or statistics performed. While other figures in the core and supplement show error bars and describe replicates, it isn't clear what statistical analysis was performed to determine which means are statistically different.

We now have performed (additional) <u>statistical</u> analyses wherever meaningful. The results fit to our conclusions. In detail:

<u>Fig. 1d:</u> We applied the statistics One-way ANOVA (after including a further replicate of the experiment).

Fig. 2b,d: One-way ANOVA

Fig. 3b,c: One-way ANOVA

<u>Fig. 3e:</u> One-way ANOVA, independently applied for the left and right parts. The new figure includes another round of replication, with virtually identical results. We realized that the old figure was erroneously mislabeled as 'PDH activity', but the similar enzyme KGDH was recorded. Both enzyme activities give virtually the same results in these assays (Uzarska et al. eLife 2016;5:e16673. DOI: 10.7554/eLife.16673). We have corrected the mistake.

<u>Fig. 4a,b:</u> This particular experiment was performed twice only in the fashion shown. The reason for n=2 is that this experiment is particularly costly and time-consuming. Since we have obtained similar results during the optimization phase of the experiment (conditions slightly different), we know that the individual data points are highly reliable (see the small error bars of the individual conditions). We also have performed One-way ANOVA showing the significance of the results.

<u>Fig. 4c:</u> We performed the statistics One-way ANOVA after including another replicate of the experiment (with virtually identical results).

Fig. 5e,f: One-way ANOVA

Fig. 6b,c,d,e: One-way ANOVA

<u>Suppl. Fig. S1:</u> For explanation see below ("Further, the order of figures...") and <u>Reviewer 3, point</u> "-Fig S1- not all the tissues overlap in analysis of protein vs mRNA"

<u>Suppl. Fig. S2:</u> The experiment shown in Fig. 1a (= original data plus the quantitation in Suppl. Fig. S2) in principle was presented in earlier publications by us (Sheftel et al., PNAS 2010) and the Rouault group (Shi et al., 2012). The mere purpose of Fig. 1a was a direct comparison to the new data presented in Figs. 1, 2 and 3 (i.e. the comparison of RNAi versus CRISPR-Cas9 approaches, the latter giving important new insights). Since the published data and the new data of Fig. 1 gave virtually identical results, we do not think that a more detailed analysis is needed.

<u>Extended Data Fig. 2 (previously Suppl. Fig. 4):</u> Examples for raw data of Fig. 1d (statistics in Fig. 1d).

Extended Data Fig. 6b (previously Suppl. Fig. 8b): This time course presents a rational for analyzing the samples by mass spec after 150 min, and was performed for setting up the appropriate reaction conditions of the LIAS assay.

Extended Data Fig. 7a (previously Suppl. Fig. 9a): Possibly the number of replicates (n=4) was hidden in the text. We now have made this clearer in the legend.

<u>Suppl. Fig. 3 (previously Suppl. Fig. 10):</u> The figure shows representative spectra of many Cu and Ele titrations (see also Fig. 4d,e). We mention the number of replicates for the conditions shown.

Further, the order of figures called out in the text should match the order in the supplement, e.g., Fig S1 is called out late in the manuscript.

<u>Suppl. Fig. S1</u> was called out already in the Introduction as "Suppl. Fig. 1". As explained in the legend, the figure presents (non-consistent) transcriptomic and proteomic data taken from a public data base. See also <u>Reviewer 3</u>, <u>point</u> "-*Fig S1- not all the tissues overlap in analysis of protein vs mRNA*".

Furthermore, it is interesting to speculate beyond the motif recognition controlling ferredoxin interaction partners and consider how these motifs might function through allosteric regulation in a manner similar to that studied by the Poulos lab for many years in the classical Pdx/P450 system. It would be interesting to reflect on this aspect at the end of the discussion. It is interesting to consider and highlight the structural questions that would be interesting for the molecular biophysicists to pursue in the future (as a broader impact of this study).

This point addresses really interesting aspects, yet we believe that these are beyond the problems of protein specificity and its structural basis (as studied here). Based on currently available experimental data the understanding of this aspect is still rather poor, and so far we have restrained from commenting on this interesting point. Since we had to cut our manuscript in length during revision, we suggest to discuss point in a dedicated review we plan to prepare, and hope the Reviewer agrees.

#### Referee #2 (Remarks to the Author):

.... (first two paragraphs deleted)

I have only minor comments and suggestions.

In the abstract, line 41, do the authors want to add "respectively" at the end of the sentence to describe the roles associated with each FDX?

At the beginning of our new work, the word "respectively" for the involvement of the FDXs in the two indicated processes was NOT justified because of the unclear substrate specificity of the two FDXs in the then available literature. However (and this may have confused the Reviewer), the findings of our new work now will justify this expression. Based on this explanation, we think addition of this expression (as requested) is inappropriate because in the relevant sentence we present the previous situation.

I do not know whether the number of words/characters allowed in the abstract was reached but adding a final conclusive sentence at the end of the abstract briefly summarizing the key insight(s), and/or providing a brief statement highlighting the advance the work provides to the field, may be considered.

We followed this advice and have moved a summarizing sentence in the middle of the abstract (summarizing what will be addressed in our work) to the end.

In the introduction: Lines 56-59: green eukaryotes also have mitochondrial FDXs, the use of "non-green" is not justified.

Correct. We have removed this expression.

Lines 79-85: As it is written, I understand that Yah1 catalyzes the introduction of the carbonyl group in heme o and catalyzes C5 hydroxylation of Coq6, while it only gives electrons to the respective enzymes involved.

We have re-written (and shortened, due to length restrictions) the relevant section to make this point clear.

Line 106: Strictly speaking, I suggest to replace mitochondria-cytoplasm by mitochondria-cytosol.

What we actually mean is not only the communication of mitochondria with the cytosol (soluble part) but also the other cellular compartments (= cytoplasm). Based on this explanation we would like to keep this term.

In the results: Line 124: comparable to a previous work
Changed as suggested.

Line 351: I suggest to replace "synthesized" by "expressed"

Changed as suggested.

Lines 354-355-356: After "critical for growth", I suggest to make a new sentence for the general conclusion of the paragraph.

Changed as suggested.

Line 363: From the figure 5d, I wonder whether the "growth restoration" observed by swapping the C-terminus of FDX1 by the one of FDX2 can really be qualified as major. It seems rather mild to me.

We have changed the wording to "partial".

In Figure 7: Do the authors want to represent NFU1 in the pathway to LIAS? because this maturation factor

We have added NFU1 as suggested.

In the discussion: Line 439: dithionite was already defined before

Changed as suggested (also in another place).

Line 443: May be good to define GCSH, both the acronym and the role of the protein.

Defined and explained as suggested, with a newly added a reference on lipoyl synthesis mechanism (Cronan, 2016).

Lines 446-447: Could the author elaborate a bit more about what prevents FDX2-LIAS in the structural modeling.

We note that in Supplementary Results we have presented a detailed account on the modelling strategies. Nevertheless, as suggested we have added to the legend of Extended data Fig. 10 (previously Suppl. Fig. 17) a more comprehensive explanation on our modeling efforts and the individual results. Of course, what molecular effect in the end prevents FDX2 from modeling onto LIAS in a functionally relevant fashion remains speculative from such theoretical analyses, but the overall result (FDX1 can, FDX2 cannot be modelled properly) excitingly and fully agrees with our experimental data.

In the methods: In the Section "Reconstitution of de novo Fe/S cluster synthesis on ISCU2", lines 799-801 describes a reaction mix with Elesclomol/copper but if I am correct there is no corresponding figure in the manuscript or even no mention of this assay in the text.

We thank the Reviewer for spotting this obvious oversight. The corresponding experiment was removed in a late stage of manuscript preparation. We now have deleted the sentence.

#### Referee #3 (Remarks to the Author):

This report by Schulz et al. assigns specific functions to the mitochondrial ferrodoxin proteins FDX1 and FDX2. Using a series of in vitro and cell-based enzyme assays, along with structure-function analysis, this manuscript presents a new paradigm for the individual cellular roles of the human FDX proteins. As previously reported, they show a role of FDX2 in Fe-S cluster biogenesis. However, they also present data to challenge previous reports that FDX1 plays a role in Fe-S cluster maturation. Rather, they show this enzyme mediates both heme a and lipoyl synthesis. While the data regarding the structure motif swapping (Figs 5-6) are elegant and convincing, the rest of the manuscript suffers from some technical and statistical limitations. I would suggest these issues be addressed before proceeding.

We thank the Reviewer for the overall positive evaluation of most parts of our manuscript. The criticized aspect of missing <u>statistics</u> has been addressed in detail above (see responses for Reviewer 1). The other points are addressed below.

One major concern is the lack of indication of statistical significance of the data reported in any of the bar graphs. For example, the data presented in Fig 6b only represent a small percentage of total activity. The text states "The triple mutant FDX2-M3+M5+ $\Delta$ C12 displayed a 5-fold activity increase compared to FDX2, again showing the importance of these segments" but this is only an increase from 0.2 to 0.9%. Is this truly statistically or even biologically significant? Without this assessment, the conclusion that the data "perfectly (lines 202, 274)" fit the models cannot be made. Also, a number of the experiments in yeast are subject to leaky expression, which could lead to alternate interpretations.

As already explained in our previous work (Sheftel et al., PNAS 2010; Fig. 5B), the formation of cortisol in the assay used in Fig. 6b,c can be measured with high accuracy. In this previous publication, we have shown that FDX2 shows a 500-fold lower activity compared to FDX1. While relative values are rather reproducible in one experiment, the absolute values of cortisol production may vary a bit from experiment to experiment. This is why the statistical analysis of Fig. 6b by One-way ANOVA does not assign statistical significance to some of the weak complementations. However, as proposed in our manuscript, the importance of R135 (and the C terminus in Fig. 6d,e) is/are nicely supported by the statistical analyses. We have adjusted the text to represent the added statistics.

Concerning the "*leaky expression*". As pointed out below ("*-Line 203: (Fig 2d) ...*"), the leaky expression of the *YAH1* promoter can even be essential for our experimental setup. We do not see the point that it would negatively impact the interpretation of our data.

#### Other specific comments are below

- how are the activity assay data being normalized relative to cell number since the FDX1-gRNA knockdowns have a significant growth defect (Supp Fig 3a)?

Since this is a long-used and well-established standardization procedure in our laboratory, our explanation may have been a bit short here. First, exploratory experiments are performed to test cell growth rates of individual cultured cells. In case of decreased growth rates due to genetic manipulations, we then start new experiments with appropriately higher cell numbers to end up with similar cell numbers (and cell density) at the times of harvesting. At this point,

additional cell counting is used to normalize the samples for small differences in cell numbers. We have added these details to the legend of Extended data Fig. 1a (previously Fig. Suppl. 3a).

-can the authors please comment in the discussion how their data addresses the elesclomol (in the absence of copper) inhibition of FDX1 Fe-S cluster activity reported in Tsvetkov et al 2019?

In fact, we have no explanation for this observation, and we do not see this effect for two reasons. First, FDX1 is NOT functional in Fe/S cluster synthesis. Second, Ele does not even inhibit *in vitro* Fe/S cluster synthesis as shown in the Figure R1 below.

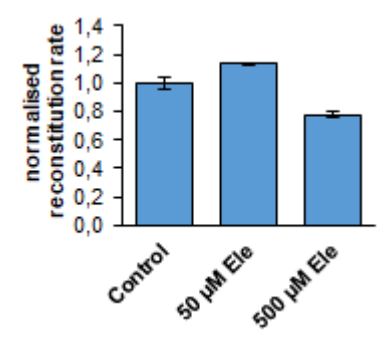


#### Figure R1 (for Reviewer only):

[2Fe-2S] cluster assembly was assayed *in vitro* under conditions of Fig. 1d with FDX2 and the indicated concentrations of elesclomol (Ele). There is virtually no effect of Ele on this biosynthetic reaction.

-Fig S1- not all the tissues overlap in analysis of protein vs mRNA

This is correct. However, the Reviewer may have missed that this figure (called out in the Introduction) presents data extracted from a public data base (Human Protein Atlas project, as indicated in the legend). Our own proteomic data have been published in Sheftel et al. PNAS 2010, and fully agree with the public data base (but are a bit less comprehensive). The data of Suppl. Fig. 1 is used to introduce the conundrum in the literature that *FDX1* is expressed in virtually all tissues based on transcriptomic data, but the protein is not "seen" by immunostaining analyses in most of the tissues. Our manuscript now clarifies this confusing issue by showing the new important function of FDX1 in lipoylation, a biosynthetic reaction needed in virtually all cells and tissues. To avoid confusion of the readers, we now have explained already at the start of the legend that this data is from a public data base. We also have added an explanation to the legend to make clear that the findings of our manuscript have solved the conundrum raised by the two data sets.

-Fig 1- it appears there is non-specific partial knockdown of FDX1 with the FDX2-si. Could this affect subsequent data interpretation?

In all likelihood, this is not a "non-specific" knockdown of FDX1 under FDX2 depletion conditions. The [2Fe-2S] cluster of FDX1 is a target of the ISC pathway including the ISC protein FDX2. As a consequence, FDX1 is not efficiently assembled when FDX2 is depleted, and hence the FDX1 apoprotein is degraded (as seen for many Fe/S apoproteins). This finding fully fits to our story. In response to this well-stated question of the Reviewer, we have added a note to explain this point in our manuscript.

-line 183: Can this statement be made if the authors weren't able to show a direct effect on heme a synthesis?

Based on the bulk of the data presented (both in human cell culture and 'humanized' yeast) and based on current literature on yeast and Trypanosomes, we believe that the statement is correct. We would like to further mention that during the experimental phase of our work we had contacted five experts of heme biosynthesis, and none of them has succeeded so far to detect heme a directly in cultured human cells. It would need a high amount of cells to detect the compound.

-Line 203: (Fig 2d) If this statement is true, why didn't addition of FDX1+FDX2 restore COX activity to FDX1 levels? What is the statistical significance?

Admittedly, we do not fully understand why complementation with both FDXs is weaker than with just FDX1. We frequently observe that yeast complementation suffers, if the mutant cells contain two or more plasmids. This may also apply here. The important result of this figure, however, is that, together with the leaky expression from the *YAH1* promoter (to support residual Fe/S protein biogenesis), FDX1 complementation efficiently restores COX activity even though the cells still do not grow, due to multiple Fe/S protein defects. The statistical analysis (see response to Reviewer 1) shows that the complementation with both FDXs is statistically significant (\*\*\* relative to empty vector control).

-Fig 4a/b: what does the 'X' refer to in the figure legend

Admittedly, we do not find an "X" in this legend. The "X"s in the figure itself are data points.

-line 316: how do the authors explain the reported direct binding of Ele to FDX1 in light of their data?

While we do not doubt this finding, we have no real explanation for the result. We emphasize that none of our results pointed to a direct effect of Ele on FDX1 or FDX2 (see Figure R1 above).

-line 398: should Glu133 be R135?

No, FDX1 contains a Glu133. The corresponding R135 is part of FDX2.

-line 443: GCSH has not been defined

Defined as suggested (see also response to Reviewer 2, point "Line 443: May be good to define GCSH").